

INFORMATION TO USERS

This manuscript has been reproduced from the microfilm master. UMI films the text directly from the original or copy submitted. Thus, some thesis and dissertation copies are in typewriter face, while others may be from any type of computer printer.

The quality of this reproduction is dependent upon the quality of the copy submitted. Broken or indistinct print, colored or poor quality illustrations and photographs, print bleedthrough, substandard margins, and improper alignment can adversely affect reproduction.

In the unlikely event that the author did not send UMI a complete manuscript and there are missing pages, these will be noted. Also, if unauthorized copyright material had to be removed, a note will indicate the deletion.

Oversize materials (e.g., maps, drawings, charts) are reproduced by sectioning the original, beginning at the upper left-hand corner and continuing from left to right in equal sections with small overlaps.

Photographs included in the original manuscript have been reproduced xerographically in this copy. Higher quality 6" x 9" black and white photographic prints are available for any photographs or illustrations appearing in this copy for an additional charge. Contact UMI directly to order.

**ProQuest Information and Learning
300 North Zeeb Road, Ann Arbor, MI 48106-1346 USA
800-521-0600**

UMI[®]

**Phosphorus Chemical Shift and Indirect ^{31}P - ^{31}P Spin-Spin Coupling
Tensors in Compounds Containing P-P Bonds: A Solid-State ^{31}P NMR
and Theoretical Study**

by

Myrlene Gee

**Submitted in partial fulfillment of the requirements for
the degree of Doctor of Philosophy**

at

**Dalhousie University
Halifax, Nova Scotia
June, 2001**

© Copyright by Myrlene Gee, 2001



**National Library
of Canada**

**Acquisitions and
Bibliographic Services**

**395 Wellington Street
Ottawa ON K1A 0N4
Canada**

**Bibliothèque nationale
du Canada**

**Acquisitions et
services bibliographiques**

**395, rue Wellington
Ottawa ON K1A 0N4
Canada**

Your file Votre référence

Our file Notre référence

The author has granted a non-exclusive licence allowing the National Library of Canada to reproduce, loan, distribute or sell copies of this thesis in microform, paper or electronic formats.

The author retains ownership of the copyright in this thesis. Neither the thesis nor substantial extracts from it may be printed or otherwise reproduced without the author's permission.

L'auteur a accordé une licence non exclusive permettant à la Bibliothèque nationale du Canada de reproduire, prêter, distribuer ou vendre des copies de cette thèse sous la forme de microfiche/film, de reproduction sur papier ou sur format électronique.

L'auteur conserve la propriété du droit d'auteur qui protège cette thèse. Ni la thèse ni des extraits substantiels de celle-ci ne doivent être imprimés ou autrement reproduits sans son autorisation.

0-612-66648-4

Canada

DALHOUSIE UNIVERSITY
FACULTY OF GRADUATE STUDIES

The undersigned hereby certify that they have read and recommend to the Faculty of Graduate Studies for acceptance a thesis entitled "Phosphorus Chemical Shift and Indirect ^{31}P - ^{31}P Spin-Spin Coupling Tensors in Compounds Containing P-P Bonds: A Solid-State ^{31}P NMR and Theoretical Study" by Myrlene Gee in partial fulfillment of the requirements for the degree of Doctor of Philosophy.

Dated: August 10, 2001

External Examiner:

Research Supervisor:

Examining Committee:

Dalhousie University

Date: August 20, 2001

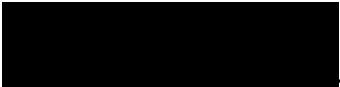
AUTHOR: Myrlene Gee

TITLE: Phosphorus Chemical Shift and Indirect ^{31}P - ^{31}P Spin-Spin Coupling Tensors in Compounds Containing P-P Bonds: A Solid-State ^{31}P NMR and Theoretical Study

DEPARTMENT OR SCHOOL: Dalhousie University

DEGREE: Ph. D. CONVOCATION: October YEAR: 2001

Permission is herewith granted to Dalhousie University to circulate and to have copied for non-commercial purposes, at its discretion, the above title upon the request of individuals or institutions.


Signature of Author

The author reserves other publication rights, and neither the thesis nor extensive extracts from it may be printed or otherwise reproduced without the author's written permission.

The author attests that permission has been obtained for the use of any copyrighted material appearing in this thesis (other than brief excerpts requiring only proper acknowledgement in scholarly writing), and that all such use is clearly acknowledged.

For Mum and Dad

"I went to the woods because I wished to live deliberately, to front only the essential facts of life, and see if I could not learn what it had to teach, and not, when I came to die, discover that I had not lived."

"I left the woods for as good a reason as I went there. Perhaps it seemed to me that I had several more lives to live, and could not spare any more time for that one."

From Walden, by Henry David Thoreau

Table of Contents

	Page
Table of Figures.....	viii
List of Tables.....	xi
Abstract.....	xii
List of Abbreviations and Symbols.....	xiii
Acknowledgments.....	xx
Chapter 1: Introduction and Scope	
1.1 Introduction	1
1.2 Thesis Outline.....	5
Chapter 2: Background Theory	
2.1 NMR Interactions	
2.1.1 Overview	8
2.1.2 Zeeman Interaction	9
2.1.3 Radio Frequency Interaction	9
2.1.4 Nuclear Magnetic Shielding and Chemical Shift	11
2.1.5 Dipolar Coupling	15
2.1.6 <i>J</i> Coupling	20
2.2 NMR Spectra Arising from Isolated Spin Pairs	
2.2.1 Overview	23
2.2.2 The Dipolar Chemical Shift Method	26
2.2.3 2D Spin-Echo Spectroscopy.....	30
2.3 <i>Ab Initio</i> Calculations of NMR Parameters	
2.3.1 Nuclear Magnetic Shielding Tensors	33
2.3.2 Indirect Spin-Spin (<i>J</i>) Tensors	38
Chapter 3: Phosphorus Chemical Shift Tensors for Tetramethyldiphosphine Disulphide: A Single-Crystal ³¹P NMR, Dipolar-Chemical Shift NMR and <i>Ab Initio</i> Molecular Orbital Study	
3.1 Introduction.....	43

3.2 Experimental and Computational Details	46
3.3 Results and Discussion	
3.3.1 Phosphorus-31 NMR of a Single Crystal.....	51
3.3.2 Phosphorus-31 NMR of Crystalline Powder Samples	60
3.3.3 <i>Ab Initio</i> Calculation of Phosphorus Shielding Tensors ...	65
3.3.4 Comparison of Results	66
3.3.5 Trends in Phosphorus Chemical Shifts for Alkyldiphosphine Disulfides	67
3.4 Conclusions	69
 Chapter 4: Characterization of Phosphorus Chemical Shift Tensors in a Phosphole Tetramer: A Combined Experimental NMR and Theoretical Study	
4.1 Introduction	70
4.2 Experimental and Computational Details	71
4.3 Results and Discussion	
4.3.1 Experimental Determination of Phosphorus Chemical Shift Tensors	74
4.3.2 <i>Ab Initio</i> Calculations of Phosphorus Shielding Tensors ..	84
4.3.3 Trends in Phosphorus Chemical Shifts for Phospholes	87
4.4 Conclusions	90
 Chapter 5: $^1J(^{31}\text{P}, ^{31}\text{P})$ Coupling Tensors - Conformational Studies in Model Systems and Structural Characterization of $[\text{Ph}_3\text{P-PPh}_2][\text{GaCl}_4]$	
5.1 Introduction	91
5.2 Experimental and Computational Details	94
5.3 Results and Discussion	97
5.3.1 Phosphorus-31 NMR Spectra of $[\text{Ph}_3\text{P-PPh}_2][\text{GaCl}_4]$	97
5.3.2 Dependence of $^1J(^{31}\text{P}, ^{31}\text{P})$ on conformation: $\text{H}_2\text{P-PH}_2$ vs. $\text{H}_3\text{P-PH}_2^+$	105
5.3.3 Estimate of r_{pp} in $[\text{Ph}_3\text{P-PPh}_2][\text{GaCl}_4]$	115
5.4 Conclusions	115

Chapter 6: Conclusions	117
Chapter 7: Future Research Directions	
7.1 Introduction	120
7.2 [Ph₂(Cl)P-PPh₂][GaCl₄]	120
7.3 <i>Ab Initio</i> Calculation of Phosphorus Chemical Shift Tensors	122
7.4 Characterization of ¹J(³¹P, ³¹P)	123
7.5 NMR Spectra Arising from Three Coupled Homonuclear Spin-½ Nuclei in the Solid State	127
Appendix 1: Performing the 2D Spin-Echo NMR Experiment on the CMX 200 at the University of Alberta	129
Appendix 2: Handling Air-Sensitive NMR Samples	131
References.....	133

List of Figures

	Page	
Figure 1.1	Structures of the compounds studied this thesis	3
Figure 2.1	Zeeman energy as a function of B_0	10
Figure 2.2	Angles defining the orientation of \mathbf{B}_0 , \mathbf{r}_{IS} , and the PAS of the nuclear magnetic shielding tensor	13
Figure 2.3	Typical line shapes for an isolated spin in a powder crystalline sample	16
Figure 2.4	Calculated NMR spectra when the Zeeman and dipolar interactions are present	19
Figure 2.5	Calculated NMR spectra illustrating the effect of dipolar and J coupling	27
Figure 2.6	Calculated NMR spectra illustrating the effect of dipolar coupling and anisotropic nuclear magnetic shielding	28
Figure 2.7	Euler angles relating the PAS of the nuclear magnetic shielding tensor to the molecular frame of reference	29
Figure 2.8	The 2D spin-echo pulse sequence	31
Figure 3.1	Structure of tetramethyldiphosphine disulfide, TMPS	45
Figure 3.2	Phosphorus-31 NMR spectra of a single crystal of TMPS	52
Figure 3.3	Example of a ^{31}P NMR spectrum of the TMPS single crystal	53
Figure 3.4	Phosphorus chemical shift as a function of crystal rotation for TMPS	55
Figure 3.5	Dipolar splitting as a function of crystal rotation angle TMPS	55
Figure 3.6	Orientation of the phosphorus chemical shift tensor for TMPS	58
Figure 3.7	Experimental and calculated ^{31}P NMR spectra of stationary powder samples of TMPS	61

Figure 3.8	Experimental and calculated ^{31}P NMR spectra of MAS samples of TMPS	62
Figure 3.9	Experimental and calculated $F1$ projections of the 2D spin-echo ^{31}P NMR spectrum of TMPS	63
Figure 4.1	Structure of the phosphole tetramer and the model system used for <i>ab initio</i> calculations	71
Figure 4.2	Experimental and calculated ^{31}P NMR spectra of stationary samples of the phosphole tetramer	75
Figure 4.3	Experimental and calculated ^{31}P NMR spectra of MAS samples of the phosphole tetramer at 4.7 T	76
Figure 4.4	Experimental and calculated ^{31}P NMR spectra of MAS samples of the phosphole tetramer at 9.4 T	77
Figure 4.5	The calculated and experimental $F1$ projections of the 2D spin-echo ^{31}P NMR spectrum of the phosphole tetramer	81
Figure 4.6	The relative orientation of the two phosphorus chemical shift tensors in the phosphole tetramer	83
Figure 4.7	The phosphorus chemical shift tensor orientations for the phosphole tetramer determined by <i>ab initio</i> calculations	84
Figure 4.8	Structures of compound 5, 6, and 7 in table 4.2	89
Figure 5.1	Structures of the molecules discussed in chapter 5	93
Figure 5.2	Experimental and calculated ^{31}P NMR spectra of MAS samples of $[\text{Ph}_3\text{P-PPh}_2][\text{GaCl}_4]$ at 4.7 T	98
Figure 5.3	Experimental and calculated ^{31}P NMR spectra of MAS samples of $[\text{Ph}_3\text{P-PPh}_2][\text{GaCl}_4]$ at 9.4 T	99
Figure 5.4	Experimental and calculated $F1$ projections of the 2D spin-echo ^{31}P NMR spectrum of $[\text{Ph}_3\text{P-PPh}_2][\text{GaCl}_4]$ at 4.7 T	103
Figure 5.5	Experimental and calculated ^{31}P NMR spectra of stationary powder samples of $[\text{Ph}_3\text{P-PPh}_2][\text{GaCl}_4]$	104

Figure 5.6	Calculated orientation of the phosphorus chemical shift tensors for $(\text{CH}_3)_3\text{P}-\text{P}(\text{CH}_3)_2^+$	106
Figure 5.7	Plot of the total energy for $\text{H}_2\text{P}-\text{PH}_2$ a function of ϕ_{PP}	108
Figure 5.8	The dependence of $^1\text{J}(^{31}\text{P}, ^{31}\text{P})$ in $\text{H}_2\text{P}-\text{PH}_2$ on ϕ_{PP}	109
Figure 5.9	The dependence of $^1\text{J}(^{31}\text{P}, ^{31}\text{P})$ in $\text{H}_3\text{P}-\text{PH}_2^+$ on ϕ_{PP^+}	111
Figure 7.1	Phosphorus-31 NMR spectra of solid $[\text{Ph}_2(\text{Cl})\text{P}-\text{PPh}_2][\text{GaCl}_4]$ (MAS)	121
Figure 7.2	Structure of a phosphorus-containing homonuclear three-spin system	128
Figure A2.1	A Varian-Chemagnetics rotor	132

List of Tables

		Page
Table 3.1	Selected bond lengths and bond angles for TMPS	47
Table 3.2	Direction cosines orienting the crystal axes of a single crystal of TMPS to the NMR cube frame	48
Table 3.3	Linear least-squares coefficients for the phosphorus chemical shift and spin-spin coupling interactions in TMPS as functions of crystal rotation	56
Table 3.4	Principal components and orientations of the phosphorus chemical shift and dipolar coupling tensors relative to the crystal axes (a^*bc) for TMPS	57
Table 3.5	Spin-spin coupling data for TMPS	57
Table 3.6	The isotropic chemical shift, principal components, Ω , and κ of the phosphorus chemical shift tensors for TMPS	64
Table 3.7	Comparison of δ_{iso} and C-P-C bond angle for $[R_2P(S)]_2$	68
Table 4.1	Experimental and calculated phosphorus chemical shift tensor principal components for the phosphole tetramer	78
Table 4.2	Phosphorus chemical shift tensor principal components for some phospholes	89
Table 5.1	Phosphorus chemical shift tensor principal components and spin-spin coupling parameters for $[Ph_3P-PPh_2][GaCl_4]$	101
Table 5.2	${}^1J(^{31}P, ^{31}P)$ for H_2P-PH_2 as a function of ϕ_{PP}	110
Table 5.3	${}^1J(^{31}P, ^{31}P)$ for $H_3P-PH_2^+$ as a function of ϕ_{PP^+}	112
Table 5.4	Geometry dependence of ${}^1J(^{31}P, ^{31}P)_{iso}$ for H_2P-PH_2	114
Table 7.1	${}^1J(X,X)$ and ${}^1K(X,X)$ for P_2H_2 and N_2H_2	124

Abstract

The combination of solid-state NMR and theoretical calculations to characterize NMR parameters is applied to compounds containing P-P bonds where phosphorus participates in a variety of bonding modes. In particular, phosphorus chemical shift tensors and one-bond indirect spin-spin or J -coupling tensors, ${}^1J(^{31}\text{P}, ^{31}\text{P})$, have been investigated experimentally by NMR and complemented by first-principles calculations.

The phosphorus chemical shift and spin-spin coupling tensors for tetramethyldiphosphine disulfide are characterized by analysis of ${}^{31}\text{P}$ NMR spectra obtained at 4.7 T for a single crystal. These results were compared to those obtained from spectra acquired at 4.7 T and 9.4 T for powder samples. The data obtained from both methods are in excellent agreement. It was also found that the upper limit on the anisotropy in ${}^1J(^{31}\text{P}, ^{31}\text{P})$, ΔJ , is approximately 450 Hz.

The phosphorus chemical shift tensors for a phosphole tetramer were characterized by analysis of ${}^{31}\text{P}$ NMR spectra acquired at 4.7 T and 9.4 T for powder samples. The experimental NMR results are supplemented by first principles calculations of the chemical shift tensor. The calculations are useful for proposing chemical shift tensor orientations.

The final example presented here is an investigation of the phosphinophosphonium salt, $[\text{Ph}_3\text{P}-\text{PPh}_2][\text{GaCl}_4]$. The structure is not available from X-ray diffraction studies, thus characterization by other means, such as solid-state NMR, is important. To determine the P-P bond length from the effective dipolar coupling constant, R_{eff} , ΔJ needs to be estimated, in this case by *ab initio* calculations on a model system, $\text{H}_3\text{P}-\text{PH}_2^+$. Combination of the calculated ΔJ value and the measured R_{eff} yields a P-P bond length of 2.25 Å. Further calculations of ${}^1J(^{31}\text{P}, ^{31}\text{P})$ for $\text{H}_2\text{P}-\text{PH}_2$ offers an opportunity to investigate the dependence of this parameter on conformation. First-principles calculations allows one to map out the detailed orientation dependence as well as the potential energy surface.

List of Abbreviations and Symbols

$ 0\rangle$	ground electronic state
\mathbf{B}	a magnetic field vector
\mathbf{B}_0	applied magnetic field vector
B_0	magnitude of \mathbf{B}_0
\mathbf{B}_{rf}	applied radio frequency field vector
B_{rf}	magnitude of \mathbf{B}_{rf}
B_1	amplitude of \mathbf{B}_{rf}
\mathbf{B}_{ind}	induced magnetic field vector
CASSCF	complete active space self-consistent field
cc-pVTZ	correlation-consistent polarization valence triple-zeta
CSGT	continuous set of gauge transformations
CP	cross polarization
\mathbf{D}	dipolar coupling tensor
DFT	density functional theory
DSO	diamagnetic spin-orbit
$E(\mathbf{B}, \mathbf{M})$	the energy of a molecule
ΔE	the energy separation between the $+1/2$ and $-1/2$ nuclear spin states of I in the presence of \mathbf{B}_0
FC	Fermi contact
FF	finite field

FID	free induction decay
FP	finite perturbation
FT	Fourier transform
GIAO	gauge-including atomic orbitals
\hbar	Planck's constant divided by 2π
$\mathcal{H}_{\text{CS}}(I)$	Hamiltonian describing the chemical shift interaction for I
$\mathcal{H}_{\text{DD}}(I,S)$	Hamiltonian describing the dipolar coupling between I and S
\mathcal{H}_{DSO}	Hamiltonian describing the DSO contribution to \mathbf{J}
\mathcal{H}_{FC}	Hamiltonian describing the FC contribution to \mathbf{J}
$\mathcal{H}_J(I,S)$	Hamiltonian describing the indirect spin-spin coupling (J-coupling) between I and S
\mathcal{H}_{PSO}	Hamiltonian describing the PSO contribution to \mathbf{J}
$\mathcal{H}_{\text{rf}}(I)$	Hamiltonian describing the interaction of I with \mathbf{B}_{rf}
\mathcal{H}_{SD}	Hamiltonian describing the SD contribution to \mathbf{J}
$\mathcal{H}_Z(I)$	Hamiltonian describing the Zeeman interaction
HF	Hartree Fock
\mathbf{I}, \mathbf{S}	nuclear spin angular momentum operators
I_i, S_i	ith component of \mathbf{I} or \mathbf{S}
I, S	nuclei with spin of $\frac{1}{2}$
IGLO	individual gauge for localized orbitals
INDO	intermediate neglect of differential overlap

J	indirect spin-spin coupling tensor
J'	tensor describing the anisotropic part of J
J_{DSO}	the DSO contribution to J
J_{FC-FC}	the FC contribution to J
J_{FC-SD}	the FC × SD contribution to J
J_{PSO-PSO}	the PSO contribution to J
J_{SD-SD}	the SD contribution to J
ⁿJ(I,S)	<i>J</i> coupling over <i>n</i> bonds between <i>I</i> and <i>S</i> (Hz)
J₁₁, J₂₂, J₃₃	principal components of J (Hz)
J_{ij}	a component of J (Hz)
J_⊥	component of an axially symmetric J which is perpendicular to the bond
J_∥	component of an axially symmetric J which is parallel to the bond
J_{iso}	isotropic <i>J</i> coupling (Hz)
Δ<i>J</i>	anisotropy in J (Hz)
K	reduced <i>J</i> -coupling tensor (N A ⁻² m ⁻³)
k_B	Boltzmann constant
L_k, L_{kN}	angular momentum operator for the <i>k</i> th electron (<i>N</i> denotes with respect to a nucleus)
LORG	localized orbital local origin
M	the set of nuclear magnetic moment vectors in a molecule
M_I	the nuclear magnetic moment vector of nucleus <i>I</i>

m_e	electron mass
m_I	z-component of the nuclear angular momentum of I
MAS	magic angle spinning
Mes [*]	(2,4,6-tri- <i>t</i> -butyl) phenyl
MCLR	multiconfigurational linear response
MCSCF	multiconfigurational self-consistent field
MP	Møller-Plesset
$ n\rangle$	n th excited electronic state
Δn_I	population difference between the $+1/2$ and $-1/2$ nuclear spin states of I
N	total number of I nuclei in a sample
NMR	nuclear magnetic resonance
o. d.	outer diameter
P_i	intensity of the ν_i transition for a homonuclear spin pair
PAS	principal axis system
PSO	paramagnetic spin-orbit
\mathbf{r}_{IS}	vector between spin I and S of magnitude r_{IS}
r_{IS}	distance between I and S
$\mathbf{r}_k, \mathbf{r}_{kN}$	position vector for the k th electron (N denotes with respect to a nucleus)
R_{DD}	the dipolar coupling constant (kHz)
R_{eff}	the effective dipolar coupling constant (kHz)
RR	rotational resonance
$s(t_1), s(t_2)$	FIDs for the 2D spin-echo NMR experiment

SD	spin-dipolar
SO	spin-orbit
SOS-CI	sum-over-states configuration interaction
SOPPA	second-order polarization propagator approximation
STO	Slater-type orbital
<i>T</i>	temperature
<i>t</i>₁	evolution time in 2D spin-echo experiment
<i>t</i>₂	acquisition time in 2D spin-echo experiment
TBPS	tetrabutylidiphosphine disulfide
TEPS	tetraethyldiphosphine disulfide
TMPS	tetramethyldiphosphine disulfide
α	phase angle for B_{rf}
α, β	polar angle defining the position of r_{IS} with respect to the PAS of σ
α, β, γ	Euler angles
$\Delta\alpha$	difference between the values of the Euler angle α for chemical shift tensors of a spin pair
γ_I	magnetogyric ratio of nucleus I (rad T⁻¹s⁻¹)
δ	chemical shift tensor (ppm)
$\delta_{11}, \delta_{22}, \delta_{33}$	principal components of δ (ppm)
δ_{ii}	a component of δ (ppm)

δ_{iso}	isotropic chemical shift (ppm)
ζ	the angle between \mathbf{B}_0 and \mathbf{r}_{IS}
η	asymmetry in \mathbf{J}
θ, ϕ	polar angles defining the position of \mathbf{B}_0 with respect to the PAS of $\mathbf{\sigma}$
θ_p	tip angle
κ	skew
λ	the set of parameters that define the wavefunction for a molecule
μ_0	permeability of vacuum
ν_i	frequency corresponding to the i th ($i = 1, 2, 3$ or 4) transition for a homonuclear spin pair
ν_{ii}	resonance frequency for a sample
ν_{ref}	resonance frequency for a reference compound
ν_{rf}	frequency of an applied radio frequency field
ν_{rot}	MAS spinning frequency
ν_0	Larmor frequency
$\mathbf{\sigma}$	nuclear magnetic shielding tensor
$\sigma_{11}, \sigma_{22}, \sigma_{33}$	principal components of $\mathbf{\sigma}$ (ppm)
σ^{d}	diamagnetic contribution to σ (ppm)
σ^{p}	paramagnetic contribution to σ (ppm)
σ_{ii}	a component of $\mathbf{\sigma}$ (ppm)
σ_{iso}	isotropic nuclear magnetic shielding (ppm)

σ_{ref}	nuclear magnetic shielding for a reference compound (ppm)
τ_p	duration of radio frequency irradiation
ϕ_{MePP}	dihedral angle for $(\text{CH}_3)_3\text{P}-\text{P}(\text{CH}_3)_2^+$
ϕ_{PP}	dihedral angle for $\text{H}_2\text{P}-\text{PH}_2$
ϕ_{PP^+}	dihedral angle for $\text{H}_3\text{P}-\text{PH}_2^+$
ϕ_{ring}	angle describing the relative orientation of adjacent phosphole rings in the phosphole tetramer
ψ	rotation angle of a single crystal in a goniometer about its X , Y or Z axis
Ω	span (ppm)

Acknowledgments

I would like to thank my Ph. D. supervisor, Rod Wasylshen, for his patience and support. For his constant encouragement and guidance, I am grateful. The members of the solid-state NMR group at Dalhousie University and at the University of Alberta are acknowledged for all their help. In particular, I would like to thank Klaus Eichele for help with the spectrometers and suggestions on many projects. I would also like to thank Dave Bryce, Guy Bernard, Shelley Forgeron, Rob Schurko, Mike Lumsden, and Scott Kroeker for their interest in my research projects. Special thanks to Dave and Guy for proofreading this thesis.

Neil Burford and Paul Ragogna at Dalhousie University and Edgar Ocando-Mavarez at IVIC are acknowledged for samples and suggestions. I am grateful to Gang Wu at Queen's University for suggestions on the phosphole tetramer project. Stan T. Cameron at Dalhousie University is acknowledged for his contribution to the phosphole tetramer project as well. I am grateful to Jim Britten at McMaster University for his contribution to the TMPS project. I would also like to thank Brian Millier at Dalhousie University for his help.

I acknowledge the financial support of the Natural Sciences and Engineering Research Council (NSERC) of Canada, the Izaak Walton Killam Trust, and the Walter C. Sumner Foundation for postgraduate scholarships. All NMR spectra were acquired at the Atlantic Regional Magnetic Resonance Centre (ARMRC) which is also funded by NSERC.

Starting my Ph. D. degree at Dalhousie University and finishing at the

University of Alberta means that I have twice the number of friends and colleagues to thank compared to the average Ph. D. candidate. To everyone I met at both places, thank you. Finally, I would like to thank my family for all their support and encouragement.

Chapter 1: Introduction and Scope

1.1 Introduction

Nuclear magnetic resonance (NMR) spectroscopy is one of the most powerful tools available for characterizing molecular structure and dynamics in chemistry. However, it is important to recognize that some fundamental questions regarding the relationship between NMR parameters and structure remain. An NMR spectrum is characterized by a number of parameters, for example the chemical shift and the indirect spin-spin coupling (or *J*-coupling) constant. The majority of the NMR literature concentrates on the measurement of the isotropic values of these parameters and the application of various empirical rules and correlations to extract information on structure and dynamics. For example, one of the most important relationships between an isotropic NMR parameter and molecular structure is the Karplus relationship, which describes how the indirect spin-spin coupling over three bonds depends on the dihedral angle.¹ However, the chemical shift and *J* coupling are tensor properties;^{2,3} hence, it is essential to characterize the anisotropic nature of these interactions to fully understand the origins of observed trends. For example, considering only the isotropic chemical shift leads to the observation of trends which often defy simple explanations in terms of local structure, particularly in the case of phosphorus chemical shifts.⁴

The determination of the chemical shift tensor, both its principal components and the orientation of its principal axis system (PAS) with respect to the molecule, is particularly valuable due to its close relationship with the local structure and electronic

properties of the molecule.⁵ Nuclear magnetic resonance spectroscopy of solids is ideal for investigating the tensor nature of these parameters since the interactions are not usually averaged as in the case of solution NMR studies. The field of solid-state NMR is currently enjoying an expanding popularity, thanks in part to a number of experimental advances which have led to applications of this technique to a range of research problems, from protein structure to materials science. Recent advances in computational chemistry, particularly with regards to *ab initio* calculation of NMR parameters,^{6,7,8,9} have resulted in the use of calculated results as a complement to experimental data.

Ideally, NMR studies using single crystals are desirable since, in principle, the chemical shift tensor as well as dipolar and *J*-coupling tensors may be determined unambiguously. Unfortunately, large single crystals are rarely available; hence, powder samples must be used. If the system of interest contains an isolated spin pair, some orientation information can be extracted from NMR studies (see section 2.2).

One objective of my Ph.D. research was to use solid-state ³¹P NMR combined with first-principles calculations to characterize the NMR parameters for systems containing P-P bonds. The three examples illustrated in figure 1.1 have been selected for discussion in this thesis. For one of these systems, tetramethyldiphosphine disulfide, **1**, abbreviated as TMPS, a single-crystal ³¹P NMR investigation was carried out. For another compound, a phosphole tetramer, **2**, the NMR parameters were characterized experimentally using a crystalline powder sample and by theoretical

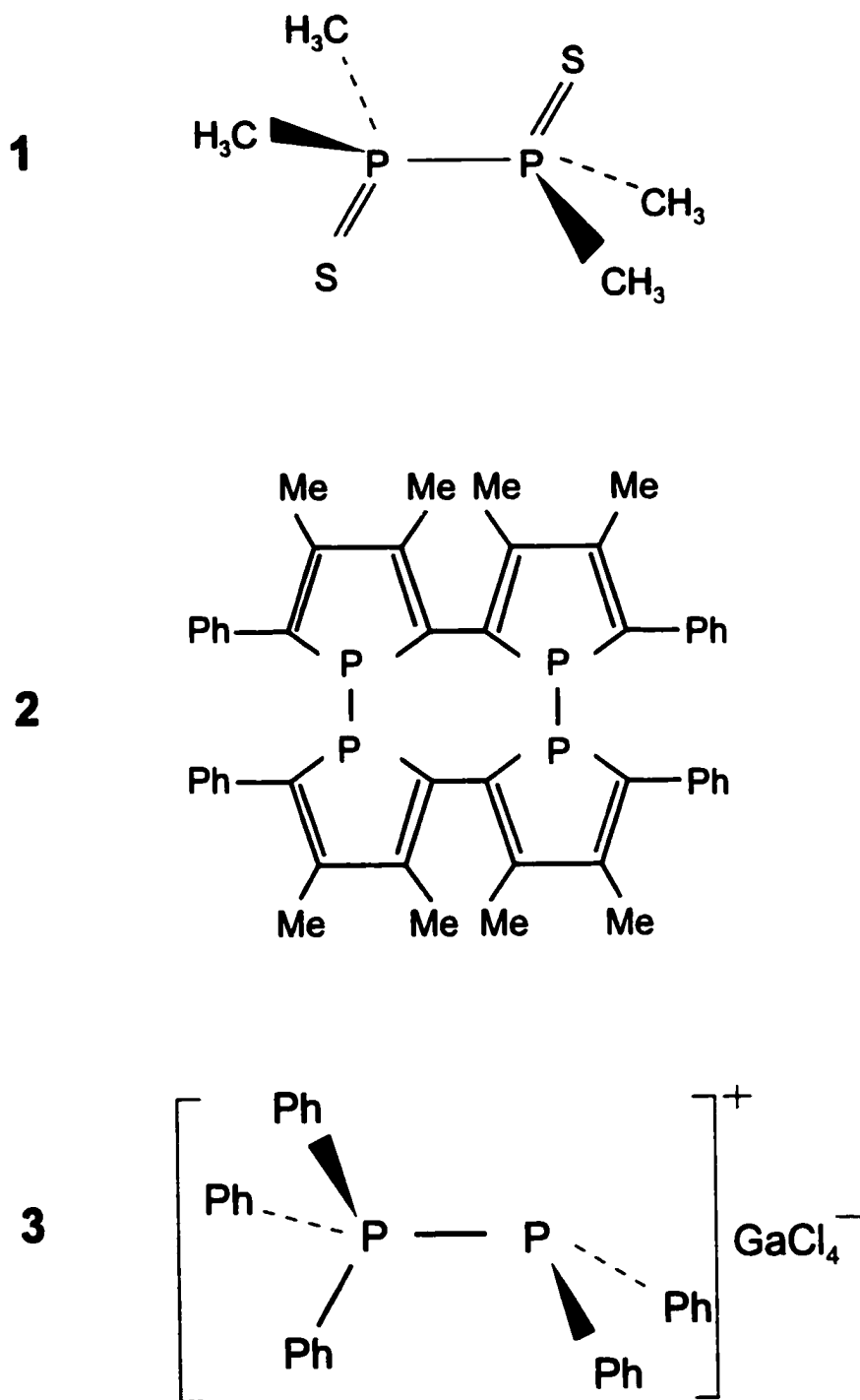


Figure 1.1 Molecular structures of the compounds studied by solid-state NMR in this thesis. 1: tetramethyldiphosphine disulfide, TMPS. 2: a phosphole tetramer. 3: pentaphenylphosphinophosphonium tetrachlorogallate.

calculations. In addition, the X-ray crystal structure was redetermined in the course of this study. For a third compound, pentaphenylphosphinophosphonium tetrachlorogallate, $[\text{Ph}_3\text{P-PPh}_2][\text{GaCl}_4]$, **3**, the X-ray structure was unavailable and NMR investigations of solid samples have provided valuable structural information.

There are three themes running through the examples presented in this thesis. The first theme concerns the orientation of the phosphorus chemical shift tensor as a reflection of molecular structure. It has been shown that for compounds such as tetraethyldiphosphine disulfide, $(\text{CH}_3\text{CH}_2)_2\text{P}(\text{S})\text{P}(\text{S})(\text{CH}_2\text{CH}_3)_2$, abbreviated as TEPS, the most shielded component of the phosphorus chemical shift tensor is directed along the P=S bond.^{10,11} This observation has also been made in $(\text{CH}_3)_3\text{PS}$.¹² Investigation of the phosphorus chemical shift tensor orientations in TMPS may aid in establishing this observation as a general phenomenon. On a related note, one assumption about chemical shift tensor orientations is that the direction of greatest shielding corresponds to the direction of greatest electron density.¹³ Studies of phosphorus shielding in a phosphole tetramer and a phosphinophosphonium cation, where there are formal lone pairs on the phosphorus nuclei, affords an opportunity to investigate these trends further.

A second theme concerns the indirect spin-spin coupling tensor between phosphorus nuclei that are bonded to each other, ${}^1\text{J}({}^{31}\text{P}, {}^{31}\text{P})$, and in particular its anisotropy, ΔJ . The investigation of ΔJ in TMPS is relevant here, as is explained in further detail in section 1.2. *Ab initio* calculations of ${}^1\text{J}({}^{31}\text{P}, {}^{31}\text{P})$ in model compounds, $\text{H}_2\text{P-PH}_2$ and $\text{H}_3\text{P-PH}_2^+$, are potentially useful for exploring the dependence of

$^1J(^{31}\text{P}, ^{31}\text{P})$ on conformation.

The third theme concerns the value of *ab initio* calculations of NMR parameters as a complement to experimental data. The accuracy of calculated chemical shift tensor orientations is explored in the chapter on TMPS (chapter 3) and calculations of J on a model system, $\text{H}_3\text{P-PH}_2^+$, are applied to the determination of the dipolar coupling constant, R_{DD} , between the phosphorus nuclei in $[\text{Ph}_3\text{P-PPh}_2][\text{GaCl}_4]$, and hence estimate the P-P bond length (chapter 5). The contents of each chapter are discussed in more detail in the following section.

1.2 Thesis Outline

Following a chapter detailing the relevant background theory (chapter 2), the work on TMPS is described in chapter 3. There have been a few NMR studies of alkyldiphosphine disulfides in the literature. Many solution studies stem from an interest in the relationship between conformation and indirect spin-spin coupling between phosphorus nuclei that are directly bonded to each other, $^1J(^{31}\text{P}, ^{31}\text{P})$.^{14,15} TEPS^{10,11} and tetrabutylidiphosphine disulfide¹⁶ (TBPS) have been testing grounds for the determination of anisotropy in indirect spin-spin coupling tensors. Early single-crystal NMR studies reported large anisotropies for $^1J(^{31}\text{P}, ^{31}\text{P})$ in TEPS and TBPS of 2.2 kHz¹¹ and 1.9 kHz,¹⁶ respectively. The phosphorus chemical shift and spin-spin coupling tensors for TMPS (figure 1.1, structure 1) are characterized by a single-crystal ^{31}P NMR study and by an independent analysis of ^{31}P NMR spectra obtained from crystalline powdered samples combined with *ab initio* calculations. As so much

information is available about this system, it also serves as a benchmark for evaluating experimental NMR methods as well as *ab initio* approaches for the characterization of NMR parameters. Since accurate P-P bond lengths are required for a reliable determination of ΔJ , the X-ray crystal structure was redetermined. Data available in the literature for related compounds provide an opportunity to consider some trends in phosphorus magnetic shielding.

Chapter 4 summarizes the results for a phosphole tetramer, figure 1.1, structure 2. This compound contains two phosphorus spin pairs, each one consisting of two three-coordinate phosphorus nuclei directly bonded to each other; characterization of phosphorus chemical shift tensors and spin-spin coupling parameters in such environments are relatively rare.^{13,17,18,19,20} *Ab initio* calculations prove to be an extremely valuable addition to the experimental ³¹P NMR data for a complete characterization of the two phosphorus chemical shift tensors since single crystals large enough for an NMR investigation were unavailable for this compound. It was found that the relative orientation of the two chemical shift tensors reflects the local structure. Inconsistencies between the NMR data and the published X-ray crystal structure²¹ prompted a redetermination of the structure.

The structural characterization of pentaphenylphosphinophosphonium tetrachlorogallate, [Ph₃P-PPh₂][GaCl₄] (figure 1.1, structure 3), by solid-state NMR is detailed in chapter 5. Phosphinophosphonium salts²² represent a new class of compounds and are thus important to characterize. X-ray crystal structures are not available in the literature; hence, characterization by other means is vital. For the

example presented in this chapter, $[\text{Ph}_3\text{P-PPh}_2][\text{GaCl}_4]$, some structural information is available from analysis of ^{31}P NMR spectra of solid samples combined with *ab initio* calculation of $^1\text{J}(^{31}\text{P},^{31}\text{P})$. Trends in $^1\text{J}(^{31}\text{P},^{31}\text{P})$ are explored by *ab initio* calculations on model systems, $\text{H}_2\text{P-PH}_2$ and $\text{H}_3\text{P-PH}_2^+$. In particular, the effect of the conformation is considered.

Finally, extensions of the research projects described here are proposed in chapter 7 of this thesis.

Chapter 2: Background Theory

2.1 NMR Interactions

2.1.1 Overview

The systems of interest in this thesis consist of homonuclear spin pairs, IS , where I and S refer to spin- $1/2$ nuclei. To analyze the NMR spectra for such a spin pair, the following Hamiltonian needs to be considered:

$$\mathcal{H} = \mathcal{H}_Z(I) + \mathcal{H}_Z(S) + \mathcal{H}_{rf}(I) + \mathcal{H}_{rf}(S) + \mathcal{H}_{CS}(I) + \mathcal{H}_{CS}(S) + \mathcal{H}_{DD}(I,S) + \mathcal{H}_J(I,S) \quad (2.1)$$

where $\mathcal{H}_Z(I)$ and $\mathcal{H}_Z(S)$ are the Hamiltonian operators that describe the interaction of I and S respectively with the applied external magnetic field, \mathbf{B}_0 , termed the Zeeman interaction. $\mathcal{H}_{rf}(I)$ and $\mathcal{H}_{rf}(S)$ describe the interaction of each spin with an applied radio frequency field, \mathbf{B}_{rf} . $\mathcal{H}_{CS}(I)$ and $\mathcal{H}_{CS}(S)$ are the nuclear magnetic shielding (or chemical shift) Hamiltonians, $\mathcal{H}_{DD}(I,S)$ describes the dipolar interaction between I and S , and $\mathcal{H}_J(I,S)$ is the indirect spin-spin or J -coupling interaction between the two nuclei. \mathcal{H}_Z and \mathcal{H}_{rf} are under the control of the spectroscopist, hence they are termed *external* Hamiltonians; the remaining terms are dependent on the nature of the system and are hence referred to as *internal* Hamiltonians.

2.1.2 The Zeeman Interaction

The fundamental phenomenon upon which NMR is based involves the interaction of the nuclear magnetic moment with \mathbf{B}_0 as described by the following Hamiltonian:

$$\hbar^{-1}\mathcal{H}_z = -\gamma_I \mathbf{I} \cdot \mathbf{B}_0 \quad (2.2)$$

where γ_I is the magnetogyric ratio (in $\text{rad T}^{-1} \text{s}^{-1}$) of nucleus I and \mathbf{I} is the nuclear spin angular momentum operator. For NMR studies of spin- $1/2$ nuclei, this is the largest of the interactions described in equation 2.1. The spin states for I are described by the quantum number m_I which gives the z-component of angular momentum. For a spin- $1/2$ nucleus, $m_I = +1/2$ or $-1/2$. In the presence of \mathbf{B}_0 , these two states are separated by an energy, ΔE , that is dependent on the magnitude of the applied magnetic field, B_0 , as illustrated in figure 2.1. The corresponding frequency,

$$\nu_0 = \frac{\gamma_I B_0}{2\pi} \quad (2.3)$$

is called the Larmor frequency.

2.1.3 Radio-Frequency Interaction

To obtain an NMR spectrum, it is necessary to induce transitions between the allowed nuclear spin states. This is achieved by applying electromagnetic radiation at or near the Larmor frequency and usually in a direction that is perpendicular to \mathbf{B}_0 .

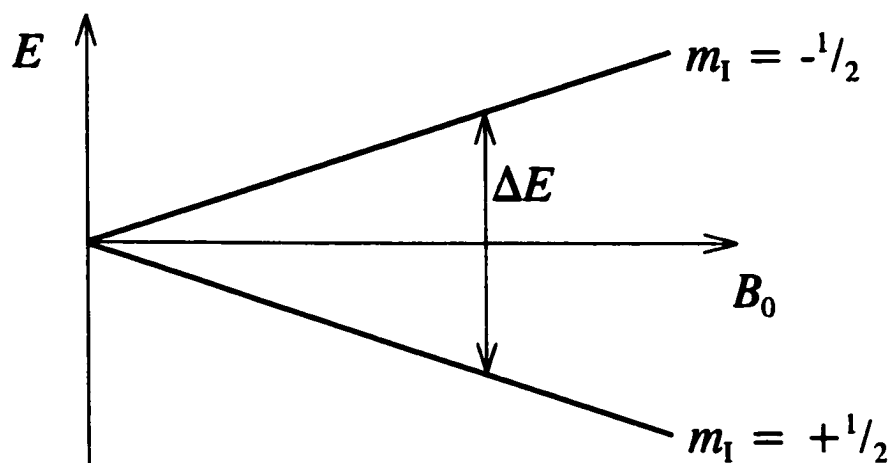


Figure 2.1 The Zeeman energy as a function of the magnitude of the applied magnetic field, B_0 , for a spin- $1/2$ nucleus with $\gamma_I > 0$.

Typically, ν_0 falls in the radio frequency region of the electromagnetic spectrum. The Hamiltonian describing the interaction between I and an applied radio frequency field, \mathbf{B}_{rf} , is identical to the Zeeman Hamiltonian (equation 2.2) except that the magnetic field is not static. The magnitude of \mathbf{B}_{rf} in a direction perpendicular to \mathbf{B}_0 is B_{rf} :

$$B_{rf} = 2B_1 \cos(2\pi\nu_{rf}t + \alpha) \quad (2.4)$$

where B_1 is the amplitude of the applied radio frequency field, ν_{rf} is its frequency (at or near ν_0), and α is its phase. Under the influence of \mathbf{B}_{rf} , the net magnetization resulting

from the nuclear magnetic moments are tipped away from their equilibrium positions by an angle $\theta_p = \gamma_1 B_1 \tau_p$ where τ_p is the duration of the radio frequency irradiation.

NMR is an inherently insensitive technique, as ΔE is much less than the thermal energy, $k_B T$. As a result, the population difference between the $m_I = +1/2$ and $m_I = -1/2$ states, Δn_I , is very small. Under the high-temperature approximation,

$$\frac{\Delta n_I}{N_I} = \frac{\Delta E}{2k_B T} = \frac{\hbar \gamma_1 B_0}{2k_B T} \quad (2.5)$$

where N_I is the total number of nuclei, I , in the sample. Typically, $\Delta n_I / N_I$ is on the order of 10^{-5} .²³

2.1.4 Nuclear Magnetic Shielding and Chemical Shift

The nuclear magnetic shielding interaction, described by a second-rank tensor, σ , arises from the interaction of electrons around the nucleus with \mathbf{B}_0 to produce a local induced magnetic field at the nucleus, \mathbf{B}_{ind} :

$$\mathbf{B}_{\text{ind}} = \sigma \cdot \mathbf{B}_0 \quad (2.6)$$

The nuclear magnetic shielding Hamiltonian is:

$$\hbar^{-1} \mathcal{H}_{\text{CS}}(I) = \gamma_1 \mathbf{I} \cdot \sigma \cdot \mathbf{B}_0 \quad (2.7)$$

In general, σ can be expressed as the sum of symmetric and antisymmetric parts.^{3,24}

The symmetric tensor, which has components such that $\sigma_{ij} = \sigma_{ji}$, influences the line shape in NMR of solids, whereas the antisymmetric part does not to first order.^{2,3} In principle, the antisymmetric part can play a role in the relaxation of the nucleus.²⁵ In this thesis, the symbol σ refers exclusively to the symmetric part:

$$\sigma = \begin{bmatrix} \sigma_{xx} & \sigma_{xy} & \sigma_{xz} \\ \sigma_{xy} & \sigma_{yy} & \sigma_{yz} \\ \sigma_{xz} & \sigma_{xy} & \sigma_{zz} \end{bmatrix} \quad (2.8)$$

in which there are six independent components. It may be transformed, as with any symmetric second-rank tensor, to a frame of reference known as the principal axis system (PAS), in which the tensor is diagonal:

$$\sigma^{\text{PAS}} = \begin{bmatrix} \sigma_{11} & 0 & 0 \\ 0 & \sigma_{22} & 0 \\ 0 & 0 & \sigma_{33} \end{bmatrix} \quad (2.9)$$

where σ_{11} , σ_{22} , and σ_{33} are the principal components (in units of ppm) of the nuclear magnetic shielding tensor. The PAS is related to the molecular frame of reference by Euler angles, α , β , and γ .²⁶ There are still six parameters to determine (three principal components and three Euler angles) to fully characterize the tensor. In the solid state,

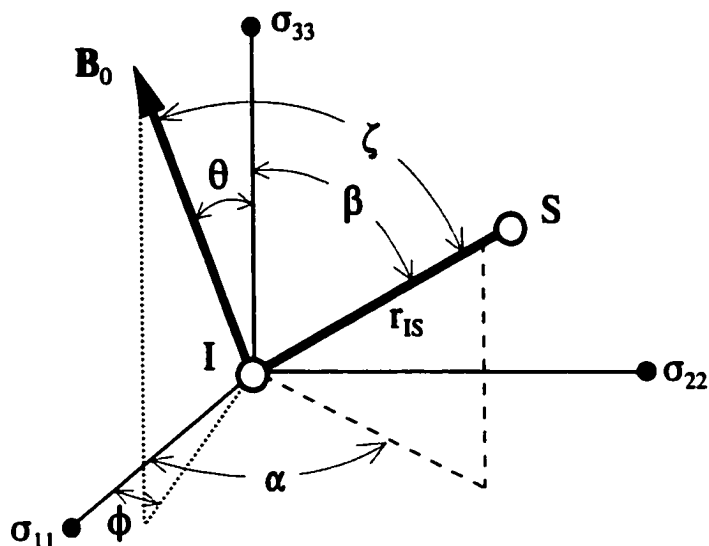


Figure 2.2 Illustration of the angles which define the orientation of the applied magnetic field, \mathbf{B}_0 , and the dipolar vector, \mathbf{r}_{IS} , with respect to each other and to the principal axis system of the nuclear magnetic shielding tensor for I .

the observed frequency is dependent on the orientation of the crystallite with respect to \mathbf{B}_0 if the shielding is anisotropic; thus equation 2.3 must be modified to include both the Zeeman and nuclear magnetic shielding interactions:

$$\nu(\theta, \phi) = \nu_0 \left[1 - (\sigma_{11} \sin^2 \theta \cos^2 \phi + \sigma_{22} \sin^2 \theta \sin^2 \phi + \sigma_{33} \cos^2 \theta) \right] \quad (2.10)$$

where θ and ϕ are polar angles defining the position of \mathbf{B}_0 in the PAS of the shielding tensor, as shown in figure 2.2.

By convention, $\sigma_{11} \leq \sigma_{22} \leq \sigma_{33}$, therefore σ_{33} corresponds to the direction of greatest shielding. Experimentally, the chemical shift tensor, $\hat{\delta}$, is measured rather than the nuclear shielding tensor, the difference being that σ is referenced to the bare nucleus while $\hat{\delta}$ is referenced to a primary standard:

$$\delta_{ii} = \frac{\nu_{ii} - \nu_{ref}}{\nu_{ref}} \times 10^6 \quad (\text{ppm}) \quad (2.11)$$

where ν_{ii} and ν_{ref} refer to the resonance frequencies of the sample and the reference respectively. The chemical shift and nuclear magnetic shielding are related as follows:

$$\delta_{ii} = \frac{\sigma_{ref} - \sigma_{ii}}{1 - \sigma_{ref}} \quad (\text{ppm}) \quad (2.12)$$

Since $1 - \sigma_{ref} \approx 1.0$, equation 2.12 simplifies to:

$$\delta_{ii} \approx \sigma_{ref} - \sigma_{ii} \quad (2.13)$$

The largest component of the chemical shift tensor, δ_{11} , corresponds to the smallest component of the nuclear magnetic shielding tensor, σ_{11} , in accordance with equation 2.13. Hence $\delta_{11} \geq \delta_{22} \geq \delta_{33}$. The isotropic nuclear magnetic shielding is $1/3$ the trace of σ :

$$\sigma_{\text{iso}} = \frac{\sigma_{11} + \sigma_{22} + \sigma_{33}}{3} \quad (2.14)$$

with an analogous expression for the isotropic chemical shift, δ_{iso} . One can also define two parameters, the span, Ω , and the skew, κ , which describe the breadth and shape of the powder pattern:²⁷

$$\text{span} = \Omega = \sigma_{33} - \sigma_{11} = \delta_{11} - \delta_{33} \quad (2.15)$$

$$\text{skew} = \kappa = \frac{3(\sigma_{\text{iso}} - \sigma_{22})}{\Omega} = \frac{3(\delta_{22} - \delta_{\text{iso}})}{\Omega} \quad (2.16)$$

Alternatively, the anisotropy and asymmetry are often used; however they have been defined in various ways by different authors.^{27,28} For a powder sample, in which all possible orientations of crystallites are present, the NMR spectrum of an isolated spin can have one of several line shapes as shown in figure 2.3, depending on the nature of the chemical shift tensor. In one case, $\delta_{11} = \delta_{22} = \delta_{33}$ (isotropic), in the second case $\delta_{11} = \delta_{22}$ or $\delta_{22} = \delta_{33}$ (axially symmetric) and in the third case none of the components are equivalent (non-axially symmetric).

2.1.5 Dipolar Coupling

Dipolar or direct spin-spin coupling is an interaction between nuclear magnetic moments separated by a vector \mathbf{r}_{IS} where the subscript indicates nuclei I and S respectively.^{29,30} This interaction is analogous to the classical interaction between two

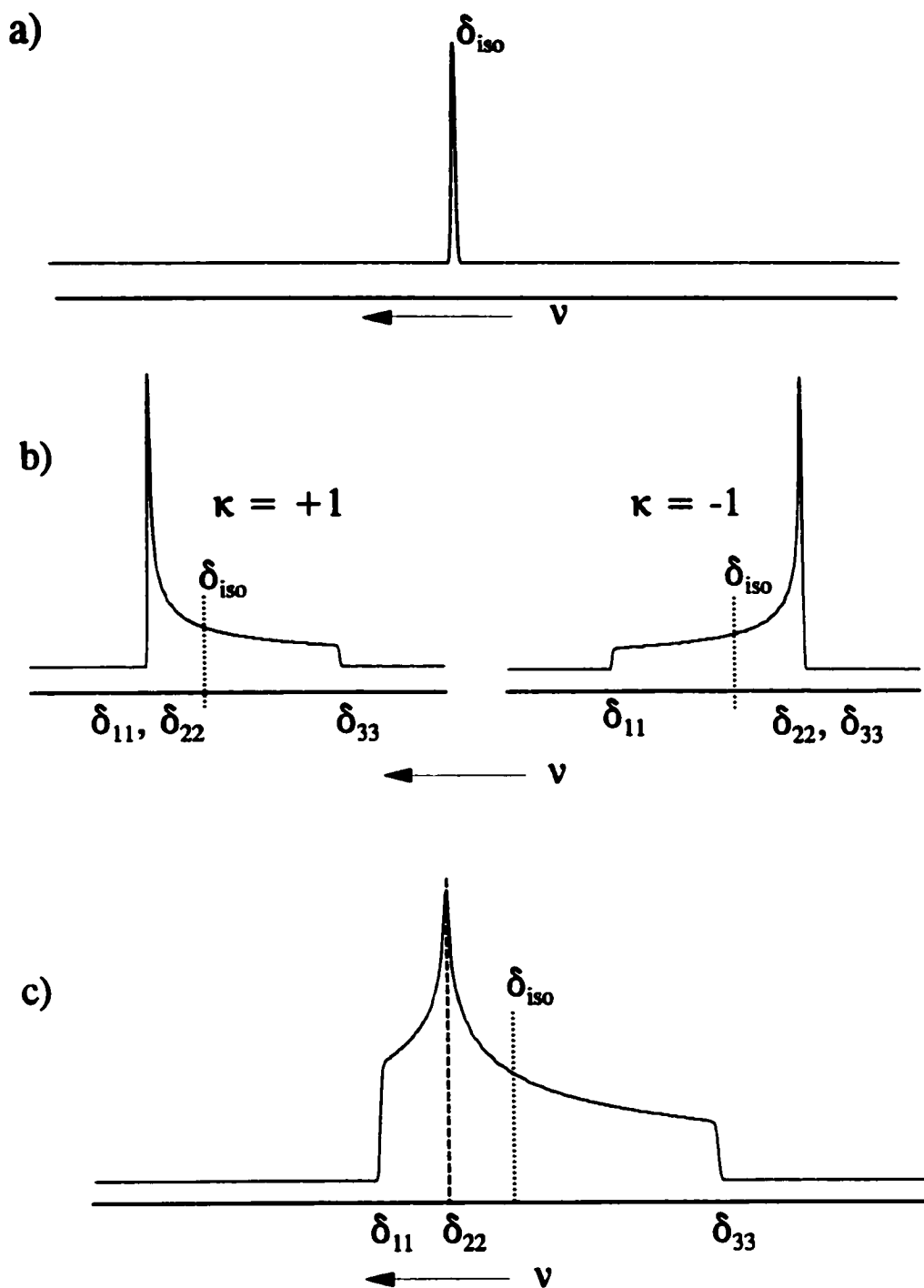


Figure 2.3 Typical line shapes for an isolated spin in a powder crystalline sample where a) all the principal components of the chemical shift tensor are equal, b) two components are equal and c) none of the components are the same. b) illustrates the difference between the two extreme values for κ , +1 and -1.

bar magnets.

The dipolar Hamiltonian is:

$$\hbar^{-1}\mathcal{H}_{DD}(I,S) = \mathbf{I} \cdot \mathbf{D} \cdot \mathbf{S} \quad (2.17)$$

where \mathbf{S} is the nuclear spin angular momentum operator for nucleus S and \mathbf{D} is the dipolar coupling tensor which is diagonal in its PAS:

$$\mathbf{D} = \begin{bmatrix} R_{DD} & 0 & 0 \\ 0 & R_{DD} & 0 \\ 0 & 0 & -2R_{DD} \end{bmatrix} \quad (2.18)$$

if I and S are not magnetically equivalent, e.g., a heteronuclear spin pair and:

$$\mathbf{D} = \begin{bmatrix} 3/2R_{DD} & 0 & 0 \\ 0 & 3/2R_{DD} & 0 \\ 0 & 0 & -3R_{DD} \end{bmatrix} \quad (2.19)$$

if I and S are magnetically equivalent, e.g., a homonuclear spin pair. Different types of homonuclear spin pairs are discussed in further detail in section 2.2. Unlike σ , \mathbf{D} is traceless; hence, dipolar interactions are not observed directly in NMR studies of isotropic fluids. The unique axis of \mathbf{D} is along \mathbf{r}_{IS} unless there is anisotropic motion.

The dipolar coupling constant, R_{DD} , in frequency units (Hz) is defined as follows:

$$R_{DD} = \frac{\mu_0}{4\pi} \left(\frac{\hbar}{2\pi} \right) \gamma_I \gamma_S \langle r_{IS}^{-3} \rangle \quad (2.20)$$

where μ_0 is the permeability of vacuum and $\langle r_{IS}^{-3} \rangle$ refers to the vibrational average of the cubed internuclear distance. Since R_{DD} depends only on $\langle r_{IS}^{-3} \rangle$, the remaining factors being constants, the dipolar coupling constant is a valuable parameter for structural determination by NMR of solids, as will be discussed in greater detail in section 2.1.6 and chapter 5. The spectrum for I coupled to a spin- $1/2$ nucleus, S , in the absence of any other interaction except the Zeeman interaction, consists of a doublet centred at the Larmor frequency of I with a splitting given by $R_{DD} (3 \cos^2 \zeta - 1)$ if I and S are not magnetically equivalent (figure 2.4(a)) and by $1/2 R_{DD} (3 \cos^2 \zeta - 1)$ if I and S are magnetically equivalent (figure 2.4(b)), where ζ is the angle between \mathbf{B}_0 and \mathbf{r}_{IS} . In a powdered crystalline sample, all possible values of ζ are present, hence a characteristic powder pattern with a Pake doublet³¹ is observed. Figure 2.4(c) shows the Pake doublet for a heteronuclear spin pair while the spectrum arising from a pair of magnetically equivalent nuclei is shown in figure 2.4(d). The two subspectra, shown by dotted lines, illustrate the fact that the dipolar line shape arises from two transitions corresponding to the two spin states of S .

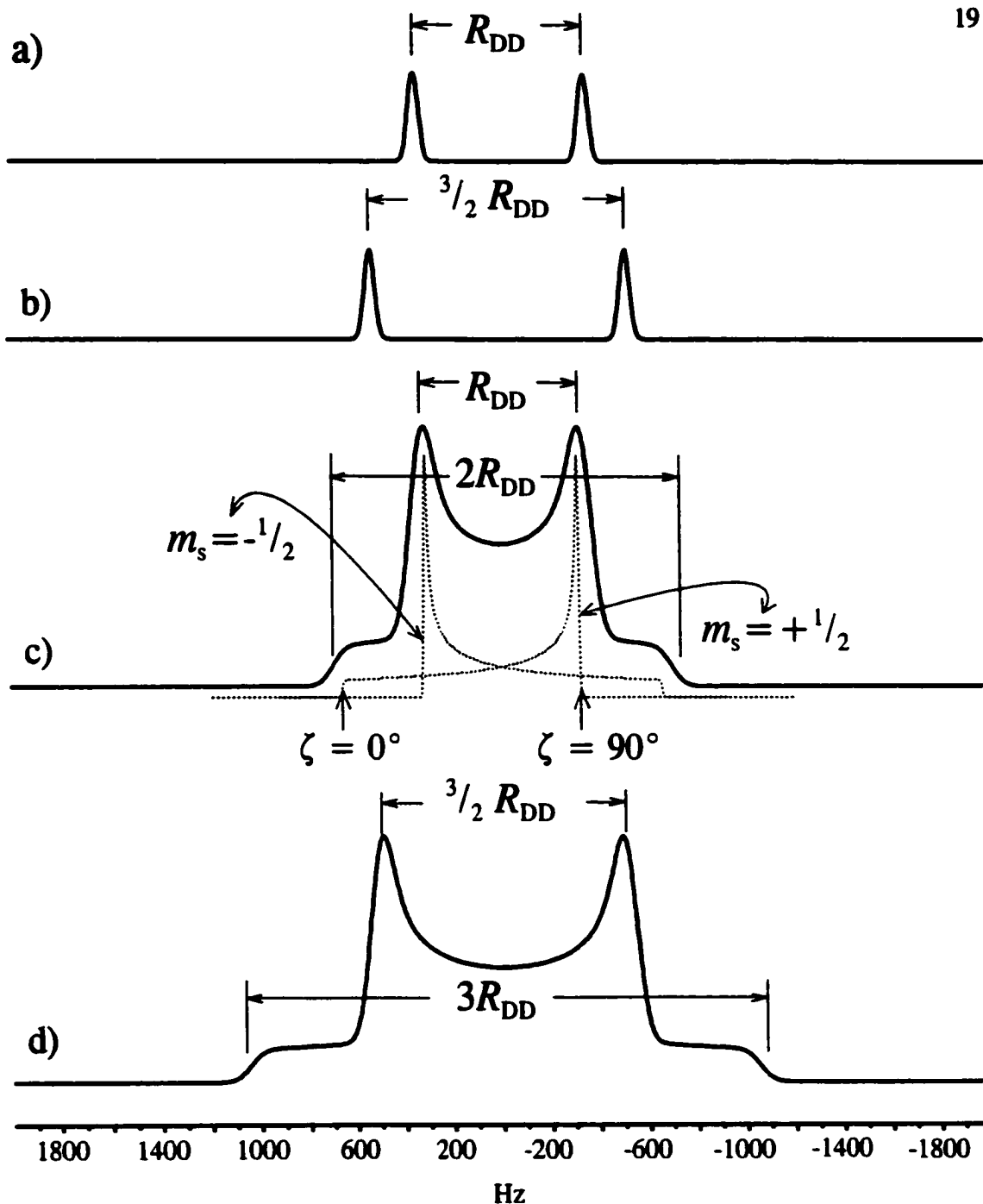


Figure 2.4 Calculated NMR spectra for the I nucleus of a spin pair where I and S are a) not magnetically equivalent and b) where they are magnetically equivalent. B_0 and r_{IS} are perpendicular in this case, i.e., $\zeta = 90^\circ$. The corresponding line shapes for powder crystalline sample, where all values of ζ are present, are shown in c) for nonmagnetically equivalence and d) for magnetic equivalence. The subspectra shown by dotted lines in c) correspond to the two spin states of S . These spectra were calculated using $R_{DD} = 700$ Hz.

2.1.6 *J* Coupling

Another interaction between two nuclei that may be measured in NMR experiments is the indirect spin-spin or *J*-coupling interaction. This is an interaction whereby a nucleus perturbs the surrounding electrons. This perturbation is subsequently transmitted to a second nucleus through the electron network of the molecule. The strength of the coupling depends on the nature of the electron network, hence *J* coupling is an extremely useful parameter for characterizing systems where nuclei are separated by one or more covalent bonds.³² The Hamiltonian for *J* coupling between two nuclei is:^{29,30}

$$\hbar^{-1}\mathcal{H}_J(I,S) = \mathbf{I} \cdot \mathbf{J} \cdot \mathbf{S} \quad (2.21)$$

where \mathbf{J} is a second-rank tensor. Like the nuclear magnetic shielding tensor, \mathbf{J} can be represented by a symmetric and antisymmetric part,³ however the antisymmetric part does not perturb the NMR line shape to first order.³³ In its PAS, the symmetric part of \mathbf{J} is given by:

$$\mathbf{J} = \begin{bmatrix} J_{11} & 0 & 0 \\ 0 & J_{22} & 0 \\ 0 & 0 & J_{33} \end{bmatrix} \quad (2.22)$$

The isotropic J coupling is:

$$J_{\text{iso}} = \frac{J_{11} + J_{22} + J_{33}}{3} \quad (2.23)$$

While J coupling is measured experimentally in units of Hz, comparison of indirect spin-spin couplings for different spin pairs is facilitated by using the reduced coupling tensor, \mathbf{K} , which is independent of the magnetogyric ratios of the coupled nuclei:

$$\mathbf{K} = \frac{4\pi^2}{h\gamma_1\gamma_s} \mathbf{J} \quad (2.24)$$

where \mathbf{K} is in units of $\text{N A}^{-2} \text{m}^{-3}$ or equivalently in $\text{T}^2 \text{J}^{-1}$.³⁴ The ensuing definitions also apply to \mathbf{K} .

The features of \mathbf{J} may be described by the anisotropy, ΔJ , and the asymmetry, η :^{29,35,36}

$$\Delta J = J_{33} - \frac{J_{11} + J_{22}}{2} \quad (2.25)$$

and

$$\eta = \frac{J_{22} - J_{11}}{J_{33} - J_{\text{iso}}} \quad (2.26)$$

where the principal components are assigned according to $|J_{33} - J_{\text{iso}}| \geq |J_{11} - J_{\text{iso}}| \geq$

$|J_{22} - J_{\text{iso}}|$. If \mathbf{J} is axially symmetric, then $\Delta J = J_{\parallel} - J_{\perp}$ where J_{\parallel} is the component along the internuclear axis while J_{\perp} is perpendicular to it. The indirect spin-spin coupling Hamiltonian (equation (2.21)) can be expressed in terms involving only J_{iso} and an anisotropic term which is identical in form to the dipolar Hamiltonian (equation 2.17):^{29,32}

$$\hbar^{-1} \mathcal{H}_J(I, S) = J_{\text{iso}}(I, S) \mathbf{I} \cdot \mathbf{S} + \mathbf{I} \cdot \mathbf{J}' \cdot \mathbf{S} \quad (2.27)$$

where

$$\mathbf{J}' = \begin{bmatrix} -\Delta J/3 & 0 & 0 \\ 0 & -\Delta J/3 & 0 \\ 0 & 0 & 2\Delta J/3 \end{bmatrix} \quad (2.28)$$

Consequently, it is impossible to experimentally distinguish between the dipolar coupling and anisotropy in \mathbf{J} . Experimentally, one measures an effective dipolar coupling constant:

$$R_{\text{eff}} = R_{\text{DD}} - \frac{\Delta J}{3} \quad (2.29)$$

In practice, R_{DD} can be calculated from equation 2.20 if the internuclear distance is known. If R_{DD} differs significantly from the experimental value of R_{eff} , then one can estimate ΔJ . R_{eff} is available from solid-state NMR experiments or, for simple diatomic

molecules, from hyperfine constants measured in molecular beam or high-resolution microwave spectroscopy experiments.³⁷ Since R_{eff} and R_{DD} can have the same or opposite signs, two possible values of ΔJ result from equation 2.29, one of which is usually discarded since it is much larger than J_{iso} . For coupling involving lighter nuclei, ΔJ is often assumed to be negligible; for heavier nuclei, ΔJ can be quite large.^{33,35} For example, in thallium fluoride, $\Delta J(^{205}\text{Tl}, ^{19}\text{F}) = -13.3 \pm 0.7 \text{ kHz}$.³⁸ While reliable experimental determinations of ΔJ are scarce,^{10,37,39,40,41,42} theoretical calculations of J offer an avenue for examining the relationship between indirect spin-spin coupling and structure. Calculations of J from first principles will be discussed in section 2.3.2.

2.2 NMR Spectra Arising from Isolated Spin Pairs

2.2.1 Overview

For a system consisting of an isolated spin where the chemical shift is the only internal interaction present, analysis of NMR spectra arising from single crystals can, in principle, yield the orientation of the chemical shift tensor with respect to the molecule. Unfortunately, single crystals of sufficient size for NMR studies are rarely available. NMR spectra of powder samples yield the three principal components of the chemical shift tensor; however there is no means of determining the tensor orientation relative to the molecular frame of reference unless the chemical shift tensor is axially symmetric. If a dipolar interaction is also present, as in the case of systems containing isolated spin pairs, then the spectra of powder samples become sensitive to the relative orientation of the chemical shift tensors with respect to r_{IS} which of course is in the molecular frame

of reference.⁴³

Systems where an isolated spin pair is present have been extensively investigated in the solid state.^{43,44} As mentioned previously, if two nuclei have the same magnetogyric ratio, the system is referred to as a homonuclear spin pair; otherwise they form a heteronuclear spin pair. For a homonuclear spin pair, a further distinction can be made between magnetic equivalence where the two nuclei are related by a centre of inversion and crystallographic equivalence where the two nuclei are related typically by a C_2 axis or a mirror plane.² In the case of magnetic equivalence, the two spins have identical chemical shift tensor components and orientations. For nuclei that are crystallographically equivalent but magnetically non-equivalent, the chemical shift tensor components are the same but their orientations differ. The most general case is observed when the two nuclei are neither magnetically nor crystallographically equivalent. Spin pairs are often classified as A_2 , AB, or AX spin systems. If the two nuclei are magnetically equivalent, they have identical resonance frequencies for any orientation of the spin pair in B_0 , hence they form an A_2 spin system. On the other hand, if the difference between their resonance frequencies is much greater than the magnitude of the spin-spin couplings (dipolar and indirect), then the spin system is designated as an AX spin system. The AB spin system lies between these two extremes. It should be noted that such a labelling system is not entirely suitable in solid-state NMR since the difference in the resonance frequencies as well as the magnitudes of the spin-spin couplings are orientation dependent. It is possible to have a spin pair that is A_2 at one crystallite orientation but AB or AX at another.

In general, homonuclear spin pairs give rise to four transitions in the solid state with intensities, P_i :^{10,44,45,46,47}

$$\nu_1 = \frac{1}{2} (\nu_I + \nu_S - A - D) \quad P_1 = 1 - \frac{B}{D} \quad (2.30)$$

$$\nu_2 = \frac{1}{2} (\nu_I + \nu_S + A - D) \quad P_2 = 1 + \frac{B}{D} \quad (2.31)$$

$$\nu_3 = \frac{1}{2} (\nu_I + \nu_S - A + D) \quad P_3 = 1 + \frac{B}{D} \quad (2.32)$$

$$\nu_4 = \frac{1}{2} (\nu_I + \nu_S + A + D) \quad P_4 = 1 - \frac{B}{D} \quad (2.33)$$

where ν_I and ν_S depend on ν_0 , σ_{11} , σ_{22} , and σ_{33} , and the orientation of PAS of the shielding tensor with respect to \mathbf{B}_0 , given by the polar angles θ and ϕ (figure 2.2), for each nucleus, according to equation 2.10. The terms A , B , and D are:

$$A = J_{\text{iso}} - R_{\text{eff}} (3 \cos^2 \zeta - 1) \quad (2.34)$$

$$B = J_{\text{iso}} + \frac{1}{2} R_{\text{eff}} (3 \cos^2 \zeta - 1) \quad (2.35)$$

$$D = [(\nu_I - \nu_S)^2 + B^2]^{\frac{1}{2}} \quad (2.36)$$

For an AX spin system, $(\nu_I - \nu_S) > B$; hence, $D = \nu_I - \nu_S$. Four peaks are observed, two

in the region of the I nucleus and two in the region of the S nucleus. In both cases, the splitting of the I and S peaks is $|J_{\text{iso}} - R_{\text{eff}}(3 \cos^2 \zeta - 1)|$. For an A_2 spin system, $\nu_I = \nu_S$, hence $D = B$, thus the intensities of ν_1 and ν_4 are zero and the remaining two peaks are split by $|J_{\text{iso}} - 3/2 R_{\text{eff}}(3 \cos^2 \zeta - 1)|$. An interesting situation arises in NMR spectra of solids containing isolated AB spin systems. It is possible for the two outer peaks to be more intense than the two inner peaks.⁴⁶ An example of this is presented in chapter 3. Such spectra are not observed for isotropic fluids. For a powder crystalline sample, the addition of J coupling modifies the splittings shown in figure 2.4, as illustrated in figure 2.5. The observed line shape is dependent on the relative signs of R_{eff} and J_{iso} .

2.2.2 The Dipolar-Chemical Shift Method

The combination of anisotropic chemical shift and dipolar coupling interactions results in a spectrum where each component of the chemical shift tensor is split according to (in units of frequency):⁴⁸

$$\Delta\nu_{11} = R_{\text{eff}} (1 - 3 \cos^2 \alpha \sin^2 \beta) \quad (2.37)$$

$$\Delta\nu_{22} = R_{\text{eff}} (1 - 3 \sin^2 \alpha \sin^2 \beta) \quad (2.38)$$

$$\Delta\nu_{33} = R_{\text{eff}} (1 - 3 \cos^2 \beta) \quad (2.39)$$

for an AX spin pair, where α and β are the polar angles defining the position of \mathbf{r}_{IS} with respect to the PAS of σ in figure 2.2. The expected line shape is illustrated in figure 2.6(a). Although one cannot measure the sign of $\Delta\nu_{ii}$, the sum of the three splittings

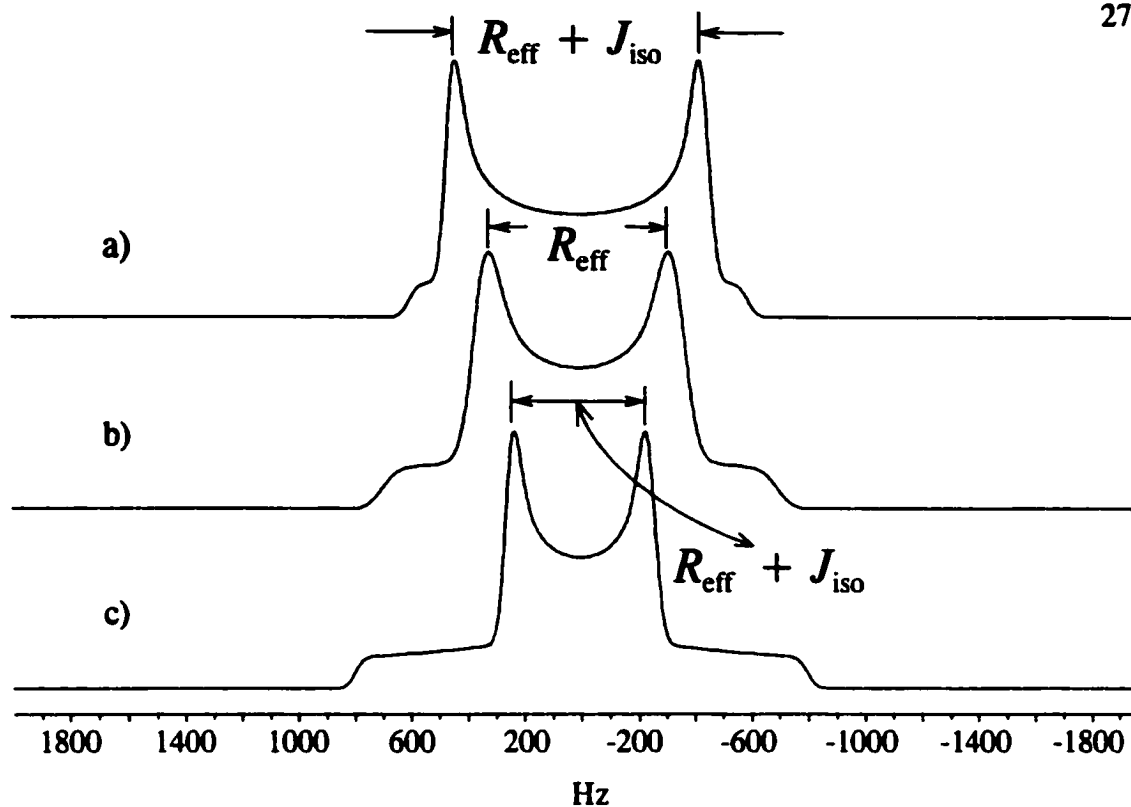


Figure 2.5 Calculated NMR spectra for the A nucleus of an AX spin pair illustrating the effect of dipolar and J coupling. For a) $J_{\text{iso}} = +200$ Hz, while $J_{\text{iso}} = 0$ Hz for b). $J_{\text{iso}} = -200$ Hz for c). All spectra were calculated using $R_{\text{eff}} = 700$ Hz and in the absence of anisotropic magnetic shielding.

must be zero since the dipolar coupling tensor is traceless. One of the subspectra shown in figure 2.4(c) is stretched out while the other is compressed, as shown in figures 2.6(b) and (c). For an AB spin system, the overlap of the subspectra due to both nuclei leads to complex line shapes, examples of which will be discussed in this thesis.

As is evident from equations 2.37 to 2.39, the spectrum is sensitive to the relative orientation of the chemical shift tensor and \mathbf{r}_{IS} , which is coincident with the unique component of the dipolar coupling tensor. Thus some information regarding the

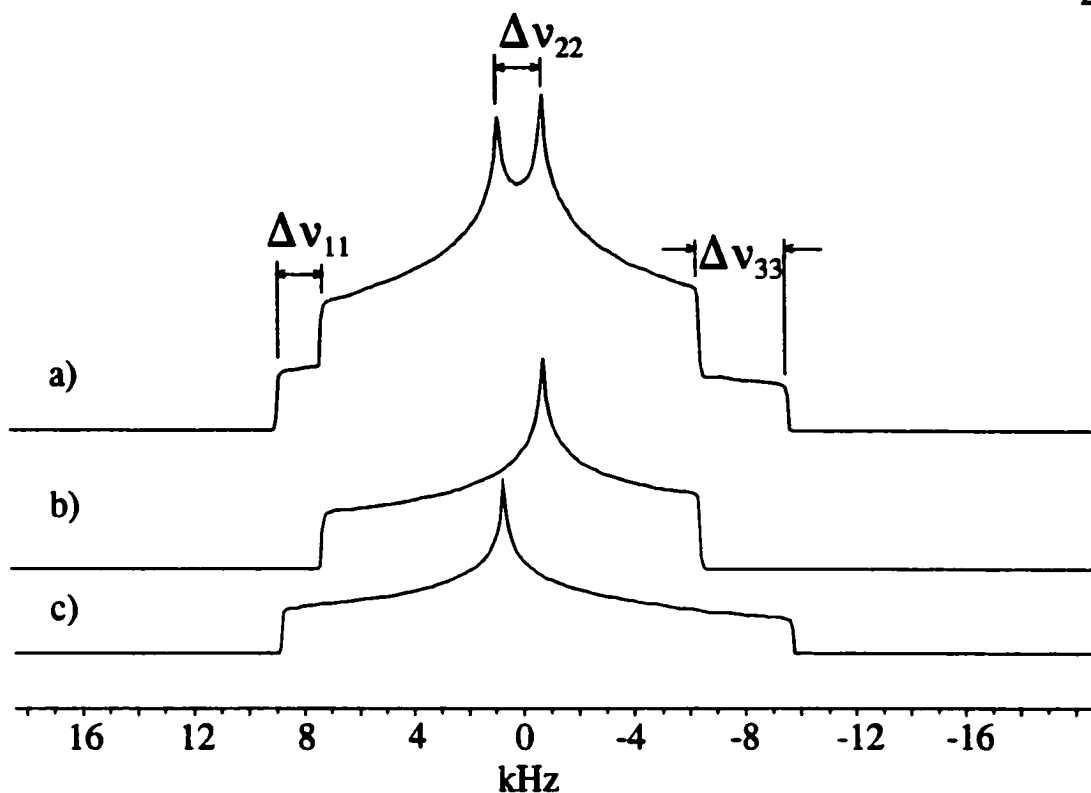


Figure 2.6 Calculated NMR spectrum for the A nucleus of an AX spin pair illustrating the effect of dipolar coupling and anisotropic nuclear magnetic shielding on the line shape. The total line shape (a) is the sum of the two subspectra, (b) and (c). For this simulation, $\nu_0 = 81.033$ MHz, $R_{\text{eff}} = 1.6$ kHz, $\Omega = 200$ ppm, $\kappa = 0.0$ and r_{IS} is coincident with σ_{33} (i.e., $\alpha = \beta = 0^\circ$).

chemical shift tensor orientation in the molecular frame of reference is available. This method of relating the chemical shift tensor to the dipolar coupling is termed the dipolar-chemical shift method for characterizing chemical shift tensors. However, since the dipolar tensor is axially symmetric, there will be an ambiguity as to the orientation of the shift tensors with respect to rotation about r_{IS} . The orientation of each shift

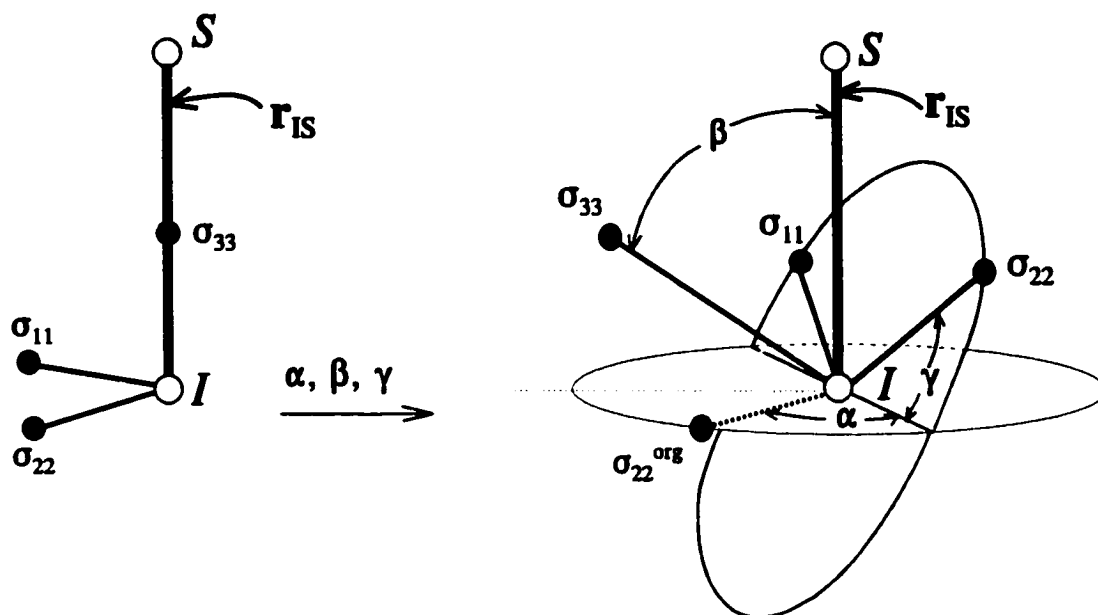


Figure 2.7 Euler angles relating the PAS of the nuclear magnetic shielding tensor to the molecular frame of reference for nucleus I of a spin pair, IS , where σ_{22}^{org} is the original position of σ_{22} .

tensor relative to r_{IS} can be described by a set of Euler angles, α , β , and γ ,²⁶ as illustrated in figure 2.7. The angle β positions r_{IS} relative to σ_{33} while γ determines whether r_{IS} is closer to σ_{11} or σ_{22} . The angle α describes the rotation of the chemical shift tensors about r_{IS} ; since the dipolar tensor is axially symmetric, α cannot be measured relative to an axis fixed in the molecular frame of reference, hence its value is arbitrary. However, the difference between the values of α for the two chemical shift tensors (which will be denoted by $\Delta\alpha$ in this thesis) may be determined. $\Delta\alpha$ defines the angle between the projections of the σ_{33} components for I and S on to the same plane. It

should be noted that the angles above are different from those defined in figure 2.2.

The analysis of spectra dependent on as many as six chemical shift tensor components, two sets of Euler angles and two spin-spin coupling parameters may seem difficult if not impossible; however, computer programs^{49,50,51} are available for calculating spectra based on the Hamiltonian presented in section 2.1, allowing a comparison with the experimental results. The dipolar coupling constant, R_{DD} , can be estimated using bond lengths from diffraction structures if available. From magic angle spinning (MAS) NMR spectra, J_{iso} , δ_{iso} , and, in some cases, the principal components of δ^{52} for I and S may be determined. As well, techniques like 2D spin-echo spectroscopy are available for homonuclear spin pairs to separate the effect of dipolar and J coupling from the chemical shift interaction (see section 2.2.3). Acquiring spectra at two or more applied magnetic fields is essential as the various spin interactions described in section 2.1 scale differently with B_0 . In practice, all the NMR spectra are simulated until one obtains a set of NMR parameters which gives a satisfactory reproduction of all experimental spectra. In addition, reliable *ab initio* calculations can provide information concerning the orientations of chemical shift tensors and spin-spin coupling tensors with respect to the molecular frame of reference. *Ab initio* calculations of these two NMR parameters are discussed in section 2.3.

2.2.3 2D Spin-Echo NMR Spectroscopy

The 2D spin-echo NMR experiment is extremely useful in the characterization of spin-spin coupling parameters in systems consisting of isolated homonuclear spin pairs.

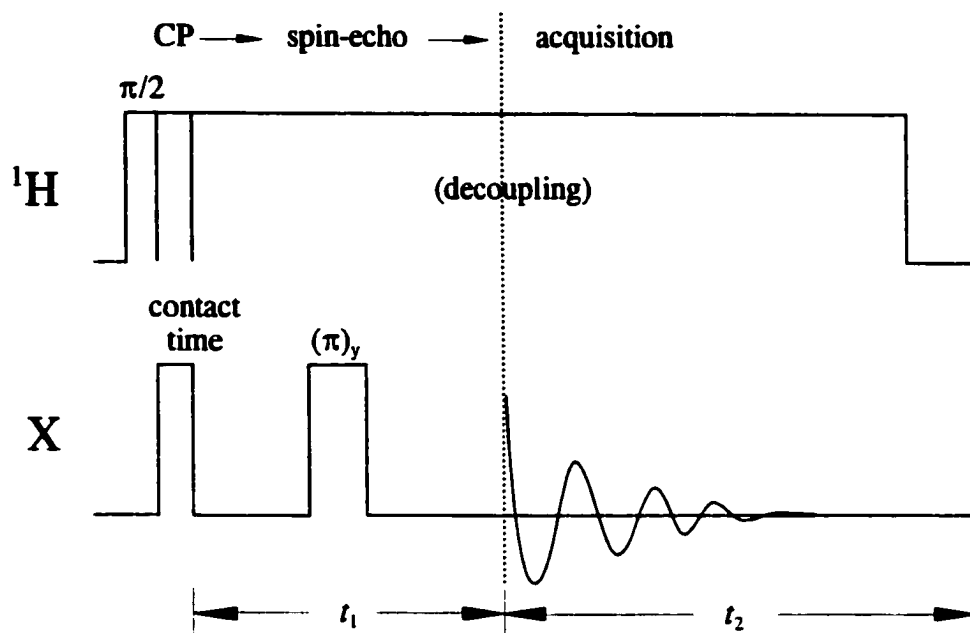


Figure 2.8 The 2D spin-echo pulse sequence which consists of a CP sequence followed by a spin-echo pulse and then the acquisition of an FID.

The spin-spin coupling interactions are separated from the chemical shift, allowing for an independent measurement of R_{eff} and determination of the relative signs of R_{eff} and J_{iso} . The basic 2D pulse sequence consists of a preparation period, an evolution time of duration t_1 followed by an acquisition time, t_2 .⁵³ The evolution time is incremented to produce a 2D data set. The 2D spin-echo pulse sequence,¹³ shown in figure 2.8, consists of the standard cross polarization⁵⁴ (CP) experiment, under the Hartmann-Hahn match condition,⁵⁵ for the preparation period followed by the evolution time during which the π spin-echo pulse is applied. The spin-echo pulse has the effect of refocusing inhomogeneities due to nuclear magnetic shielding, leaving the magnetization to evolve

exclusively under the influence of spin-spin coupling. In the resulting 2D spectrum, the *F1* projection contains the spin-spin coupling data while the *F2* projection is the normal 1D powder pattern of a stationary sample. Nakai and McDowell^{13,56} have derived expressions for the free induction decays (FIDs), $s(t_1)$ and $s(t_2)$, of the 2D spin-echo NMR experiment:

$$\begin{aligned}
 s(t_1) = & \cos^2 2\xi [\exp(i\pi A t_1) + \exp(-i\pi A t_1)] \\
 & + \frac{1}{2} \sin 2\xi (1 + \sin 2\xi) [\exp(i\pi(D-A)t_1) + \exp(-i\pi(D-A)t_1)] \\
 & - \frac{1}{2} \sin 2\xi (1 - \sin 2\xi) [\exp(i\pi(D+A)t_1) + \exp(-i\pi(D+A)t_1)]
 \end{aligned} \quad (2.40)$$

$$\begin{aligned}
 s(t_2) = & (1 - \sin 2\xi) \exp(i2\pi v_1 t_2) + (1 + \sin 2\xi) \exp(i2\pi v_2 t_2) \\
 & + (1 + \sin 2\xi) \exp(i2\pi v_3 t_2) + (1 - \sin 2\xi) \exp(i2\pi v_4 t_2)
 \end{aligned} \quad (2.41)$$

where $\cos 2\xi = (v_1 - v_5)/D$, $\sin 2\xi = B/D$ and the v_i s ($i = 1$ to 4) are given by equations 2.30 to 2.33. For an A_2 or AX spin system in the absence of J coupling, the dipolar splittings at the ‘horns’ of the Pake doublet in the *F1* projection will be $^{3/2} R_{\text{eff}}$ or R_{eff} respectively; however, the analysis of 2D spin-echo spectra is complicated by the possibility of the spin system being A_2 , AB or AX at different orientations, as mentioned previously (section 2.2.1). If J_{iso} is also present then the splitting in the *F1* projection is modified, similar to the case illustrated in figure 2.5. A centre artifact is often observed which has been attributed to imperfect rf pulses.¹³ Fortunately, the *F1* projection can still be calculated and compared to the experimental results to extract the coupling constants. Two-dimensional spin-echo spectroscopy has been used extensively

to investigate homonuclear spin pairs in the solid, especially in molecules containing P-P bonds, for example, Mes*P=PMes* (Mes* =(2,4,6-tri-*t*-butyl) phenyl),¹⁷ [Mes*NP-PPh₃][SO₃CF₃],⁵⁷ Ph₂PPPh₂,¹³ the pyrophosphate anion in Na₄P₂O₇·10H₂O,^{13,58} and Lawesson's reagent, (C₆H₄OCH₃PS₂)₂.⁵⁹ Specific details regarding performance of this experiment on the CMX Infinity 200 spectrometer at the University of Alberta are given in Appendix 1.

2.3 Ab Initio Calculations of NMR Parameters

2.3.1 Nuclear Magnetic Shielding Tensors

The theoretical basis for understanding nuclear magnetic properties in terms of modern quantum chemistry was established by Ramsey in a series of papers published between 1950 and 1953.^{60,61,62} A commentary on the significance of these papers was published in 2000.⁶³ In this section, Ramsey's formulation for nuclear magnetic shielding and modern approaches to the calculation of this parameter will be discussed.

Ramsey's perturbation approach separates nuclear magnetic shielding into a diamagnetic, σ^d , and paramagnetic, σ^p , contribution:⁶⁰

$$\sigma = \sigma^d + \sigma^p \quad (2.42)$$

This partitioning is analogous to the separation of magnetic susceptibility into diamagnetic and paramagnetic parts.⁶⁴ For shielding, the full expressions for σ^d and σ^p are:^{60,65}

$$\sigma^d = \frac{\mu_0}{4\pi} \frac{e^2}{2m_e^2} \langle 0 | \sum_{k=0} r_{kN}^{-3} (\mathbf{r}_k \cdot \mathbf{r}_{kN} \mathbf{1} - \mathbf{r}_k \mathbf{r}_{kN}) | 0 \rangle \quad (2.43)$$

$$\sigma^p = \frac{\mu_0}{4\pi} \frac{e^2}{2m_e^2} \sum_{n \neq 0} \frac{\langle 0 | \sum_k r_{kN}^{-3} \mathbf{L}_{kN} | n \rangle \langle n | \sum_k \mathbf{L}_k | 0 \rangle + \langle 0 | \sum_k \mathbf{L}_k | n \rangle \langle n | \sum_k r_{kN}^{-3} \mathbf{L}_{kN} | 0 \rangle}{E_n - E_0} \quad (2.44)$$

where \mathbf{r}_k is the position vector for electron k and \mathbf{L}_k is its angular momentum operator, both with respect to a chosen origin. The position vector and angular momentum operator of electron k with respect to the nucleus of interest are denoted by \mathbf{r}_{kN} and \mathbf{L}_{kN} respectively. One important conclusion from the above equations is that σ^d depends only on the ground electronic state, $|0\rangle$, hence it is a first-order property and easily calculated by *ab initio* methods. However, σ^p is a second-order property, involving mixing between ground and excited electronic states, $|n\rangle$, and is thus more challenging to calculate.

Nuclear magnetic shielding is very sensitive to the molecular electronic structure, hence very accurate electronic wavefunctions are required for *ab initio* calculations at any level of theory.^{6,7,8,9,66} The development and implementation of methods to overcome the gauge origin problem (*vide infra*) has led to further progress in calculations of shielding tensors. *Ab initio* calculation of nuclear magnetic shielding tensors may be useful to resolve the ambiguity involved in assigning tensor orientations obtained from a dipolar-chemical shift analysis (section 2.2.2).^{20,67,68} The present status of theoretical methods has been summarized in a number of recent reviews^{6,7,8,9,66,69} and

will be discussed only briefly in this thesis.

Rather than using Ramsey's formulation for nuclear magnetic shielding directly, most modern *ab initio* computational approaches use an equivalent expression for the shielding for I in terms of a second derivative of the total electronic energy, E , which is dependent on a magnetic field, \mathbf{B} , and the set of all nuclear magnetic moments, \mathbf{M} , for a molecule:⁸

$$\sigma = \left[\frac{\partial^2 E(\mathbf{B}, \mathbf{M})}{\partial \mathbf{M}_I \partial \mathbf{B}} \right]_{\mathbf{M}, \mathbf{B} = 0} \quad (2.45)$$

where \mathbf{M}_I is the nuclear magnetic moment of I . The calculation of σ thus reduces to evaluating derivatives of molecular electronic energies. Methods in which the derivatives are evaluated numerically are termed finite perturbation (FP) or finite field (FF). In general, though, quantum chemical programs evaluate the derivatives analytically, which is more computationally efficient than numerical analysis. In an analytical evaluation, it is necessary to determine how the wavefunction responds to the perturbation arising from the presence of \mathbf{B} and/or \mathbf{M} . Below, equation 2.45 is stated more explicitly to show the dependence on the wavefunction:

$$\sigma = 1 + \left[\frac{\partial^2 E(\mathbf{B}, \mathbf{M})}{\partial \mathbf{M}_I \partial \mathbf{B}} \right]_{\mathbf{M}, \mathbf{B} = 0} + \left[\frac{\partial^2 E(\mathbf{B}, \mathbf{M})}{\partial \mathbf{M}_I \partial \lambda} \right]_{\mathbf{M}, \mathbf{B} = 0} \frac{\partial \lambda}{\partial \mathbf{B}} \quad (2.46)$$

where λ is the set of parameters that define the wavefunction. For a given molecule, it is necessary to determine the response of the wavefunction with respect to the magnetic

field, via the factor $\partial\lambda/\partial\mathbf{B}$, to calculate the shielding for all the nuclei.

With the introduction of a magnetic field, a problem arises due to the need to describe \mathbf{B} using a vector potential.^{60d,70,71,72} It was recognized early on that calculated nuclear magnetic shielding varied depending on where one placed the origin of the vector potential, termed the gauge origin problem. While the choice of gauge does not affect the results of an exact quantum mechanical treatment, this type of calculation is generally impractical; hence, the gauge origin will be a factor in the quality of the results when one uses approximate wavefunctions constructed from standard basis sets included in quantum chemistry programs. Several methods are used to overcome this difficulty, including GIAO⁷³ and IGLO.⁷⁴ The GIAO (gauge-including atomic orbitals) method places the gauge origin for the atomic orbitals at the nucleus on which the orbitals are centred. The GIAOs are also referred to as London orbitals.⁸ The IGLO (individual gauge for localized orbitals) method uses the origin of the molecular orbital as the gauge origin. Other methods include LORG (localized orbital local origin method)⁷⁵ and CSGT (continuous set of gauge transformations method).⁷⁶

The Hartree-Fock (HF) approach, a common model for shielding calculations, describes the electronic wavefunction by a single electronic configuration and the influence of the other electrons is introduced as an effective, static field. This approximation obviously does not account for the effect arising from the motion of electrons. Electron correlation is the term used to describe the difference between the HF model and an exact description of the system. The neglect of electron correlation can cause severe errors in the calculated nuclear magnetic shielding for systems with

multiple bonds or formal lone pairs.^{6,8,9,66} *Ab initio* methods which allow for electron correlation, such as Møller-Plesset (MP) perturbation theory⁷⁷ or multiconfigurational self-consistent field (MCSCF) theory,^{78,79} often give better results than HF in such situations.⁸ Although not strictly an *ab initio* method, density functional theory (DFT) has also been applied to the calculation of nuclear magnetic shielding.^{80,81} Recently, relativistic effects have been considered in conjunction with DFT.⁸² While the Gaussian suite of programs^{83,84} includes DFT methods, the currently available functionals do not include a dependence on the magnetic field, hence it is not an improvement on HF methods in this case.⁸⁵

To assess the quality of an *ab initio* calculation of nuclear magnetic shielding, it is necessary to compare calculated results with experiment. However, it is the chemical shift, δ , and not the nuclear magnetic shielding, σ , which is measured experimentally. Conversion from one scale to the other requires an absolute shielding scale.⁸⁶ If the shielding for the nucleus of interest is known for a reference compound, then measurement of the chemical shift relative to this compound can be converted to shielding according to equation 2.13. Absolute shielding scales have been established for a number of elements, including carbon,⁸⁷ oxygen,⁸⁸ fluorine,⁸⁹ and phosphorus.⁹⁰ Recently, we proposed a revised absolute shielding scale for chlorine.⁹¹

With advances in computational techniques and faster computers, the quality of the calculations is certain to improve. Significant progress has been made in the last few years and *ab initio* calculations of nuclear magnetic shielding are becoming integrated into the methodology for analyzing NMR spectra.^{92,93,94}

2.3.2 Indirect Spin-Spin Coupling (J) Tensors

For reasons outlined below, reliable *ab initio* calculations of J coupling are challenging. Thus, reports have been relatively scarce compared to calculations of nuclear magnetic shielding tensors. However, the introduction of some new computational approaches has prompted interest in the *ab initio* calculation of J . In addition, the recent observation of J coupling across hydrogen bonds⁹⁵ has resulted in a number of papers focussing on the calculation of J coupling in such systems.^{96,97,98} The current state of J -coupling calculations has been recently reviewed.^{8,99}

In Ramsey's theory of J coupling,^{61,62,100} several mechanisms for the interaction between the nuclei and electrons are identified. One mechanism involves the coupling between the nuclear spin and the orbital motions of the electron, termed the *spin-orbit* (SO) mechanism. A formal distinction is usually made between a diamagnetic (DSO) and paramagnetic (PSO) contribution. Another mechanism is the dipolar interaction between the nuclear and electron magnetic moments, called the *spin-dipolar* (SD) mechanism. The *Fermi contact* (FC) mechanism describes the interaction between a nucleus and electrons that have a finite probability of being at the nucleus of interest.

The J -coupling Hamiltonian may be expressed in terms of a contribution from each mechanism:

$$\mathcal{H}_J = \mathcal{H}_{\text{DSO}} + \mathcal{H}_{\text{PSO}} + \mathcal{H}_{\text{SD}} + \mathcal{H}_{\text{FC}} \quad (2.47)$$

Second-order perturbation theory is used to solve the above Hamiltonian for expressions

describing each contribution to \mathbf{J} :

$$\mathbf{J} = \mathbf{J}_{\text{DSO}} + \mathbf{J}_{\text{PSO-PSO}} + \mathbf{J}_{\text{SD-SD}} + \mathbf{J}_{\text{FC-FC}} + \mathbf{J}_{\text{FC-SD}} \quad (2.48)$$

where \mathbf{J}_{DSO} involves only the ground electronic states of the molecule. $\mathbf{J}_{\text{PSO-PSO}}$ has contributions involving ground and excited singlet electronic states, while the contributions involving SD and FC ($\mathbf{J}_{\text{SD-SD}}$, $\mathbf{J}_{\text{FC-FC}}$, and $\mathbf{J}_{\text{FC-SD}}$) depend on ground and excited triplet states. The full expressions for each term are given elsewhere.^{32,101} It is important to note that $\mathbf{J}_{\text{FC-FC}}$ is completely isotropic; hence, it contributes only to J_{iso} . The FC-SD cross term, $\mathbf{J}_{\text{FC-SD}}$, is completely anisotropic; hence, it contributes only to ΔJ . Ramsey's formalism for J coupling does not account for relativistic effects. An extension of Ramsey's theory to include relativistic effects was developed by Pyykkö.¹⁰²

As with calculations of nuclear magnetic shielding, modern *ab initio* programs calculate \mathbf{J} as a second derivative of E , in this case with respect to the nuclear magnetic moments of the coupled nuclei, \mathbf{M}_I and \mathbf{M}_S . Here, it is given in terms of the reduced coupling tensor, $\mathbf{K}(I,S)$:^{8,103}

$$\mathbf{K}(I,S) = \left[\frac{\partial^2 E(\mathbf{B}, \mathbf{M})}{\partial \mathbf{M}_I \partial \mathbf{M}_S} \right]_{\mathbf{B}, \mathbf{M} = 0} \quad (2.49)$$

As with nuclear magnetic shielding, the derivatives can be evaluated numerically,^{104,105,106} or analytically. Equation 2.49 may be rewritten as follows to show explicitly the dependence of the wavefunction on \mathbf{M} :

$$\mathbf{K}(I,S) = \left[\frac{\partial^2 E(\mathbf{B},\mathbf{M})}{\partial \mathbf{M}_I \partial \mathbf{M}_S} \right]_{\mathbf{B},\mathbf{M}=0} + \left[\frac{\partial^2 E(\mathbf{B},\mathbf{M})}{\partial \mathbf{M}_I \partial \lambda} \right]_{\mathbf{B},\mathbf{M}=0} \frac{\partial \lambda}{\partial \mathbf{M}_I} \quad (2.50)$$

For each $\mathbf{K}(I,S)$ it is necessary to determine the response of the wavefunction with respect to the magnetic moment of one of the nuclei, via the factor $\partial \lambda / \partial \mathbf{M}_I$.

Determination of the full set of J -coupling tensors for a molecule is thus considered computationally more expensive than calculations of nuclear magnetic shielding, where $\partial \lambda / \partial \mathbf{B}$ need only be determined once to obtain all the shielding tensors.

A number of different models have been used for the calculation of J coupling. While HF methods have been applied, this approach usually fails because it cannot accurately describe the contribution from triplet states to the FC and SD mechanisms, termed the “triplet instability” problem.^{8,99} This can lead to calculations of J -coupling constants with significantly different magnitudes compared to experiment¹⁰⁷ or even the wrong sign. It has been generally recognized that molecules containing multiple bonds and/or electron lone pairs should not be investigated using the HF approach.^{8,99} More success has been obtained with the MCSCF approach. Calculations of J coupling using MCSCF theory with analytical evaluation of the derivatives in equation 2.49 (termed multiconfigurational linear response (MCLR) theory) were first reported in 1992.¹⁰⁸ The agreement between calculated and experimental results are generally very good,^{37,109,110} although this method is still limited to small molecules. A coupled cluster approach has also been used in the calculation of J coupling.^{111,112,113} Polarization propagator methods with acronyms such as SOPPA (second-order polarization

propagator approximation) and CCDPPA (coupled cluster doubles polarization propagator approximation) focus on the perturbation rather than the wavefunction.^{114,115,116,117} Density functional theory has also been applied; the first attempt was by Fukui in 1976.¹¹⁸ The combination of DFT methods with a completely analytical evaluation of the derivatives in equation 2.49 was reported recently.¹⁰³ Some recent examples of J coupling where relativistic effects are accounted for include results for MH_4 ($M=C, Si, Ge, Sn, Pb$) and $Pb(CH_3)_3H$.¹¹⁹ A relativistic correction to just the FC term within the DFT formalism has been discussed.¹²⁰ Examples of systems where relativistic corrections have been applied to DFT calculation of J coupling have been reported.^{121,122,123}

The choice of basis set is crucial in calculations of J coupling. In particular, accurate representation of the electronic structure near the nucleus is necessary. The convergence behaviour of correlation-consistent basis sets (denoted cc-pVXZ, where $X=2$ to 6) indicates that the good results are obtained when core-valence s -type orbitals (cc-pCVXZ) are included, and the best results are obtained with the cc-pVXZ-*sun* basis set, where the s -type functions are decontracted and n tight s -functions are added.¹²⁴ Unfortunately, these basis sets are not generally available for all elements.

If reports of reliable first-principles calculations of J -coupling constants are scarce, then reports of calculations of \mathbf{J} are rarer still. As discussed previously (section 2.1.6), experimental measurement of \mathbf{J} is difficult. However, it is imperative to characterize the tensor nature of this interaction to understand its relationship to molecular and electronic structure. Some examples of *ab initio* calculations of \mathbf{J} include

work on $J(X, ^{19}\text{F})$ ($X = ^1\text{H}, ^{13}\text{C}, ^{19}\text{F}$)¹²⁵ and $J(^{13}\text{C}, ^{29}\text{Si})$.^{109d} Extensive calculations of J in diatomic molecules established the importance of spin-spin coupling mechanisms other than FC.^{37,123} The symmetry properties of $J(^{35}\text{Cl}, ^{19}\text{F})$ and $J(^{19}\text{F}, ^{19}\text{F})$ for ClF_3 and $J(^{19}\text{F}, ^{17}\text{O})$ for OF_2 were explored in a subsequent publication.¹¹⁰ It has been demonstrated that the inclusion of relativistic considerations tends to increase ΔJ .¹²⁶

Chapter 3: Phosphorus Chemical Shift Tensors for Tetramethyldiphosphine Disulphide: A Single-Crystal ^{31}P NMR, Dipolar-Chemical Shift NMR and *Ab Initio* Molecular Orbital Study

3.1 Introduction

Alkyldiphosphine disulfides have been of some interest to NMR spectroscopists due to the relationship between the indirect ^{31}P - ^{31}P spin-spin coupling and structure. The investigation of diphosphine disulfides with various alkyl groups bonded to the phosphorus nuclei allows one to examine the effect of geometry differences such as the P-P bond length or the C-P-C bond angle on the phosphorus chemical shift and spin-spin coupling tensors. Solution NMR studies have been performed,¹⁴ and a few alkyldiphosphine disulfides have been investigated by NMR in the solid state, for example TEPS (tetraethyldiphosphine disulfide)^{10,11} and TBPS (tetrabutylidiphosphine disulfide).¹⁶ Initial reports indicated that anisotropy in $^1J(^{31}\text{P}, ^{31}\text{P})$ for both TEPS and TBPS was substantial, 2.2 kHz¹¹ and 1.9 kHz,¹⁶ respectively. However, subsequent work on TEPS indicated that the upper limit is 462 Hz.¹⁰

There are no extensive *ab initio* studies of phosphorus magnetic shielding tensors in the literature for these compounds and *ab initio* calculations of J in molecules of this size are impractical at the present time. Some experimental and *ab initio* shielding investigations of related compounds, the dithiadiphosphetanes, $[\text{RSP}(\text{S})\text{S}]_2$ ($\text{R} = \text{H}$, CH_3 , CH_2CH_3 , Ph , $\text{cyclo-C}_6\text{H}_{11}$, CH_2Ph , or 4-methylphenyl), and dithioxophosphoranes, RPS_2 ($\text{R} = \text{H}$, CH_3 , phenyl, or 2,6-dimethylphenyl) have been

reported.¹²⁷ For $\text{Ag}_4\text{P}_2\text{O}_6$, a significant anisotropy in $^1\text{J}(^{31}\text{P}, ^{31}\text{P})$ has been reported, $\Delta J = 800 \pm 80 \text{ Hz}$.¹²⁸

In this chapter, the characterization of phosphorus chemical shift and spin-spin coupling tensors for TMPS, **1**, by ^{31}P single-crystal NMR is described. The structure is shown again in figure 3.1(a) for convenience. These results are compared with those obtained from an independent analysis of ^{31}P NMR spectra of crystalline powder samples. In addition, the quality of *ab initio* calculations of phosphorus magnetic shielding tensors is evaluated by comparison with the experimental results. Finally, our analysis leads to an upper limit on the anisotropy of $^1\text{J}(^{31}\text{P}, ^{31}\text{P})$ for TMPS.

Comparison of results obtained from combining NMR studies of crystalline powder samples with *ab initio* calculations vs results from a single-crystal NMR study allows one to evaluate the various methods for characterizing chemical shift and spin-spin coupling tensors.^{19,129} In principle, the latter experiments provide the principal components and orientations of the chemical shift tensors, as well as dipolar and indirect spin-spin coupling tensors. Recent advances in hardware and software have made the single-crystal NMR experiment more efficient.¹³⁰ This NMR investigation of TMPS is ideal for such a comparison of data obtained from single-crystal NMR studies vs data from NMR studies of crystalline powder samples and *ab initio* shielding calculations. It is straightforward to grow a large single crystal of TMPS and the molecule is sufficiently small, allowing for *ab initio* calculations with acceptably large basis sets and various levels of theory.

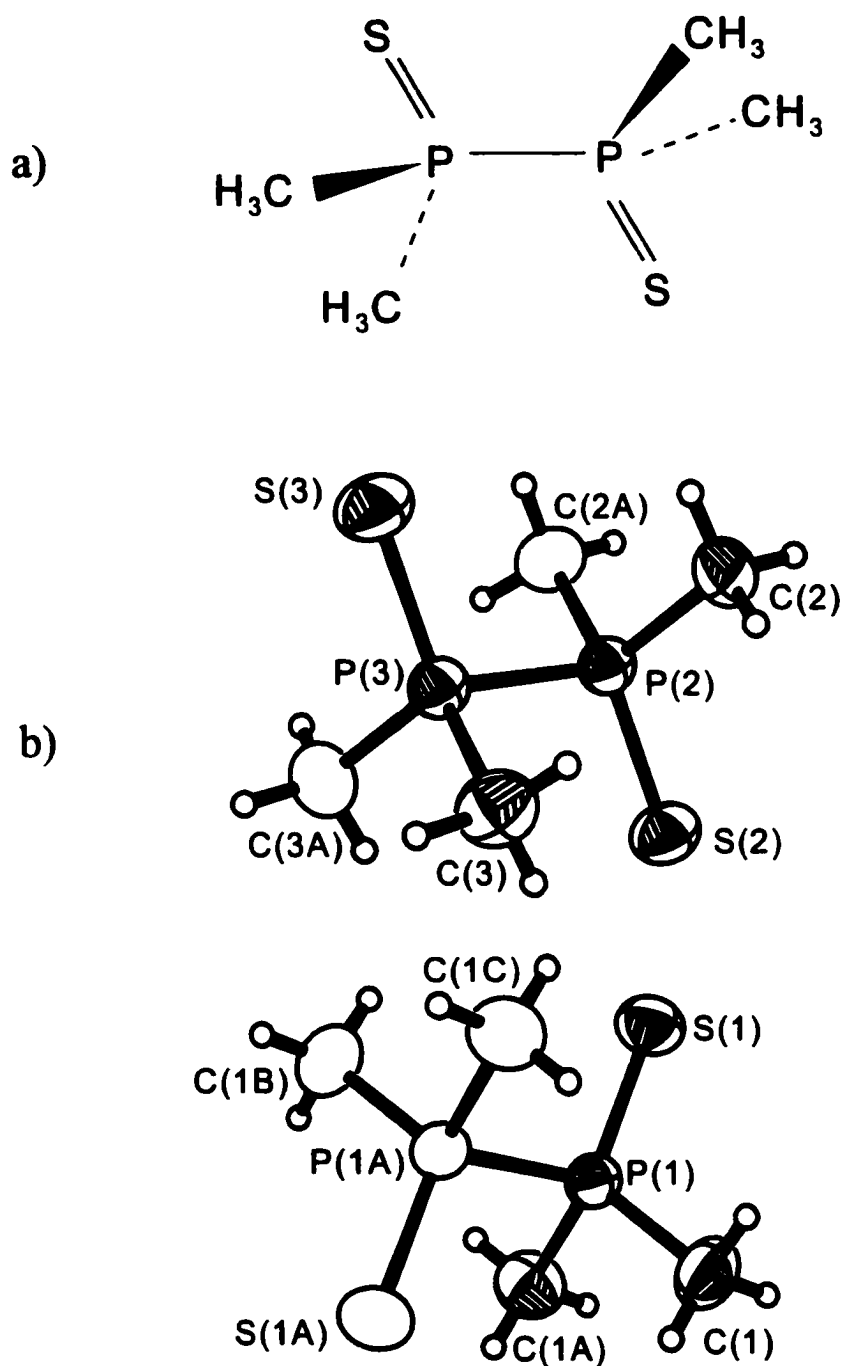


Figure 3.1 (a) Schematic representation of tetramethyldiphosphine disulfide, TMPS. (b) Labelling scheme for the TMPS structure obtained from an X-ray diffraction study (see table 3.1). Note that there are two molecules in the asymmetric unit.

3.2 Experimental and Computational Details

A sample of TMPS was obtained from Johnson Matthey Electronics.

X-ray Data Collection and Processing: For reasons discussed below, the X-ray structure of TMPS was redetermined by J. F. Britten at McMaster University. A single crystal of dimensions 0.02 mm × 0.20 mm × 0.45 mm, from a sample of TMPS recrystallized in CH₂Cl₂, was mounted on a glass fiber. X-ray diffraction experiments were carried out on a Siemens P4RA diffractometer (Mo K α , $\lambda = 0.710\ 69\ \text{\AA}$, graphite monochromator) at room temperature, using the ω and ϕ scan technique with a CCD area detector. The maximum 2θ value was 55.0°. The parameters for the monoclinic cell were $a = 18.860(6)\ \text{\AA}$, $b = 10.693(6)\ \text{\AA}$, $c = 7.021(4)\ \text{\AA}$, and $\beta = 94.608(3)^\circ$, with $Z = 6$. With formula weight of 186.20 g/mol, the calculated density is 1.311 g/cm³. Of the 5143 reflections collected, 1686 were unique. The data were corrected for Lorentz and polarization effects and for absorption using an empirical model.¹³¹

The structure was refined in $C2/m$,¹³² where all atoms with the exception of hydrogen atoms were refined using anisotropic temperature factors. Hydrogen atoms in their observed positions were refined isotropically. The final cycle of full-matrix least-squares refinement, using all unique reflections ($I > 3\sigma(I)$) with 101 variable parameters, converged with unweighted and weighted agreement factors of $R = 0.0327$ and $R_w = 0.0706$, respectively. On the final difference Fourier map, the maximum and minimum peaks corresponded to 0.384 and -0.260 electrons \AA^{-3} . All calculations were performed with SHELXTL.¹³³ Structural parameters are given in table 3.1 and the atom labelling scheme is shown in figure 3.1(b).

Table 3.1: Selected bond lengths (Å) and bond angles (°) for TMPS.

Site 1		Site 2	
P(1)-P(1A)	2.2137 (14)	P(2)-P(3)	2.2144 (10)
S(1)-P(1)	1.9569 (11)	S(2)-P(2)	1.9596 (10)
P(1)-C(1)	1.799 (3)	S(3)-P(3)	1.9560 (11)
P(1)-C(1A)	1.799 (3)	P(2)-C(2)	1.796 (2)
C(1)-P(1)-C(1A)	105.7 (2)	P(2)-C(2A)	1.796 (2)
C(1A)-P(1)-S(1)	115.50 (11)	P(3)-C(3)	1.803 (3)
C(1)-P(1)-P(1A)	103.56 (10)	P(3)-C(3A)	1.803 (3)
S(1)-P(1)-P(1A)	111.65 (5)	C(2)-P(2)-S(2)	115.35 (9)
		C(3)-P(3)-S(3)	115.25 (10)
		C(2)-P(2)-P(3)	103.90 (9)
		S(2)-P(2)-P(3)	111.58 (4)
		C(3)-P(3)-P(2)	104.02 (10)
		S(3)-P(3)-P(2)	111.11 (5)
		C(2)-P(2)-C(2A)	105.5 (2)
		C(3)-P(3)-C(3A)	106.0 (2)

Phosphorus-31 Single-Crystal NMR: A large single crystal of TMPS, grown in CH_2Cl_2 with dimensions of approximately 3 mm \times 3 mm \times 3.7 mm, was glued into the corner of a hollow three-sided crystal holder, made from aluminum oxide, measuring 4 mm on each side. X-ray diffraction methods were used to determine the orientation of the monoclinic crystal system with respect to the cube axes (table 3.2). The cell axes were

orthogonalized using Rollett's convention.¹³⁴ The rotation matrix, $\mathbf{R}_z(\gamma)\mathbf{R}_y(\beta)\mathbf{R}_x(\alpha)$,¹³⁵ relates the orthogonalized crystal system and the cube frame of reference. For our sample, $\alpha = 120.33^\circ$, $\beta = 3.04^\circ$, and $\gamma = 242.72^\circ$.

Table 3.2: Direction cosines to orient the monoclinic crystal axes (a , b , c) with respect to the orthogonal NMR cube frame (X , Y , Z) as determined by X-ray diffraction.

	X	Y	Z
a	0.9972	0.0398	-0.0446
b	-0.0525	0.9980	-0.0458
c	-0.0268	0.0458	0.9983

Phosphorus-31 NMR data from the single crystal were obtained on a Bruker MSL 200 spectrometer (4.7 T, corresponding to a ^{31}P NMR frequency of 81.03 MHz), using an automated single-crystal goniometer probe manufactured by Doty Scientific. Rotations were performed about each of the X , Y , and Z axes of the cube, from 0° to 180° in 9° increments. All ^{31}P NMR spectra were acquired using CP⁵⁴ with high power proton decoupling. A ^1H $\pi/2$ pulse width of 3.1 μs , contact time of 5.0 ms, acquisition time of 41 ms, and a recycle delay of 6 s were used. For each spectrum the sweep width was 50 kHz; 64 transients were adequate to obtain a good signal-to-noise ratio. For the FID, 3072 K of zero points were added to give a total of 4096 K data points

before Fourier transformation with 50 Hz of gaussian line broadening. All spectra are referenced to 85% $\text{H}_3\text{PO}_4(\text{aq})$. The peaks in each spectrum were fitted with a gaussian function to obtain the frequencies of the peak maxima. The ^{31}P single-crystal NMR data for each site were analyzed by linear least squares fit to:¹³⁶

$$f_i(\psi) = A_i + B_i \cos 2\psi + C_i \sin 2\psi \quad (3.1)$$

where f_i is the NMR parameter of interest and ψ tracks the rotation angle of the crystal in the goniometer about the i^{th} axis ($i = X, Y, Z$). For the ^{31}P chemical shift data of each site, the position at the centre of each doublet was plotted. In the analysis of the ^{31}P - ^{31}P dipolar coupling interaction, the splitting between the doublets was plotted for both sites. Phase angles of -2° for the X rotation, -3° for the Y rotation and -6° for the Z rotation were introduced in order to compensate for errors in the initial goniometer positions. The standard analysis of single-crystal NMR data is described elsewhere.^{19,136}

Phosphorus-31 NMR of Powder Samples: Phosphorus-31 NMR spectra of stationary or MAS powdered samples were acquired on a Bruker MSL 200, a Chemagnetics CMX Infinity 200 (4.7 T for both, corresponding to a frequency of 81.03 MHz for ^{31}P), or a Bruker AMX 400 spectrometer (9.4 T, corresponding to a frequency of 161.90 MHz for ^{31}P). CP⁵⁴ and high power proton decoupling were used for all experiments.

Double-air bearing MAS probes were used throughout. Samples were packed into 7 mm (MSL), 7.5 mm (Infinity) and 4 mm (AMX) o.d. zirconium oxide rotors. Typical parameters were ^1H $\pi/2$ pulse widths of 4 μs , contact times of 1 ms, and recycle delays

of 4 s for MAS and 8 s for stationary samples. The sweep width was 62.5 kHz with typical acquisition times of 41 ms. The FIDs were zero filled by 4096 K points to a total of 8192 K points before Fourier transformation. All spectra are referenced to 85% $\text{H}_3\text{PO}_4(aq)$ by using solid $\text{NH}_4\text{H}_2\text{PO}_4$ which has an isotropic phosphorus chemical shift of 0.8 ppm from 85% $\text{H}_3\text{PO}_4(aq)$.

Phosphorus-31 NMR spectra of stationary samples were simulated using WSOLIDS,⁴⁹ a program developed in this laboratory which incorporates the POWDER routine of Alderman *et al.*¹³⁷ NMR spectra of MAS samples were calculated using NMRLAB,⁵⁰ which uses the Monte Carlo method to sample crystal orientations for powder averaging. In our calculations 10,000 crystallite orientations were used for the powder averaging.

The 2D spin-echo NMR spectrum was acquired on the CMX Infinity 200, using a standard spin-echo pulse sequence with the phase cycling of Rance and Byrd.¹³⁸ The experimental parameters were similar to those used for the 1D experiments. To obtain a 2D data set, 64 increments of t_1 (see figure 2.8) were sufficient. A sweep width of 12.5 kHz in the F_1 dimension was used. The data size for the 2D spectrum was 512×128 after zero filling. Gaussian line broadening of 100 Hz was applied to both dimensions, then the data were processed in magnitude mode. The F_1 projection of the 2D spectrum was calculated using SpinEcho¹³⁹ which uses equations 2.40 and 2.41.

Computational Details: *Ab initio* calculations were performed using the Gaussian 98 suite of programs⁸⁴ running on an IBM RS/6000 computer. The phosphorus nuclear magnetic shielding was calculated using the atomic coordinates from the X-ray structure

determined in this work. Calculations were performed using the GIAO method⁷³ at the HF level of theory as well as with DFT. For the DFT calculations, the Becke three parameter functional¹⁴⁰ using the Lee, Yang, and Parr correlation functional¹⁴¹ (B3LYP) was used. To compare calculated results with experimental results, the calculated phosphorus nuclear magnetic shielding was converted to chemical shift using the absolute shielding of 328.35 ppm for the phosphorus nucleus in the reference, 85% $\text{H}_3\text{PO}_4(aq)$.⁹⁰

3.3 Results and Discussion

3.3.1 Phosphorus-31 NMR of a Single Crystal

The ^{31}P NMR spectra obtained from a single crystal of TMPS are shown in figure 3.2. The X-ray structure of TMPS indicates the presence of six molecules in the unit cell. In two of the six molecules, the two phosphorus nuclei are related by inversion symmetry, hence they are crystallographically and magnetically equivalent, i.e., they form an A_2 spin pair² (site 1). In the single-crystal NMR study, site 1 gives rise to a doublet where the splitting is the ^{31}P - ^{31}P effective spin-spin coupling at that particular orientation of the crystal in the applied magnetic field, B_0 . Since $|^1J(^{31}\text{P}, ^{31}\text{P})|$ measured in solution is less than 20 Hz,¹⁴² the splitting is dominated by R_{eff} . The remaining four molecules (site 2) in the unit cell of TMPS possess mirror planes that include the S-P-P-S plane; however the phosphorus nuclei are not related by a centre of inversion; hence, they are not crystallographically equivalent.

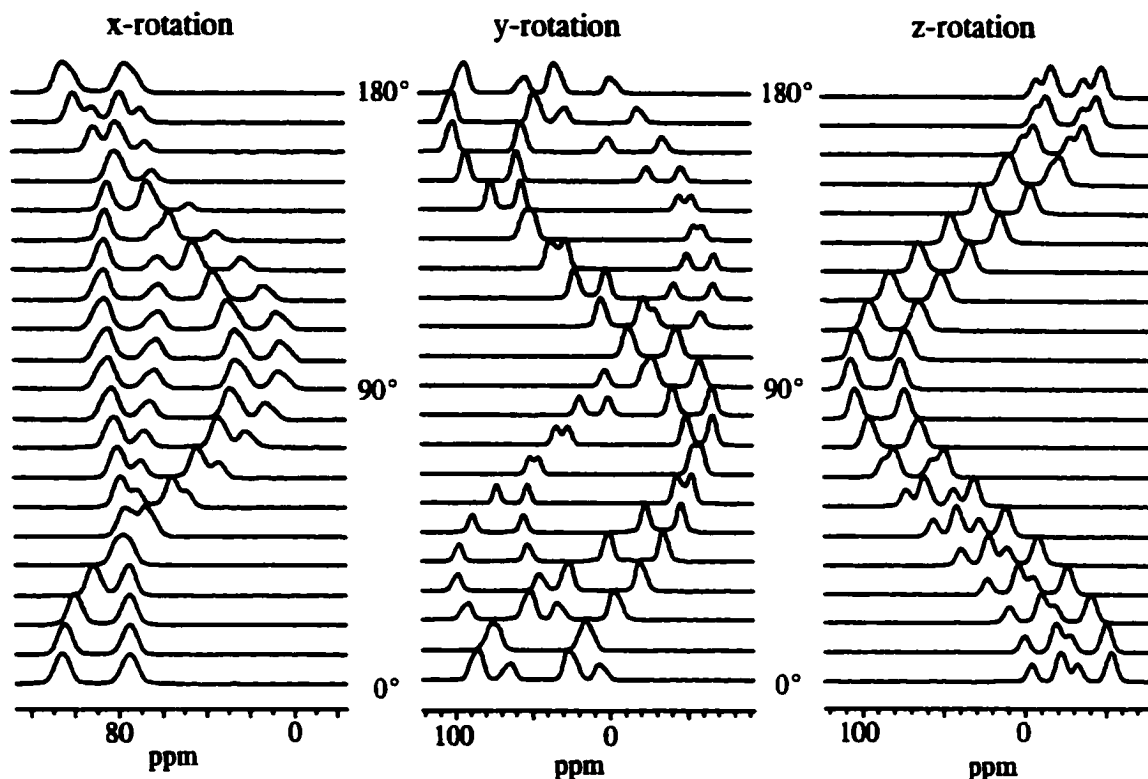


Figure 3.2 Phosphorus-31 NMR spectra of a single crystal of TMPS for rotations of the crystal holder about its X, Y, and Z axes, acquired at 4.7 T.

In most of the NMR spectra of the TMPS single crystal (figure 3.2), four peaks are evident. The two of lesser intensity are assigned to site 1 and the more intense set is assigned to site 2 since the two sites are present in a 1:2 ratio. It is not obvious in figure 3.2 that site 2 is an AB spin system, since the expected four transitions (section 2.2.1) are not immediately apparent. In fact, very few of the rotations produce NMR spectra where there is any evidence of an AB quartet; one example is shown in figure 3.3. Since there are insufficient data to analyze site 2 as an AB spin system, it has been analyzed as an A_2 spin system. The plots of the chemical shift and the dipolar splitting

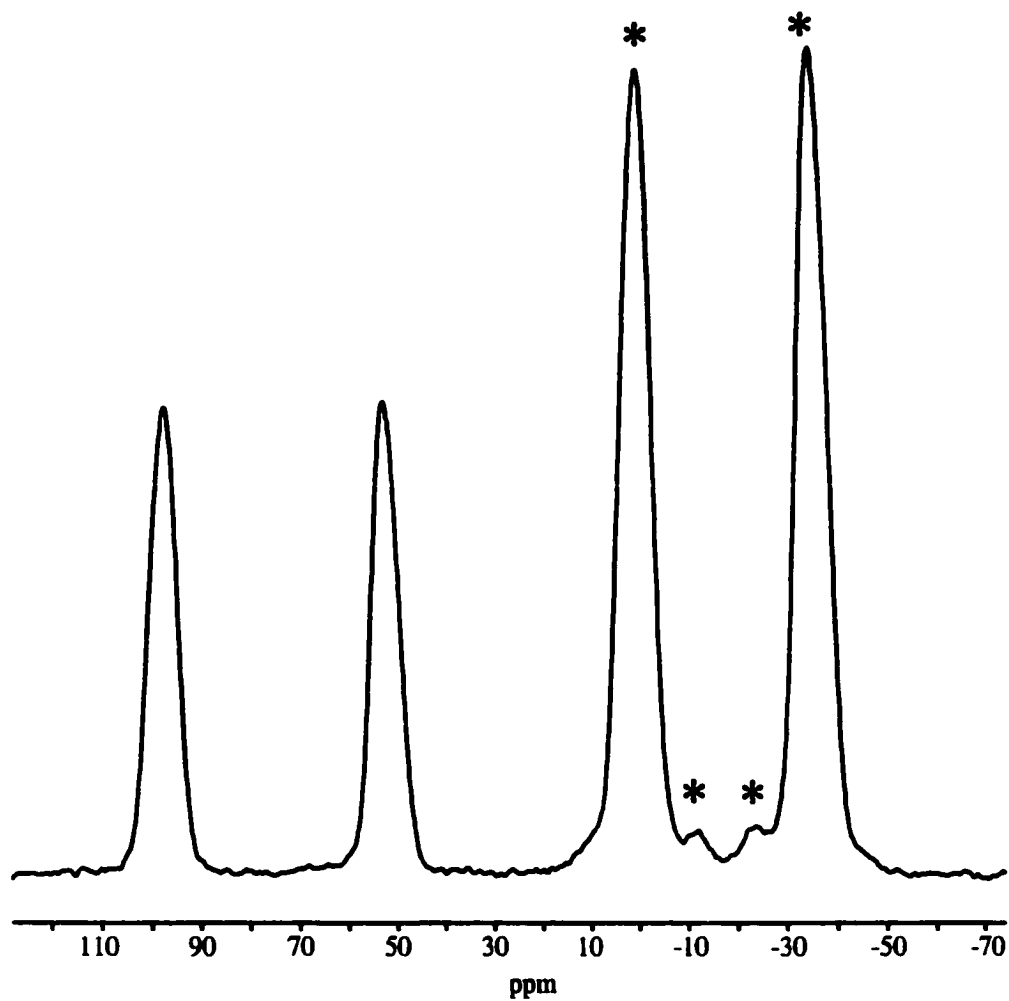


Figure 3.3 Example of a ^{31}P NMR spectrum of the TMPS single crystal (from the rotation about the Y axis of the crystal holder, at 36° from the initial position). The asterisks indicate the four peaks attributed to site 2.

as a function of crystal rotation are shown in figures 3.4 and 3.5, respectively. The coefficients of the linear least squares fit to equation 3.1 for the chemical shift tensors are given in table 3.3. The components of the chemical shift tensors, δ_{11} , δ_{22} and δ_{33} , and their respective direction cosines relative to the orthogonalized crystal frame of reference are given in table 3.4. As is evident in this table, the principal components of the phosphorus chemical shift tensors for sites 1 and 2 are virtually identical. The orientation of the tensor is illustrated in figure 3.6(a) for site 1. The principal component of the phosphorus chemical shift tensor which corresponds to the direction of greatest shielding, δ_{33} , is closest to the P-S bond, while δ_{11} is approximately perpendicular to the plane containing the S-P-P-S bonds, with a P-P- δ_{11} angle of 83° . The angle between δ_{33} and the P-P bond is 124° for site 1. The chemical shift tensor orientation at the other phosphorus nucleus of site 1 is simply an inversion of the one shown in figure 3.6(a). For site 2, the phosphorus chemical shift tensor is oriented in a similar fashion with respect to the molecule, with δ_{33} at 2.5° from the P-S bond and the P-P- δ_{11} angle of 100° . The presence of a mirror plane in site 2 requires that the P-P- δ_{11} angle be exactly 90° ; however, the magnitude of δ_{11} and δ_{22} are similar, thus it is difficult to determine their orientations independently.¹⁰

The principal components of the dipolar coupling tensors are given in table 3.4 with their respective direction cosines. The spin-spin coupling data for TMPS are also summarized in table 3.5. As mentioned in section 2.1.5, the dipolar coupling tensor in its principal axis system is axially symmetric and traceless, with the unique axis along the internuclear vector. The non-zero trace and very slight non-axial symmetry of our

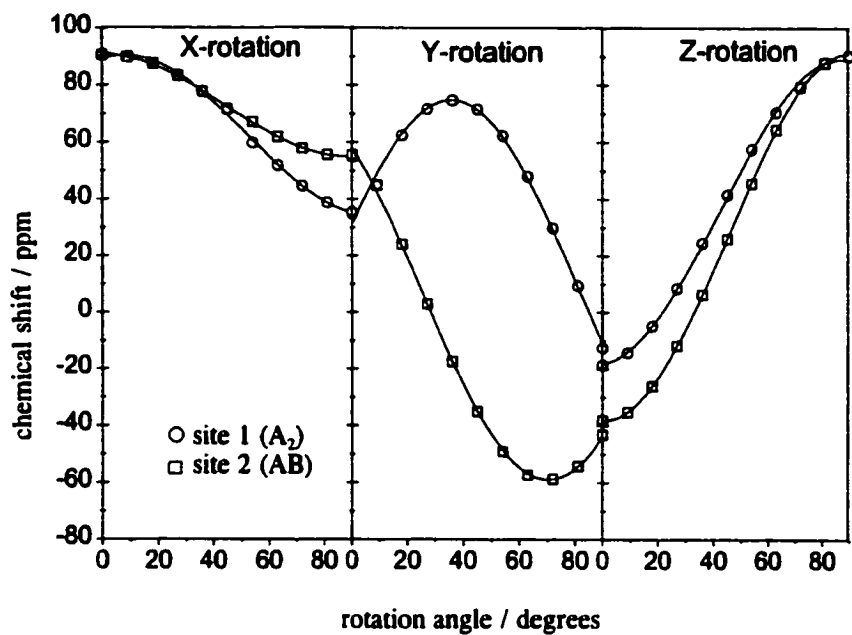


Figure 3.4 Phosphorus chemical shift as a function of rotation angle, ψ , for sites 1 and 2. The curves represent the linear least-squares best fit to the experimental data, shown as \circ for site 1 and as \square for site 2.

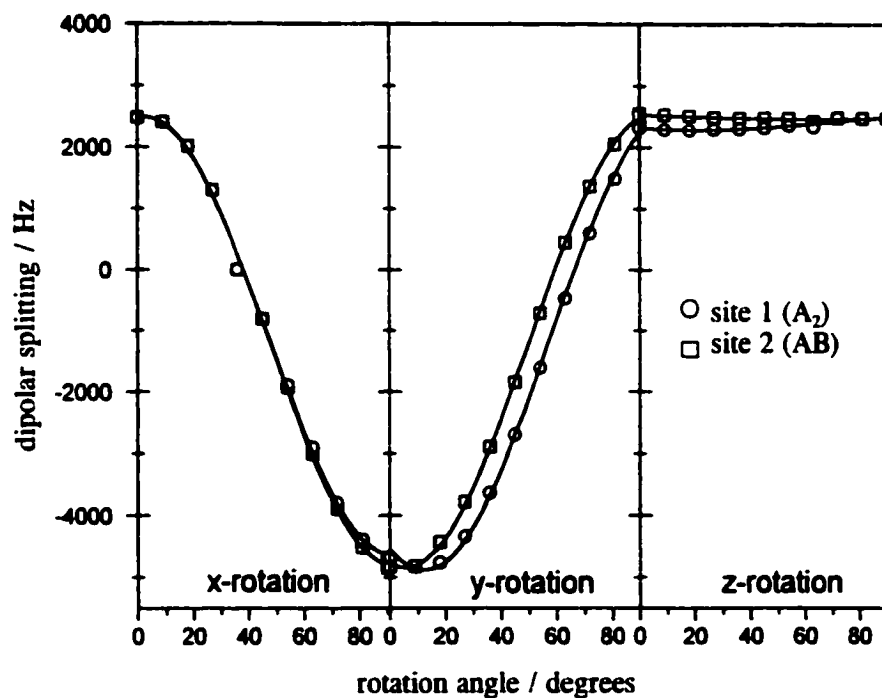


Figure 3.5 Dipolar splitting as a function of rotation angle, ψ , for sites 1 and 2. The curves represent the linear least squares best fit to the experimental data, shown as \circ for site 1 and as \square for site 2.

Table 3.3: Linear least-squares coefficients for the phosphorus chemical shift and spin-spin coupling interactions in TMPS as functions of crystal rotation about the cube *X*, *Y*, *Z* axes.^a

	rotation	A_i	B_i	C_i
site 1 (A_2)				
chemical shift ^b	<i>X</i>	60.18(4)	26.93(6)	8.851(6)
	<i>Y</i>	7.406(6)	25.85(8)	62.88(8)
	<i>Z</i>	34.72(5)	-53.47(7)	17.77(7)
spin-spin coupling ^c	<i>X</i>	-1.37(5)	3.54(7)	0.48(7)
	<i>Y</i>	-1.15(2)	-3.50(2)	-1.22(2)
	<i>Z</i>	2.410(7)	-0.09(1)	-0.06(1)
site 2 (AB)				
chemical shift ^b	<i>X</i>	71.98(2)	17.72(2)	-0.295(2)
	<i>Y</i>	8.046(4)	47.54(5)	-48.33(5)
	<i>Z</i>	27.45(3)	-62.51(3)	11.74(4)
spin-spin coupling ^c	<i>X</i>	-1.45(4)	3.62(6)	0.52(6)
	<i>Y</i>	-1.11(2)	-3.70(3)	-0.37(3)
	<i>Z</i>	2.490(4)	0.013(6)	-0.01(6)

^a The phase angles for the best fit to the experimental data are -2° for *X*, -3° for *Y* and -6° for *Z*.

^b Units of ppm.

^c Units of kHz.

Table 3.4: Principal components and orientations (direction cosines) of the phosphorus chemical shift and dipolar coupling tensors relative to the orthogonalized crystal axes (a^*bc) for TMPS.

		a^*	b	c
site 1 (A_2)				
δ_{11} /ppm	90.6	-0.1417	0.9836	0.1140
δ_{22} /ppm	74.9	-0.5171	-0.1717	0.8385
δ_{33} /ppm	-63.2	0.8441	0.0599	0.5328
D_{11} /kHz	2.538	0.9805	-0.1405	0.1373
D_{22} /kHz	2.365	0.1430	0.9897	-0.0081
D_{33} /kHz	-5.008	-0.1348	0.02753	0.9905
site 2 (AB)				
δ_{11} /ppm	91.8	-0.1120	0.9795	-0.1621
δ_{22} /ppm	74.4	0.3955	0.1964	0.8971
δ_{33} /ppm	-58.8	0.9106	0.0435	-0.4110
D_{11} /kHz	2.566	0.9916	-0.1273	0.0237
D_{22} /kHz	2.358	0.1280	0.9946	-0.0239
D_{33} /kHz	-4.994	-0.0204	0.0268	0.9994

Table 3.5: Spin-spin coupling data for TMPS.

Method	D_{iso} / kHz	R_{eff} / kHz	R_{DD} / kHz	$ J_{iso} $ / Hz	ΔJ / Hz
single crystal					
site 1 (A_2)	-0.035	1.669 ^a	1.818	18.7 ^b	447
site 2(AB)	-0.023	1.665 ^a	1.816	-	453
2D spin echo	-	1.690 ^c	-	-	-

^a Estimated experimental error is ± 0.050 kHz.

^b From reference 142.

^c Experimental error is ± 0.080 kHz.

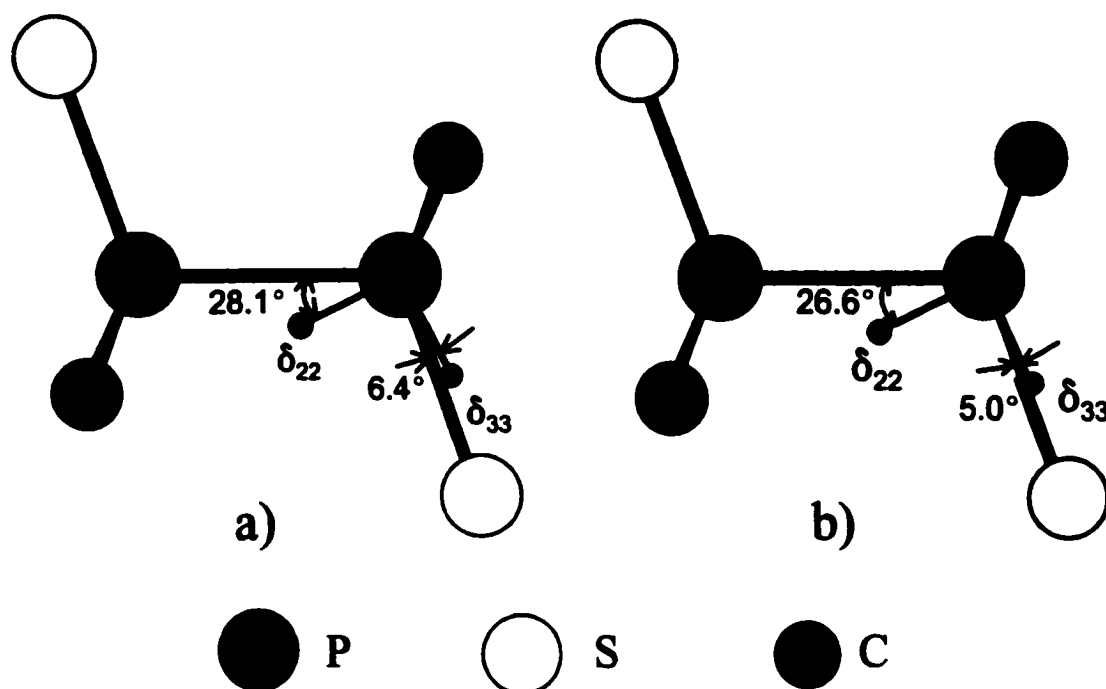


Figure 3.6 Orientation of the phosphorus chemical shift tensor for TMPS as determined by (a) a single-crystal NMR study and (b) *ab initio* (HF) calculations. The orientations are shown for site 1. The plane of the page contains the S-P-P-S moiety. In both cases, δ_{11} is approximately perpendicular to the plane of the page.

dipolar coupling tensors is likely a consequence of experimental errors in the single-crystal NMR experiment. In addition, anisotropic molecular motion may contribute.^{29,143} The experimental values of R_{eff} are 1.669 ± 0.050 kHz for site 1 and 1.665 ± 0.050 kHz for site 2, determined by averaging R_{eff} obtained from each of the diagonal components of \mathbf{D} (table 3.4). The rotation plot for the dipolar splitting (figure 3.5) indicates that the unique axis of the dipolar tensor, which is along the P-P bond, is very close to the Z-axis of the cube, since the dipolar splitting for both sites is

essentially invariant to rotation of the crystal about that axis. This implies that r_{pp} and B_0 are approximately perpendicular ($\zeta=90^\circ$) during the rotation about the Z axis; hence, a splitting of $3/2 R_{eff}$ is observed.

From R_{DD} calculated using the P-P bond lengths reported in the X-ray crystal structure¹⁴⁴ and R_{eff} determined experimentally, one can estimate ΔJ as described in section 2.1.6.²⁹ The most recently published crystal structure of TMPS¹⁴⁴ reports a significant and unexplained difference in the P-P bond lengths of sites 1 and 2, $r = 2.245(6) \text{ \AA}$ and $r = 2.161(4) \text{ \AA}$ respectively, corresponding to $R_{DD} = 1.74 \pm 0.04$ kHz and, using equation 2.29, $\Delta J = 0.3 \pm 0.05$ kHz for site 1, while $R_{DD} = 1.95 \pm 0.03$ kHz and $\Delta J = 0.9 \pm 0.05$ kHz for site 2. This is clearly suspicious, prompting our redetermination of the X-ray crystal structure. From our investigation, the general features of the X-ray structure are similar to those previously reported; however the difference in the geometry between the two sites is much less dramatic. The P-P bond lengths from our X-ray data are $2.2137(14) \text{ \AA}$ and $2.2144(10) \text{ \AA}$ for site 1 and site 2 respectively, resulting in more reasonable values of R_{DD} (table 3.5). For site 2, the major structural difference between the two $(CH_3)_2PS$ fragments is the C-P-C bond angle ($106.0(2)^\circ$ vs $105.5(2)^\circ$; see table 3.1). Using our values of R_{DD} for both sites, the upper limit on $\Delta J(^{31}P, ^{31}P)$ is approximately 450 Hz. In addition, there may also be a contribution from librational motion of the molecule, which results in a smaller observed value for the dipolar coupling constant. The reduction in the dipolar coupling constant has been estimated to be between 3 and 5%.^{45(a),145,146}

3.3.2 Phosphorus-31 NMR Spectra of Crystalline Powder Samples

The ^{31}P NMR spectra of powder samples of TMPS were analyzed independently of the single-crystal work. Before analyzing the ^{31}P NMR spectra of stationary (figure 3.7) and MAS (figure 3.8) crystalline powder samples of TMPS, the effective dipolar coupling constant can be measured independently using the 2D spin-echo experiment.¹³ From simulations of the F_1 projection (figure 3.9) of the 2D spin-echo NMR spectrum, $R_{\text{eff}} = 1.69 \pm 0.08$ kHz, in good agreement with the single crystal data. In the simulations, it is assumed that $|^1J(^{31}\text{P}, ^{31}\text{P})| = 18.7$ Hz which is the value measured in a previous solution NMR study.¹⁴²

The NMR spectra of the stationary samples (figure 3.7) are simulated using the value of R_{eff} from the 2D spin-echo NMR spectrum to obtain the chemical shift tensor principal components given in table 3.6 and tensor orientation information discussed below. The principal components of the phosphorus chemical shift tensors as obtained from the single-crystal NMR study (table 3.4) are reproduced in table 3.6 for comparison. The NMR spectra of MAS samples, spinning at various frequencies, ν_{rot} , (figure 3.8) were calculated using the same parameters as obtained from the stationary samples, with the exception of the isotropic phosphorus chemical shifts for sites 1 and 2. More accurate isotropic chemical shifts are available from the ^{31}P NMR spectra of MAS samples. For site 1, $\delta_{\text{iso}} = 34.9$ ppm while for site 2, two peaks are evident at 37.4 ppm and 37.0 ppm (figure 3.8(a), inset). The ^{31}P NMR spectra of MAS samples can be successfully simulated based on this information and the data obtained from the

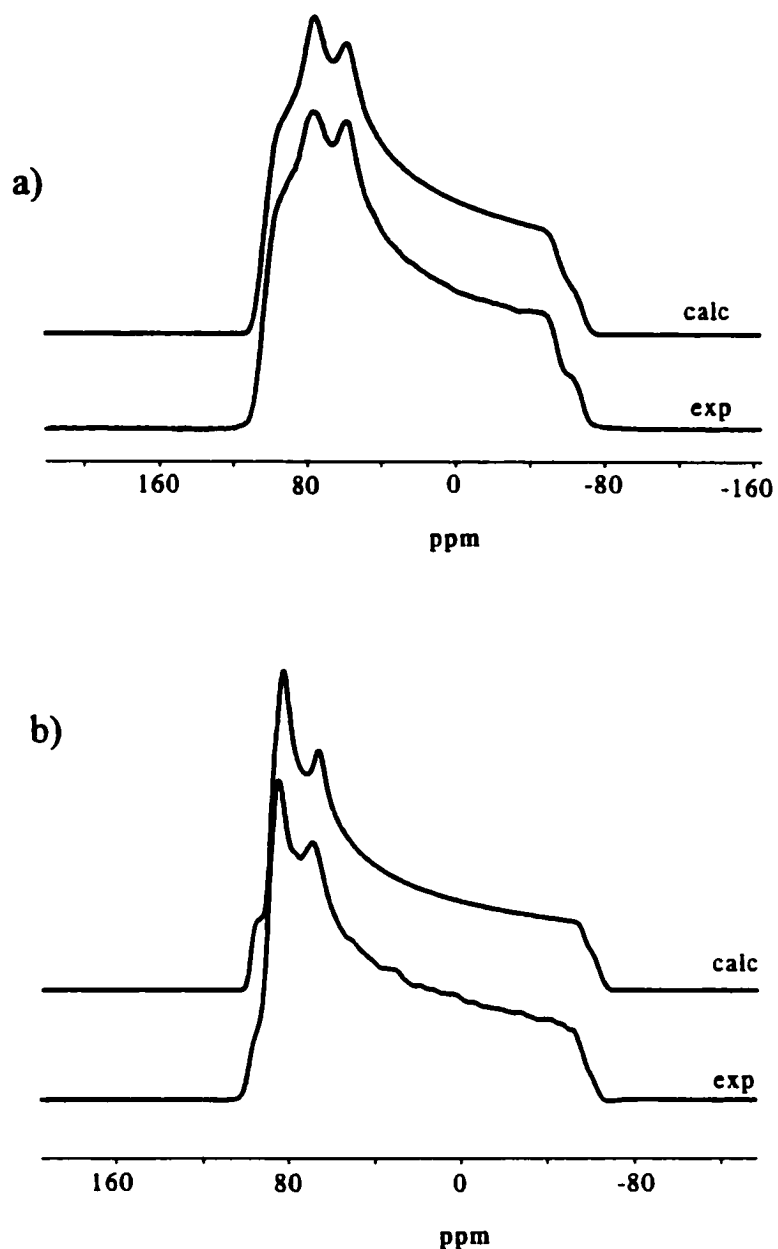


Figure 3.7 Experimental and calculated ^{31}P NMR spectra of stationary powder samples of TMPS, acquired at (a) 4.7 T (500 transients, 20 Hz gaussian line broadening) and (b) 9.4 T (7010 transients, 25 Hz gaussian line broadening). The same experimental NMR parameters were used to simulate the observed spectra at both fields.

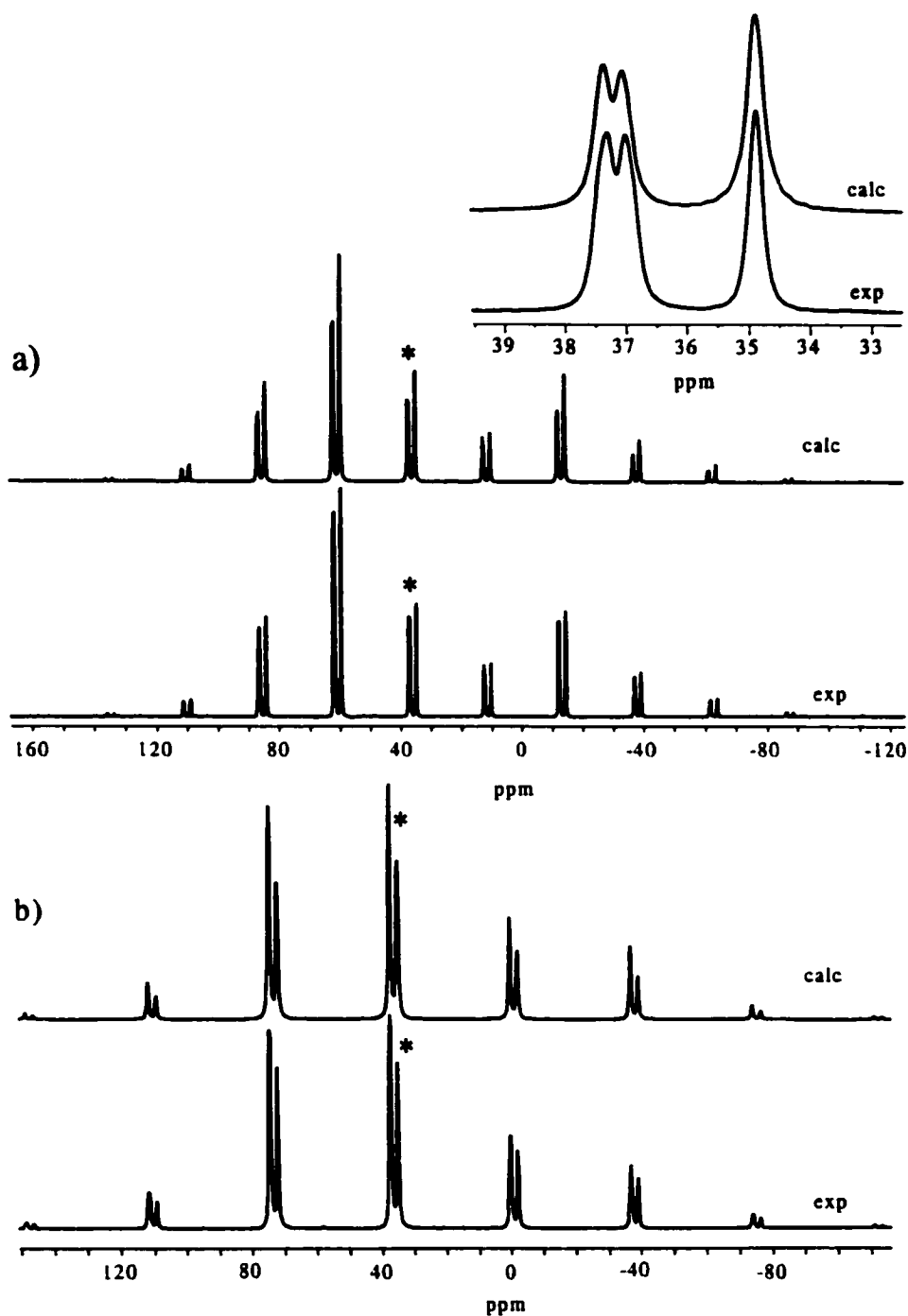


Figure 3.8 Experimental and calculated ^{31}P MAS NMR spectra of TMPS acquired at (a) 9.4 T with $\nu_{\text{rot}} = 4.00$ kHz (172 transients, 10 Hz gaussian line broadening). The inset shows details of the isotropic region. The bottom spectrum (b) was obtained at 4.7 T with $\nu_{\text{rot}} = 4.00$ kHz (64 transients, 10 Hz gaussian line broadening). The asterisks indicate the isotropic regions.

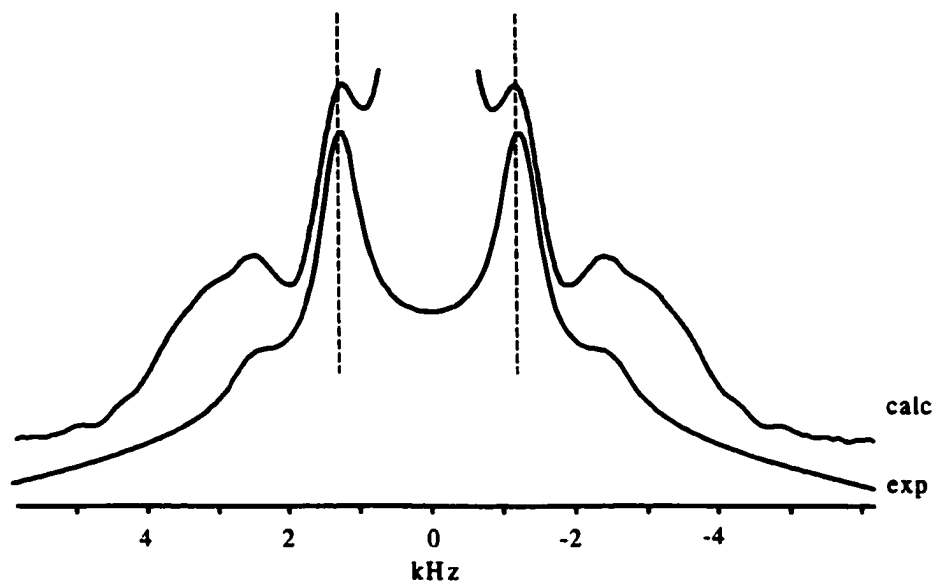


Figure 3.9 Experimental and calculated $F1$ projection of the 2D spin-echo ^{31}P NMR spectrum acquired at 4.7 T. The large centre peak (truncated in this figure) is an experimental artifact.

simulation of the NMR spectra of stationary samples. Since the single-crystal NMR spectra exhibited very little AB character, the subtle difference between the non-equivalent phosphorus environments in site 2 was not apparent from that analysis.

While one can, in principle, fit the ^{31}P NMR spectra to obtain all the chemical shift and coupling information, these spectra (figure 3.8) are essentially featureless, hence it was necessary to also analyze the NMR spectra of stationary samples, acquired at different applied magnetic fields (figure 3.7). In addition, one cannot apply the Herzfeld-Berger approach¹⁴⁷ to the spinning sideband manifold of the MAS spectra due to the presence of strong dipolar coupling.¹⁴⁸

Table 3.6: The isotropic phosphorus chemical shift (ppm), principal components of the chemical shift tensor (ppm), Ω (ppm), and κ , for TMPS.

	δ_{iso}	δ_{11}	δ_{22}	δ_{33}	Ω^a	κ^a
single crystal						
site 1	34.3	91	75	-63	154	0.79
site 2	35.7	92	74	-59	151	0.76
stationary powder (4.7 T, 9.4 T)						
site 1	34.3	91 ^b	75	-63	154	0.79
site 2	36.0	91	76	-59	150	0.80
MAS powder (4.7 T, 9.4 T) ^c						
site 1	34.9	-	-	-	-	-
site 2 ^d	37.0	-	-	-	-	-
	37.4	-	-	-	-	-
HF/6-311G**						
site 1	-19	41	17	-114	155	0.69
site 2 ^d	-19	41	18	-115	156	0.71
	-17	42	17	-111	153	0.66
HF/6-311G(3df,3pd)						
site 1	10	66	56	-93	159	0.88
site 2 ^d	10	67	58	-94	161	0.89
	11	67	57	-90	157	0.89
B3LYP/6-311G(d,p)						
site 1	52	132	97	-74	206	0.66
site 2 ^d	50	131	98	-79	210	0.69
	52	132	97	-74	206	0.66

$$^a \Omega = \delta_{11} - \delta_{33}; \kappa = 3(\delta_{22} - \delta_{\text{iso}}) / \Omega.$$

^b Experimental error in the principal components is ± 2 ppm.

^c Experimental error in δ_{iso} for site 1 is ± 0.03 ppm and ± 0.04 ppm for site 2.

^d The phosphorus nuclei at site 2 are not chemically equivalent; hence, two sets of principal components are given.

In addition to obtaining the principal components of the phosphorus chemical shift tensors, some tensor orientation information is available from the analysis of NMR spectra of powders containing isolated spin pairs such as those in TMPS. As described in section 2.2.2 the orientations are commonly described in terms of Euler angles, α , β and γ .²⁶ The ^{31}P NMR spectra of stationary samples (figure 3.7) were successfully simulated using $\Delta\alpha = 0^\circ$ for both site 1 and 2, indicating that the δ_{33} components for adjacent phosphorus nuclei lie in the same plane. The angle between δ_{33} and the P-P bond, β , is $63^\circ \pm 3^\circ$ for site 1 and $65^\circ \pm 3^\circ$ for site 2, equally well-described by the supplement angles, 117° and 115° , respectively. The orientation of the principal components of the phosphorus shielding tensor obtained from a dipolar-chemical shift analysis is clearly consistent with the single-crystal NMR results.

3.3.3 *Ab Initio* Calculation of Phosphorus Shielding Tensors

The calculated principal components of the phosphorus shielding tensors for TMPS are given in table 3.6 and the orientation for one phosphorus nucleus in site 1 is shown in figure 3.6(b). The calculated phosphorus chemical shift tensor orientations for site 2 are similar. Using the 6-311G** basis set, the HF results for δ_{iso} are about 53 ppm too shielded for both sites; however, the line shapes, as described by Ω and κ , are remarkably accurate. Increasing the size of the basis set to 6-311++G(3df,3pd) improves the calculated value of δ_{iso} ; however, it is still too shielded by about 24 ppm for both sites. The values from DFT calculations are deshielded by only 16 ppm compared to experimental results, but Ω is overestimated. Differences between the

isotropic chemical shift measured in the solid state compared with results from *ab initio* calculations are expected since the calculations are performed on an isolated molecule. The intermolecular effects may be substantial. For example, $\text{PH}_3(g)$ is more shielded by 28 ppm compared to $\text{PH}_3(l)$ ⁹⁰ and $\text{P}_4(g)$ is more shielded by 93.0 ppm compared to $\text{P}_4(l)$.¹⁴⁹ This is a general trend that nuclei in the gas phase are invariably shielded compared to the condensed phase.¹⁵⁰ The *ab initio* methods reproduce phosphorus shielding tensor orientations quite well (figure 3.6).

3.3.4 Comparison of Results

The phosphorus chemical shift and spin-spin coupling tensors for TMPS obtained by analysis of ^{31}P NMR spectra of crystalline powder samples are in excellent agreement with the single-crystal NMR study. The value of R_{eff} measured by both single-crystal NMR and the 2D spin-echo experiment compared to R_{DD} calculated from P-P bond lengths places an upper limit ΔJ (about 450 Hz), substantially smaller than originally estimated for similar compounds.^{11,16} The phosphorus chemical shift tensors obtained from both single-crystal and powder methods are virtually identical. In addition, analysis of ^{31}P NMR spectra of MAS samples at 9.4 T provide additional details regarding the chemically non-equivalent phosphorus nuclei of site 2. From the analysis of the NMR spectra of stationary powder samples, the principal components of the phosphorus chemical shift tensors are determined. The orientations of the most shielded components relative to the P-P bond as well as to each other are obtained. For both site 1 and 2, the direction of greatest shielding is in the same plane and are closest

to the P-S bond. This is consistent with the orientation in other systems containing P=S bonds.^{10,11,12} Unfortunately, the orientation of the tensor in the molecular frame of reference can not be determined by powder NMR methods. The full tensor orientation is available experimentally from the single-crystal NMR study (figure 3.6(a)). The orientation information obtained from the powder methods are consistent with the single-crystal results.

The *ab initio* methods employed in this work produce line shapes that are in good agreement with experimental results. In addition, the calculated nuclear magnetic shielding tensor orientations are almost identical to those obtained from the single-crystal NMR study. The invariance of the nuclear magnetic shielding tensor orientation with basis set suggests that calculations at the HF level of theory with moderate-sized basis sets are adequate for obtaining the shielding tensor orientation. This is particularly useful for large systems, where high-level calculations are very difficult due to limited computational resources.

3.3.5 Trends in Phosphorus Chemical Shifts for Alkyldiphosphine Disulfides

It has been suggested that the isotropic chemical shift at the phosphorus nucleus is directly related to the C-P-C bond angle in alkyldiphosphine disulfides.¹⁵ With the characterization of the phosphorus chemical shift tensor in TMPS, this correlation can be examined more rigorously. Table 3.7 lists the phosphorus chemical shift data and the C-P-C bond angle for $[R_2P(S)]_2$ where R = CH₃ (this work), CH₂CH₃,¹⁰ *n*-propyl,¹⁵¹ or *n*-butyl.¹⁶ It is difficult to draw any definite conclusion based on the first three

compounds in the series, partly due to the experimental uncertainty in the C-P-C bond angle; however, it appears that the isotropic shielding trend does not follow the bond angle, i.e., increasing bond angle does not correlate directly with an increase or decrease in the isotropic chemical shift. Attempts have also been made to explain the difference between the phosphorus chemical shift for R=*n*-propyl and R = *n*-butyl by an effect similar to the γ -effect in ^{13}C NMR.^{14b} Trends in the principal components of the phosphorus shift tensors should be considered, as has been done, for example, in the case of the dithiadiphosphetanes, $[\text{RSP}(\text{S})\text{S}]_2$ (R = alkyl or aryl).¹²⁷ For the alkyldiphosphine disulfides, the limited data available on the phosphorus chemical shift tensors (table 3.7) indicate that the intermediate component, δ_{22} , changes the most (by about 23 ppm) upon going from R = CH₃ to R = CH₂CH₃. The smallest component, δ_{11} , changes by about 17 ppm and δ_{33} by about 7 ppm. By contrast, all the principal components are similar for R = CH₂CH₃ compared to R = *n*-butyl. Unfortunately, no data on the phosphorus chemical shift tensor are available for R = *n*-propyl.

Table 3.7: Comparison of δ_{iso} and C-P-C bond angle for $[\text{R}_2\text{P}(\text{S})]_2$.

R	δ_{iso} / ppm	δ_{11} / ppm	δ_{22} / ppm	δ_{33} / ppm	C-P-C / deg
CH ₃ (site 1) ^a	34.1	91	75	-63	105.7(2)
CH ₂ CH ₃ ^b	50.7	108	98	-54	107.52(9)
<i>n</i> -propyl ^c	45.9	-	-	-	107.8(2)
<i>n</i> -butyl	49.5	104.7	97.5	-53.7	-
(multiple sites) ^d	49.7	106.3	96	-53.1	

^a This thesis.

^b Reference 10.

^c NMR data from reference 15, X-ray crystal structure from ref 151.

^d NMR data from reference 16, no crystal structure available.

3.4 Conclusions

The characterization of the phosphorus chemical shift and spin-spin coupling tensors for TMPS presented in this paper serves as a benchmark for the evaluation of experimental NMR powder methods as well as the reliability of *ab initio* methods. The excellent agreement between the calculated and experimental phosphorus chemical shift tensor orientations is particularly encouraging. For TMPS, as for TEPS,¹⁰ $\Delta J(^{31}\text{P}, ^{31}\text{P})$ is less than 500 Hz. A number of alkyldiphosphine disulfides have been characterized by NMR and attempts have been made to account for trends in the isotropic phosphorus chemical shifts; however, it is clear that the entire phosphorus chemical shift tensor must be considered. In addition, the structural data available in the literature for alkyldiphosphine disulfides are limited, hence correlations between a particular structural feature in this class of compounds and the phosphorus chemical shifts are tenuous at best.

Chapter 4: Characterization of Phosphorus Chemical Shift Tensors in a Phosphole Tetramer: A Combined Experimental NMR and Theoretical Study

4.1 Introduction

The phosphole tetramer, **2** (figure 4.1), was first synthesized in 1982¹⁵² and the X-ray crystal structure was reported subsequently.²¹ Solid-state NMR investigations of similar systems where two three-coordinate phosphorus nuclei are directly bonded are relatively rare.^{13,17,19,20} In the case of the phosphole tetramer, analysis of the ³¹P NMR spectra acquired with cross polarization and MAS revealed a difference in the isotropic phosphorus chemical shifts of 1.7 ppm with $^1J(^{31}\text{P}, ^{31}\text{P})_{\text{iso}} = -362$ Hz.^{153,154} Here, we use the presence of phosphorus spin pairs to characterize the phosphorus chemical shift tensors via the dipolar-chemical shift NMR method (section 2.2). In contrast to the earlier ³¹P NMR investigations of MAS samples,^{153,154} NMR spectra of stationary samples obtained at different applied magnetic fields are fully analyzed. It is also demonstrated that analysis of the ³¹P 2D spin-echo NMR spectrum of the phosphole tetramer is invaluable for refining the coupling parameters. *Ab initio* calculations complement the experimental data and suggest orientations of the phosphorus chemical shift tensors in the molecular frame of reference. Inconsistencies between the NMR data (*vide infra*) and the original X-ray data²¹ prompted a redetermination of the crystal structure.

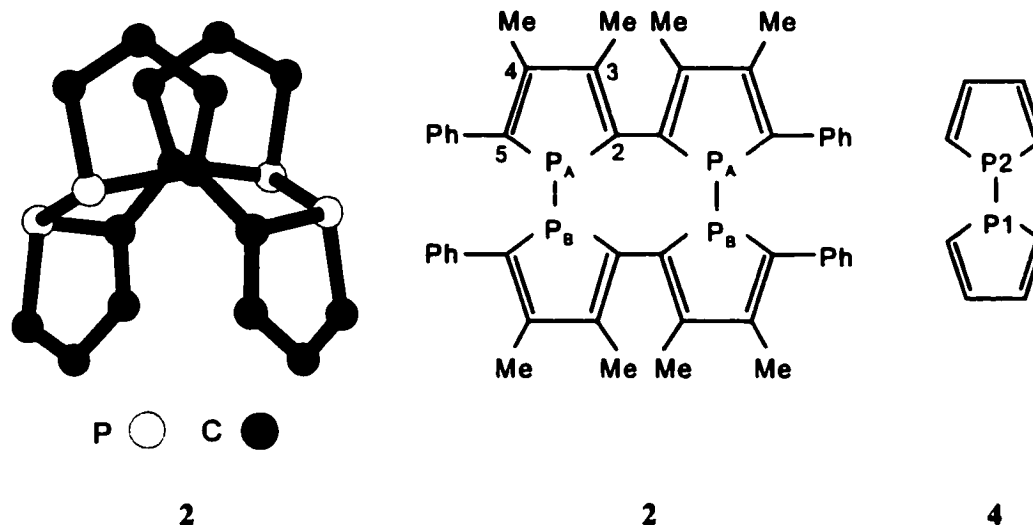


Figure 4.1 Molecular structures of the phosphole tetramer (2) and the model structure for 2 used for *ab initio* calculations (4). For clarity, the methyl and phenyl groups have been removed from the 3D representation on the left.

4.2 Experimental and Computational Details

The synthesis of the phosphole tetramer has been described previously.¹⁵² A sample was provided by Professor F. Mathey (DCPH Ecole Polytechnique).

Phosphorus-31 NMR Spectra: All ³¹P NMR spectra of stationary and MAS samples were acquired on Bruker MSL 200 (4.7 T), Chemagnetics CMX Infinity 200 (4.7 T) and Bruker AMX 400 (9.4 T) spectrometers operating at ³¹P NMR frequencies of 81.03 MHz and 161.98 MHz, respectively. Cross polarization⁵⁴ under the Hartmann-Hahn match condition and high-power proton decoupling were used for all NMR experiments.

At the lower field, double air bearing MAS probes were used with the sample packed in 7 mm o.d. (for the MSL) and 7.5 mm o.d. (for the CMX) zirconium dioxide rotors.

For the stationary sample, a ^1H $\pi/2$ pulse of 3.6 μs , contact time of 5 ms, acquisition time of 43 ms, and a recycle delay of 5 s were used. A sweep width of 24 kHz was used and 100 Hz of gaussian line broadening was applied before Fourier transformation. For spectra acquired with MAS at 1.50 or 2.00 kHz, similar pulse widths were used. The acquisition time was 20 ms and the sweep width was 40 kHz. A total of 4096 data points were acquired. Before Fourier transformation, 4096 zero points were added and 10 Hz of gaussian line broadening was applied.

A double air bearing MAS probe was used at the higher field as well, with the sample packed in a zirconium dioxide rotor (4 mm o.d.). For both MAS and stationary samples, a ^1H $\pi/2$ pulse of 3.6 μs with a contact time of 3 ms and a recycle delay of 10 s were used. For the stationary sample, an acquisition time of 8 ms was used. The sweep width was 65 kHz and 1024 points were acquired. The data were zero filled by 1024 points and 100 Hz of gaussian line broadening was applied. With MAS at 2.00 or 4.00 kHz the sweep width was 100 kHz and acquisition time was 30 ms. In total, 4096 points were acquired and zero filled by 4096 points. Gaussian line broadening of 20 Hz was applied before Fourier transformation. All ^{31}P NMR spectra are referenced to the primary standard, 85% $\text{H}_3\text{PO}_4(\text{aq})$ by setting the ^{31}P isotropic peak of solid $\text{NH}_4\text{H}_2\text{PO}_4$ to +0.8 ppm. Spectra of stationary samples at both fields were simulated using WSOLIDS.⁴⁹ Spectra of MAS samples were calculated using NMRLAB.⁵⁰ In our simulations, 10,000 crystallite orientations were used.

2D Spin-Echo ^{31}P NMR Spectrum: The 2D spin-echo NMR spectrum was acquired at 4.7 T (Bruker MSL 200) with a standard spin-echo pulse sequence using the phase cycling of Rance and Byrd.¹³⁸ A ^1H $\pi/2$ pulse of 5.5 μs was used with a contact time of 5.5 ms and a recycle delay of 10 s. For each t_1 increment, 64 transients were acquired for a total of 64 increments. Gaussian line broadenings of 200 Hz and 100 Hz were applied to the $F1$ and $F2$ projections respectively. The experimental and calculated 2D NMR spectra were processed in magnitude mode. The $F1$ projection was calculated using SpinEcho.¹³⁹

X-Ray Data Collection and Processing: The X-ray diffraction study was carried out by T. Stanley Cameron at Dalhousie University. A crystal of approximate dimensions 0.10 \times 0.10 \times 0.10 mm, recrystallized from chlorobenzene, was mounted on a glass fibre. A Rigaku AFC5R diffractometer was used for all measurements. Calculations were performed using teXsan.¹⁵⁵ The crystals have cell dimensions $a = 11.523$ (4) \AA , $b = 23.083$ (1) \AA , $c = 15.115$ (1) \AA , $\alpha = 89.99$ (1) $^\circ$, $\beta = 92.71$ (1) $^\circ$ and $\gamma = 89.99$ (1) $^\circ$. The merging R_{int} for the reflection data, merged on the assumption that the cell is monoclinic, is 3.04% for 244 equivalent reflections with $I > 5\sigma(I)$. The reflections for which $h = 2n + 1$ are weak in intensity and are generally diffuse. The strong reflections thus belong to a cell where $a = 5.762$ (1) \AA . Both cells have systematic absences consistent with a space group $P2_1/c$. The molecule for the structure in the larger cell refines to $R = 4.7\%$. The refinement used unit weights.

Computational Details: Theoretical calculations were performed with the Gaussian 94 suite of programs⁸³ running on an IBM RISC/6000 computer. Using RHF theory and

the GIAO method,⁷³ the phosphorus nuclear magnetic shielding tensors were determined for the model geometry, **4** (figure 4.1), of the phosphole tetramer based on the X-ray crystallography results for half of the molecule with the methyl and phenyl groups replaced by hydrogen atoms. A partial geometry optimization using HF theory with the 6-311G basis set on all the atoms was carried out. The P-P bond length, the dihedral angle between the rings, and the C-H bond lengths were fixed at the X-ray structure values for the optimization. *Ab initio* calculations of nuclear magnetic shielding were performed using the 6-311++G(d,p) basis set on phosphorus and neighbouring nuclei, while the 6-311G basis set was used on the remaining atoms to keep computation times within reasonable limits.¹⁵⁶ To compare with experimental results, the calculated phosphorus shielding is converted to chemical shift by using the absolute shielding of 328.35 ppm for the phosphorus reference, 85% H₃PO₄(aq).⁹⁰

4.3 Results and Discussion

4.3.1 Experimental Determination of Phosphorus Chemical Shift Tensors

The observed and calculated ³¹P NMR spectra of stationary samples of the tetramer are shown in figure 4.2, while NMR spectra of MAS samples are shown in figures 4.3 and 4.4. Best-fit parameters are given in table 4.1. In the text to follow, a brief account of how these parameters were obtained is presented.

The ³¹P NMR spectra of the phosphole tetramer with MAS indicate the presence of a unique phosphorus spin pair in the crystal^{153,154} and, as indicated in table 4.1, the

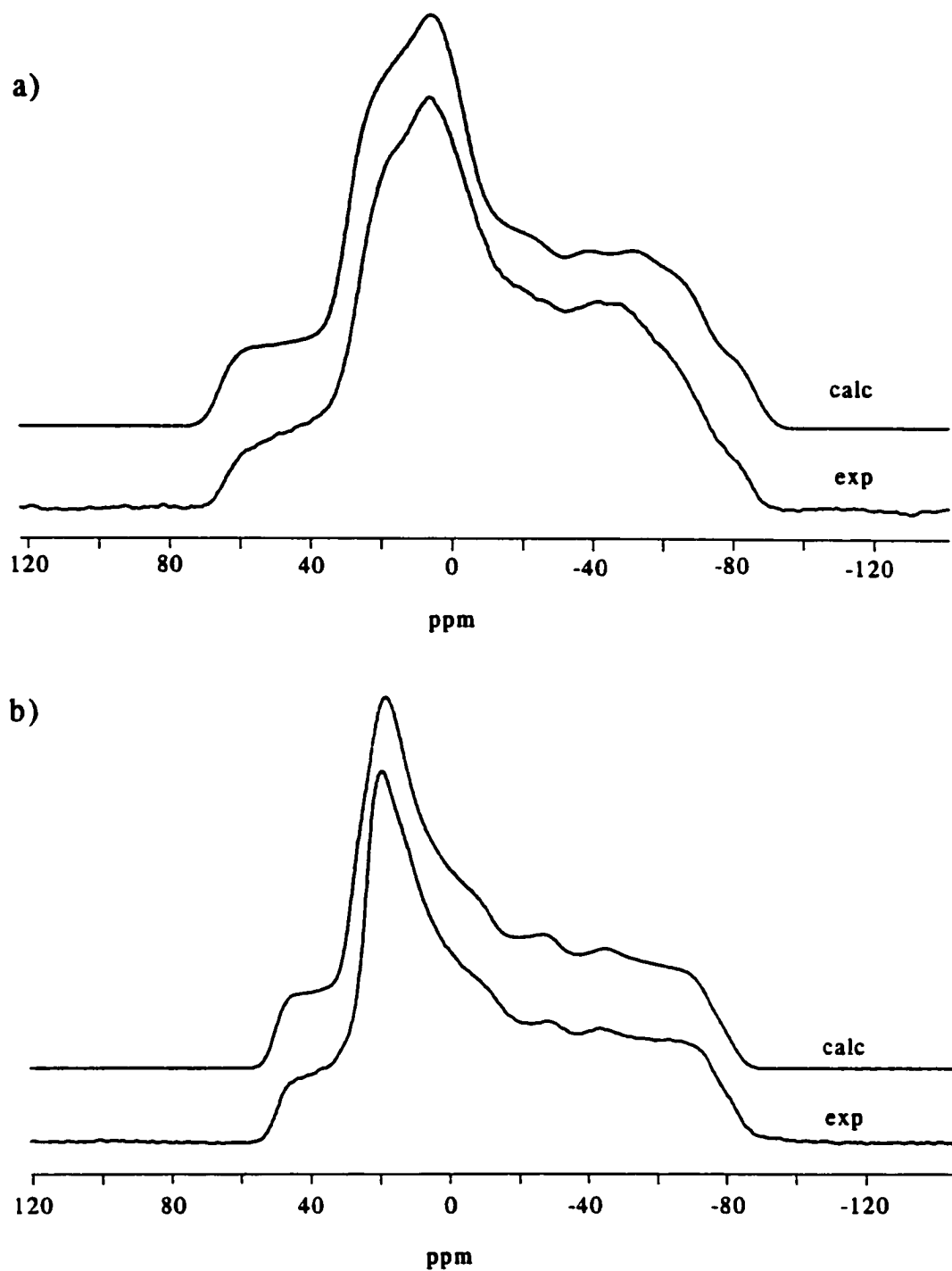


Figure 4.2 Experimental and calculated ^{31}P NMR spectra of stationary samples of the phosphole tetramer acquired at a) 4.7 T (2180 transients) and b) 9.4 T (458 transients). In both cases, 100 Hz gaussian line broadening was applied.

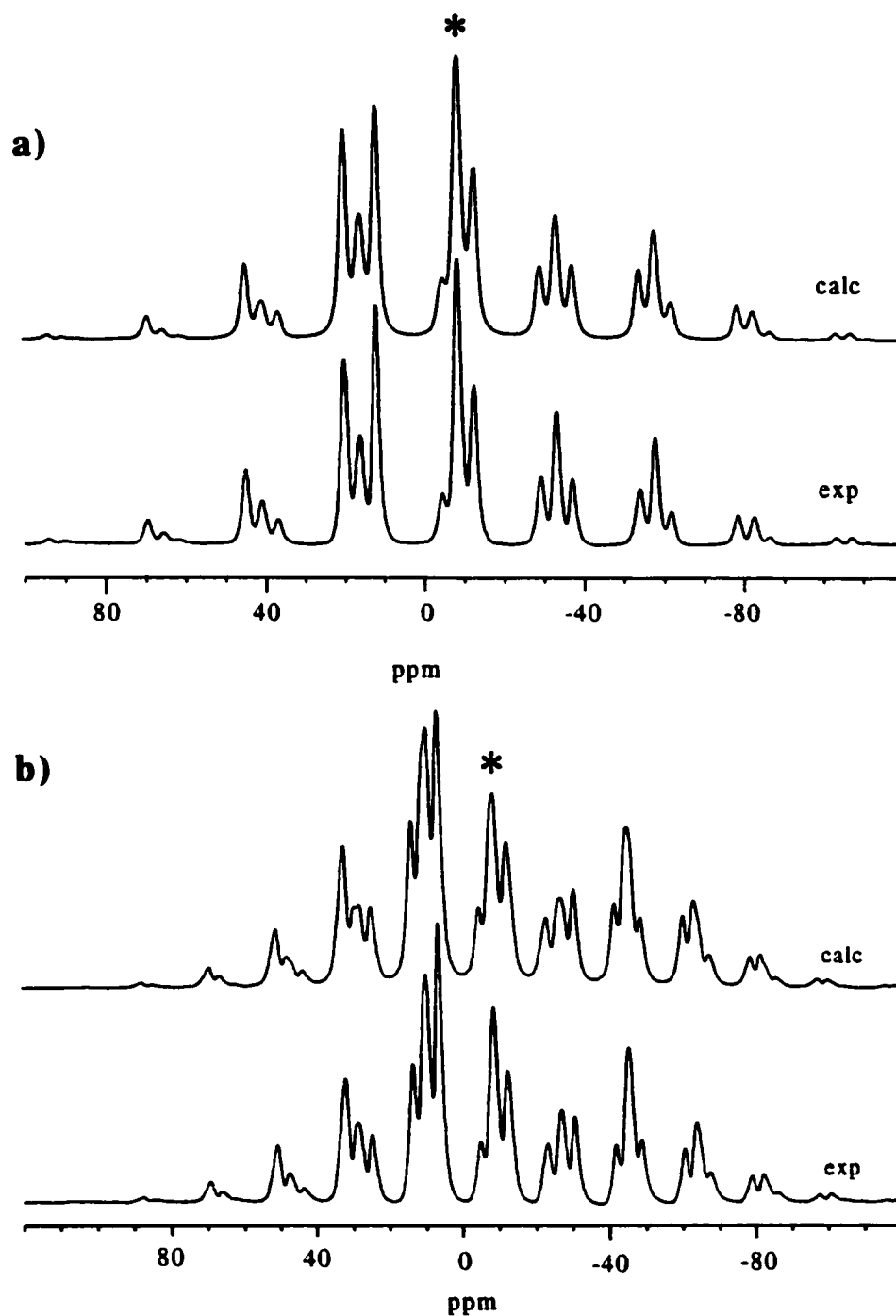


Figure 4.3 Experimental and calculated ^{31}P NMR spectra of crystalline powder samples of the phosphole tetramer spinning at the magic angle, acquired at 4.7 T for ν_{rot} of a) 2 kHz or b) at 1.5 kHz. For each spectrum 256 transients were acquired and 10 Hz of gaussian line broadening was applied. The asterisk indicates δ_{iso} .

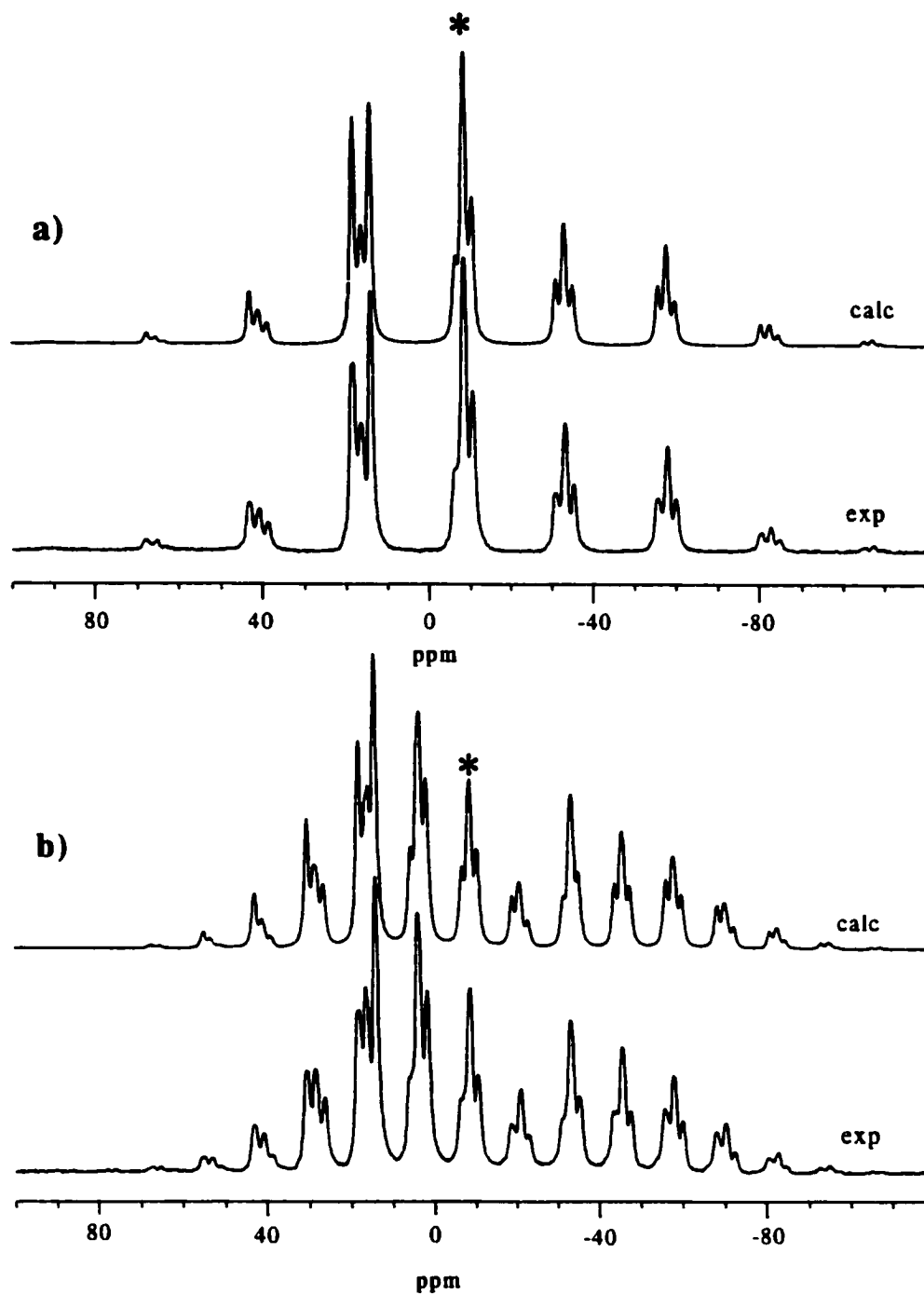


Figure 4.4 Experimental and calculated ^{31}P NMR spectra of crystalline powder samples of the phosphole tetramer spinning at the magic angle, acquired at 9.4 T for ν_{rot} of a) 4 kHz or b) 2 kHz. For each spectrum 512 transients were acquired and 20 Hz of gaussian line broadening was applied. The asterisk indicates δ_{iso} .

Table 4.1: Experimental and calculated isotropic phosphorus chemical shift, principal components^a of the phosphorus chemical shift tensors, Ω , and κ for the phosphole tetramer.

	Site	δ_{iso}	δ_{11}^b	δ_{22}^b	δ_{33}^b	Ω	κ
Experimental	P _A	-7.3	36	19	-77	113	0.7
	P _B	-9	35	18	-80	115	0.7
HF ^c	P1	-49.7	29	-18	-160	189	0.5
	P2	-53.7	23	-21	-163	186	0.5

^a All chemical shifts and Ω are given in ppm.

^b Estimated error on the principal components is ± 5 ppm.

^c GIAOs were used with the 6-311++G(d,p) basis set on phosphorus and adjacent atoms for structure 4. The 6-311G basis set was used on the remaining atoms.

NMR spectra have been analyzed accordingly. However, in the previously reported crystal structure of the phosphole tetramer²¹ there are two molecules in the asymmetric unit related by a pseudo mirror plane, hence four unique P-P bond lengths were reported; $r = 2.198(6)$, $2.191(6)$, $2.201(6)$ and $2.175(6)$ Å.²¹ Given the reported X-ray structure, one would expect to see potentially 8 different phosphorus sites in the ³¹P MAS NMR spectrum; similarly up to 16 different methyl carbon sites could be anticipated in the ¹³C MAS NMR spectrum. Experimentally, we observe only two unique ³¹P sites at both 4.7 and 9.4 T. Carbon-13 NMR spectra of MAS samples revealed two ¹³C sites at both fields ($\delta_{\text{iso}} = 15.5 \pm 0.1$ ppm and 17.1 ± 0.1 ppm). This apparent disagreement between our NMR results and the reported X-ray data

prompted a redetermination of the X-ray data. Repeated attempts were made to grow suitable single crystals; however, the best crystals obtained were less than ideal for X-ray diffraction. The R factor for our X-ray data is 0.047, compared to the R factor of 0.089 reported previously.²¹

The space group obtained from the new X-ray data is $P2_1/c$ with the asymmetric unit consisting of one molecule, rather than a space group of $P\bar{1}$ with two molecules in the asymmetric unit as had been previously reported,²¹ hence there are four crystallographically non-equivalent phosphorus sites and potentially eight non-equivalent methyl groups. In both cases, the unit cell contains four molecules. The molecular structure obtained from our X-ray data is essentially the same as the reported structure;²¹ however, our results indicate that the molecule contains a near perfect C_2 axis which relates the two phosphorus spin pairs (figure 4.1, structure on the left). This also reduces the number of different phosphorus sites from four to two and the number of different methyl carbons down to four. Given that the isotropic ^{31}P chemical shifts of the two phosphorus sites only differ by 1.7 ppm,^{153,154} it is not surprising that the four methyl carbons in the C_3 position (figure 4.1, middle structure) are isochronous; similarly for those in position 4.

Within the unit cell the two phosphorus spin pairs related by the near perfect C_2 axis have very similar environments though the two atoms of each pair are in different environments. From the diffuse reflections for which $h = 2n + 1$, it would appear that there are stacking errors in the a direction. The molecules are packed in layers approximately perpendicular to the a direction; however, there are too few reflections

for which $h = 2n + 1$ (51 out of a total of 766) to test this suggestion. Using equation 2.20, and an average P-P bond length of 2.192(9) Å from the new X-ray crystal structure, $R_{DD} = 1.873$ kHz with an estimated error of ± 0.05 kHz, based on the error in the X-ray data. Also, with four phosphorus nuclei in each molecule, each ^{31}P - ^{31}P spin pair is not truly isolated since there will be mutual dipolar coupling. From the internuclear distances between phosphorus nuclei that are not directly bonded to each other, the values of R_{DD} are 233 Hz ($r = 4.392$ Å) and 169 Hz ($r = 4.882$ Å), hence the NMR spectral features are largely determined by the much larger dipolar coupling between phosphorus nuclei that are directly bonded to each other rather than the phosphorus nuclei forming the other spin pairs in the molecule.

The value of R_{eff} and the relative signs of R_{eff} and $^1J(^{31}\text{P}, ^{31}\text{P})_{\text{iso}}$ are obtained from the 2D spin-echo experiment. Figure 4.5 shows the experimental and calculated $F1$ projections of the ^{31}P 2D spin-echo NMR spectrum of the phosphole tetramer. Using $J_{\text{iso}} = -362$ Hz,^{153,154} the best value of R_{eff} is 1.80 ± 0.05 kHz (figure 4.5(a)), which is in good agreement with the value calculated from the crystal structure. The difference, $R_{\text{eff}} - R_{DD} = 73 \pm 50$ Hz, is very small and could arise from vibrational averaging and possibly ΔJ . The smaller dipolar couplings between the phosphorus nuclei that are not directly bonded to each other most likely contribute to line broadening; however, it is possible they could slightly modify the value of R_{eff} . The sensitivity of the $F1$ projection to R_{eff} can be seen in figure 4.5(b), where the agreement between the experimental spectrum and one calculated using $R_{\text{eff}} = R_{DD} = 1.873$ kHz is not as good. As well, the

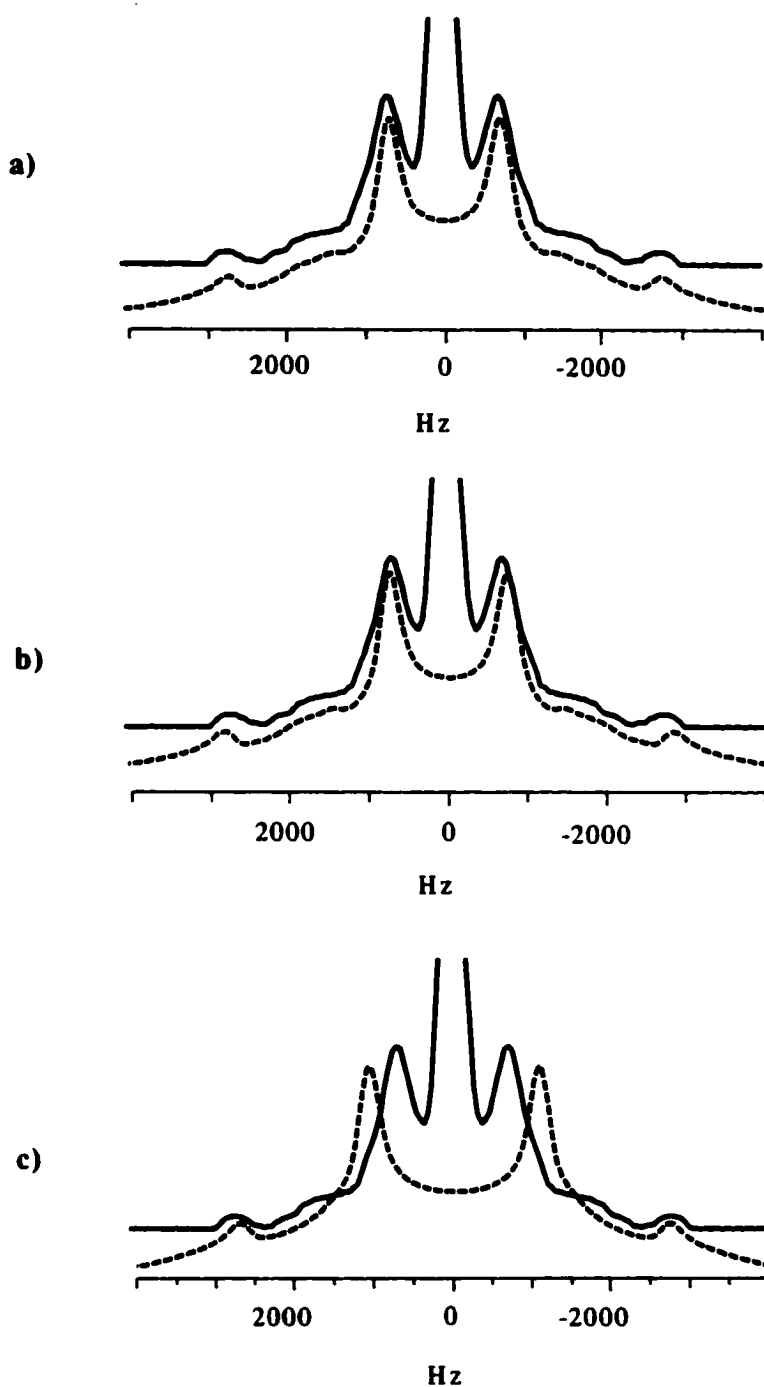


Figure 4.5 The calculated (dashed line) and experimental (solid line) *F1* projections of the 2D spin-echo ^{31}P NMR spectrum of the phosphole tetramer, acquired at 4.7 T. The best fit is obtained for a) $R_{\text{eff}} = 1.80$ kHz, $J_{\text{iso}} = -362$ Hz. If $R_{\text{eff}} = R_{\text{DD}} = 1.873$ kHz and $J_{\text{iso}} = -362$ Hz, the projection shown in b) is obtained. If $R_{\text{eff}} = 1.80$ kHz and $J_{\text{iso}} = +362$ Hz the splitting between the ‘horns’ is increased, as shown in d).

poor fit in the simulation using ${}^1J({}^{31}\text{P}, {}^{31}\text{P})_{\text{iso}} = + 362$ Hz with $R_{\text{eff}} = 1.80$ kHz (figure 4.5(c)) indicates that R_{eff} and ${}^1J({}^{31}\text{P}, {}^{31}\text{P})_{\text{iso}}$ must have opposite signs. In fact, for ${}^1J({}^{31}\text{P}, {}^{31}\text{P})_{\text{iso}}$ to be positive, R_{eff} must be less than 1.20 kHz to obtain a satisfactory fit of the two most intense peaks, which seems unreasonable in light of previous investigations ${}^1J({}^{31}\text{P}, {}^{31}\text{P})$.¹⁰ A negative J -coupling constant is consistent with INDO (intermediate neglect of differential overlap) calculations of ${}^1J({}^{31}\text{P}, {}^{31}\text{P})$. For example, the calculated ${}^1J({}^{31}\text{P}, {}^{31}\text{P})$ in $(\text{CH}_3)_2\text{P}-\text{P}(\text{CH}_3)_2$ is -254 Hz for a dihedral angle between the formal lone pairs of 74° ,¹⁵⁷ which is similar to the dihedral angle for the phosphole tetramer, 78° . The dependence of J on conformation is discussed in more detail in chapter 5.

The spin-spin coupling data (${}^1J({}^{31}\text{P}, {}^{31}\text{P})_{\text{iso}} = -362$ Hz and $R_{\text{eff}} = 1.80$ Hz) were used to simulate the experimental ${}^{31}\text{P}$ NMR spectra of a stationary sample shown in figure 4.2 to obtain the principal components of the chemical shift tensor given in table 4.1 and tensor orientation information discussed below. The experimental error in the principal components of the two chemical shift tensors is estimated to be ± 5 ppm. As a result, δ_{11} , δ_{22} , and δ_{33} are virtually identical for the two phosphorus chemical shift tensors.

The NMR spectra of MAS samples, shown in figure 4.3 and 4.4, demonstrate that the quality of the simulations using these new parameters is comparable to previously published work.^{153,154} Although the agreement between the calculated and experimental NMR spectra is good at both fields for stationary and MAS samples, there are some subtle differences between observed and calculated NMR spectra. These differences probably arise because neither of the two phosphorus spin pairs in the

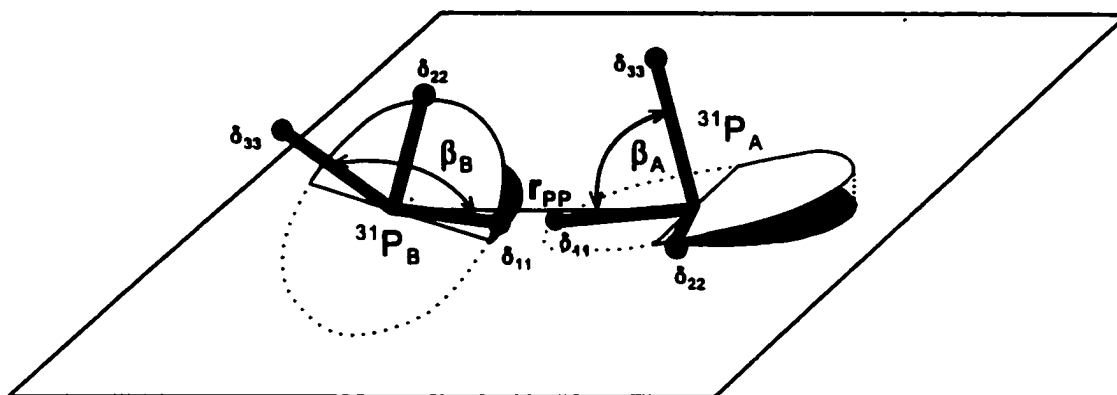


Figure 4.6 The relative orientation of the two phosphorus chemical shift tensors in the phosphole tetramer, determined from simulation of the ^{31}P NMR spectra acquired at 4.7 T and 9.4 T. For P_A , the Euler angles are $\alpha = 0^\circ$, $\beta = 78^\circ$ and $\gamma = 167^\circ$. For P_B , $\alpha = 82^\circ$, $\beta = 78^\circ$ and $\gamma = 167^\circ$.

molecule is strictly isolated (i.e., these spin pairs interact with one another).

As detailed in section 2.2, it is possible to obtain some chemical shift tensor orientation information from the NMR spectra of systems containing spin pairs. For the phosphole tetramer, the NMR line shape is particularly sensitive to $\Delta\alpha$, which is the dihedral angle between the δ_{33} components of the two phosphorus chemical shift tensors. Best-fit calculated NMR spectra were obtained with $\Delta\alpha = 82 \pm 3^\circ$. For both phosphorus chemical shift tensors, the δ_{33} component is tipped away from the

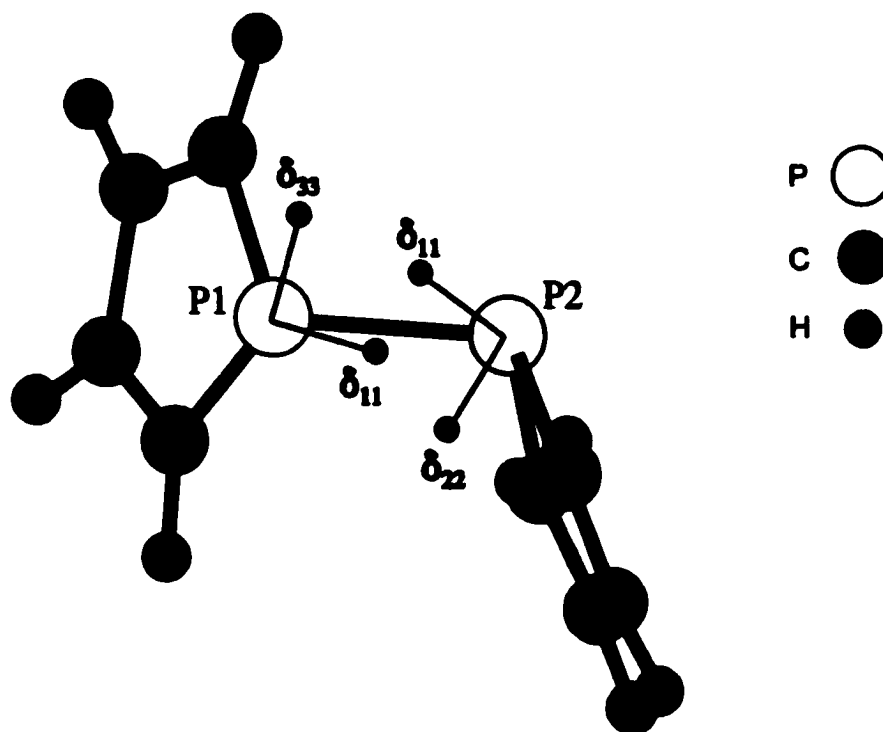


Figure 4.7 The phosphorus chemical shift tensor orientations for **4** determined by *ab initio* calculations. For P1, δ_{22} is out of the plane of the page, while for P2, δ_{33} is approximately out of the plane. In the case of P1, the δ_{11} and δ_{33} components are situated at angles of 19.3° and 79.1° respectively from r_{PP} . For P2, δ_{11} is at an angle of 27.5° and δ_{33} at an angle of 79.0° from r_{PP} .

internuclear vector by $\beta = 78 \pm 5^\circ$. In figure 4.6, the relative orientation of the two phosphorus chemical shift tensors is illustrated. In both cases, $\gamma = 167 \pm 5^\circ$ places the least shielded component, δ_{11} , closest to r_{PP} . Unfortunately, the ambiguities associated with the dipolar-chemical shift method prevent the determination of the absolute orientation of the chemical shift tensor in the molecular frame of reference.

4.3.2 *Ab Initio* Calculations of Phosphorus Shielding Tensors

As already mentioned, *ab initio* calculations may be used to help fix the relative

orientations (figure 4.6) in the molecular axis system (figure 4.7). *Ab initio* calculation results for the phosphorus nuclear magnetic shielding tensors in the model system, 4, for the phosphole tetramer are given in table 4.1. The two phosphorus sites are labelled as P1 and P2 rather than P_A and P_B (figure 4.1) since it is not known how the two sites in the NMR spectra should be assigned to the molecule. In a partial optimization of the geometry, the P-C bond lengths and the ring bond angles were allowed to change, resulting in changes that were largely within the errors stated in the crystal structure.²¹

The calculated tensor orientations, depicted in figure 4.7, are similar for both P1 and P2 with respect to the local geometry about each phosphorus nucleus. The δ_{11} components are closest to the P-P bond at angles of 19.3° and 27.5° for P1 and P2, respectively while the δ_{33} component for P1 forms an angle of 79.1° with the internuclear vector, and the corresponding angle for P2 is 79.0°. The calculated orientations of δ_{11} and δ_{33} for both phosphorus nuclei are consistent with the experimental observations. In addition, the dihedral angle between the δ_{33} principal components is 87.8°, in good agreement with the value of 82° determined by analysis of ³¹P NMR spectra. These *ab initio* calculations indicate that the δ_{33} components are not aligned in the general direction of the formal lone pairs, as had been previously suggested.^{153,154} In fact, δ_{22} is closest to the direction of the formal lone pairs. For the phosphole tetramer, the δ_{33} components are in the plane of the respective phosphole rings and approximately perpendicular to the P-P bond.

With respect to the magnitudes of the principal components, the experimental and calculated results show similar trends (table 4.1). The small calculated isotropic ³¹P

chemical shift difference, 4 ppm, between the two sites is consistent with experiment. The calculations also predict that δ_{11} and δ_{22} are similar, while δ_{33} is quite distinct, as reflected in the skews of about 0.5, comparable to the skews of 0.7 observed experimentally. However, the calculated isotropic chemical shifts are too small by about 43 ppm and the values of Ω are significantly larger than the experimental results.

Some reasons for this discrepancy between calculated and experimental results have been discussed in the previous chapter (section 3.3.3). In addition, the presence of formal lone pairs in the phosphole tetramer makes *ab initio* calculations more challenging. Inclusion of electron correlation has been shown to be important for obtaining good quantitative agreement between calculated and experimental shielding tensors in systems with formal lone pairs and multiple bonds.^{6,8,9,66} The importance of lone pairs in determining the nuclear magnetic shielding in phospholes has been demonstrated in a series of *ab initio* calculations on phospholes and the phospholide ion.¹⁵⁸ A recent investigation of some model phosphorus systems, for example PH_3 , indicates that the inclusion of electron correlation in *ab initio* calculations yields improved results for isotropic shielding.¹⁵⁹ The use of a model geometry consisting of half of the phosphole tetramer may also contribute to this discrepancy. Given these factors, quantitative agreement between the experimental and *ab initio* values is not expected, and seemingly good calculated results may be due to the fortuitous cancellation of errors. The primary goal with respect to *ab initio* calculations of nuclear magnetic shielding tensors is to obtain the tensor orientation in the molecular frame of reference. The results for TMPS (chapter 3) and previous results^{67,68,160} suggest that *ab*

ab initio methods reproduce well the experimental tensor orientation.

The relative orientation of the δ_{33} components of the two phosphorus shielding tensors in the phosphole tetramer appears to be related to the relative orientation of the adjacent phosphole rings (see figure 4.7). In the crystal structure, the rings are arranged such that the ring planes are approximately parallel to each other and twisted about the bridging P-P bond (figure 4.1, structure on the left). The twist angle between adjacent phosphole rings, ϕ_{ring} , ranges between 102° - 105° , which can be equally well described by the supplement angle range of 75° - 78° . This agrees well with $\Delta\alpha$ which is 82° determined experimentally and 87.8° from *ab initio* calculations. This structure-tensor relationship can be further demonstrated by *ab initio* calculation of the phosphorus tensor orientations at various values of ϕ_{ring} . Further calculations on our model system using $\phi_{\text{ring}} = 0^\circ, 70^\circ, 110^\circ$ and 180° indicate that the δ_{33} components are oriented relative to the local geometry in a similar manner as shown in figure 4.7, with $\Delta\alpha$ reflecting ϕ_{ring} ($\Delta\alpha = 0^\circ, 60.5^\circ, 109.5^\circ$ and 180° for the corresponding ϕ_{ring} listed above).

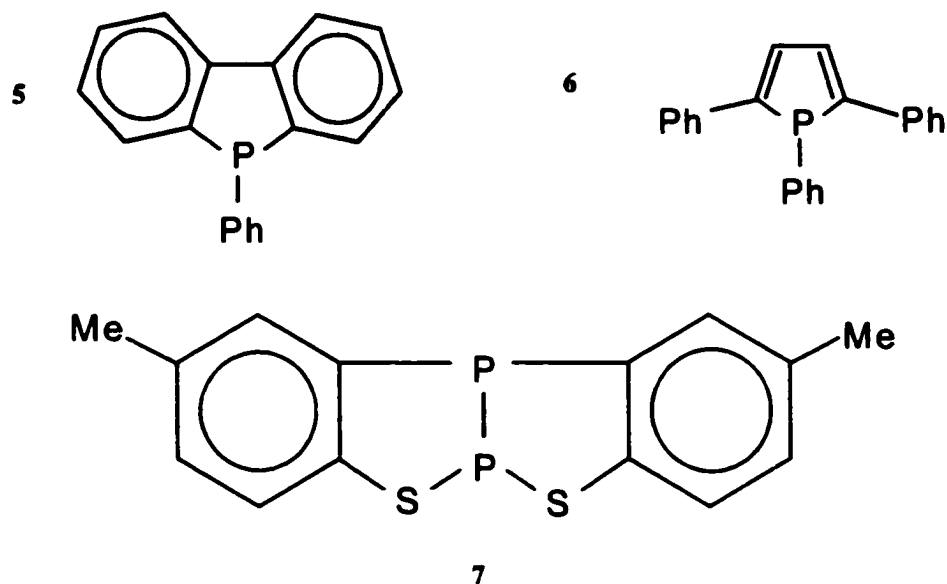
4.3.3 Trends in Phosphorus Chemical Shifts for Phospholes

There has been some discussion in the literature over the aromaticity of phospholes,¹⁶¹ recently revived by the synthesis of some planar phospholes.¹⁶² Aromaticity in phosphorus heterocycles was recently reviewed.¹⁶³ While ^{31}P solution NMR has been used routinely to characterize this important class of compounds, there are few comprehensive NMR investigations of the chemical shift tensors. The

phosphorus chemical shift tensors of several phosphole derivatives have also been characterized recently by solid-state NMR.¹⁶⁴ Comparison of the phosphorus chemical shift tensors in phospholes (table 4.2 with structures given in figure 4.8), reveals that δ_{33} in the phosphole tetramer is smaller compared to the other phospholes. For all phospholes investigated by ³¹P solid-state NMR thus far, the spans of the phosphorus chemical shift tensors are relatively small compared with systems where the phosphorus nucleus is known to be participating in a delocalized electron framework. For example, the span of the phosphorus chemical shift tensors in $\text{Mes}^*\text{P}=\text{PMes}^*$ is 1239 ppm¹⁷ and $\Omega = 779$ ppm in benzo-1,3,2-dithiaphospholium aluminum chloride.¹⁶⁵ The large spans in these systems have been attributed to the presence of low-lying excited states with the proper symmetry to mix with the highest occupied molecular orbitals (equation 2.44).¹⁶⁶

Table 4.2: Phosphorus chemical shift tensor principal components^a for some phospholes^b.

Compound	δ_{iso}	δ_{11}	δ_{22}	δ_{33}	Ω	κ	Ref.
5-phenyldibenzophosphole (two sites) (5)	-17.3	12	-19	-45	57	0	163 164
	-19	9	-21	-45	54	0	
1,2,5-triphenylphosphole (6)	0.7	30	-6	-22	52	0	167
<i>cis</i> -2,10-dimethyl[1,2,3]benzothia-diphospholo[2,3 <i>b</i>][1,2,3]benzothiadiphosphole (7)	75.3 (PS ₂)	129	122	-25	154	0.9	168
	53.7 (PC ₂)	190	25	-54	244	0	

^a All chemical shifts and Ω are given in ppm.^b Structures are shown in figure 4.8.**Figure 4.8** Molecular structures of compounds 5, 6, and 7 in table 4.2.

4.4 Conclusions

The analysis of ^{31}P NMR spectra of a stationary and MAS samples of the phosphole tetramer indicates that the principal components of the two phosphorus chemical shift tensors are virtually identical. Regarding the phosphorus chemical shift tensor orientation, the δ_{11} components of both tensors are closest to \mathbf{r}_{PP} , while the δ_{33} components are tilted away at an angle of 78° , in addition to being twisted relative to each other by an angle of 82° . This latter angle is thought to reflect the relative orientation of the phosphole rings, which are related by a dihedral angle ranging from 75° to 78° . *Ab initio* results support the experimental conclusions and indicate that the δ_{33} components are not aligned with the formal lone pairs on the phosphorus nuclei. The characterization of the phosphorus chemical shift tensors in the phosphole tetramer is greatly aided by the 2D spin-echo experiment as well as by employing *ab initio* calculations to suggest an orientation of the tensor in the molecular frame.

Chapter 5: $^1J(^{31}\text{P}, ^{31}\text{P})$ Coupling Tensors - Conformational Studies in Model Systems and Structural Characterization of $[\text{Ph}_3\text{P-PPh}_2][\text{GaCl}_4]$

5.1 Introduction

Phosphinophosphonium cations are representative of a new class of compounds;²² however, the lack of X-ray diffraction data^a means that alternative methods such as NMR are vital for characterizing these compounds in the solid state. In addition, $^1J(^{31}\text{P}, ^{31}\text{P})$ is not observed in solution NMR for some of these compounds,¹⁶⁹ most likely due to intermolecular exchange. One can apply the dipolar-chemical shift method (section 2.2.2) to characterize the phosphorus chemical shift tensors as well as the $^{31}\text{P}, ^{31}\text{P}$ spin-spin coupling interactions. From the dipolar coupling constant, the P-P bond length may be estimated according to equation 2.20. However, as discussed in section 2.1.6, the Hamiltonians describing the dipolar interaction and the contribution from the anisotropy in \mathbf{J} are identical in form; hence, they are inseparable experimentally. For this reason, accurate measurement of internuclear distances via R_{DD} requires some knowledge of ΔJ .

Comprehensive understanding of how trends in \mathbf{J} reflect molecular and electronic structure is still lacking, primarily a consequence of the difficulty in characterizing the complete tensor experimentally. For one-bond J -coupling involving phosphorus nuclei,

^a Since the preparation of this chapter, the X-ray crystal structures of $[\text{Ph}_3\text{P-PPh}_2][\text{GaCl}_4]$ and $[\text{Ph}_3\text{P-PPh}_2][\text{SO}_3\text{CF}_3]$ have been obtained (N. Burford, T. Stanley Cameron, P. J. Ragoonna, E. Ocampo-Mavarez, M. Gee, Robert McDonald, and R. E. Wasylshen, *J. Am. Chem. Soc.* 123, 7947 (2001)).

reports in the literature indicates that ΔJ may be substantial,^{128,170} however, as is evident from the work on TMPS (chapter 3) and the phosphole tetramer (chapter 4), it is difficult to distinguish the effect of ΔJ from the consequences of vibrational averaging. A possible avenue for determining the contribution of ΔJ to R_{eff} is via *ab initio* calculations. Details of *ab initio* methods for calculating J have been discussed in section 2.3.2. In addition, first-principles calculations of $^1J(^{31}\text{P}, ^{31}\text{P})$ allow one to investigate the influence of formal electron lone pairs as well as determine the dependence on conformation of the lone pairs with respect to rotation about the P-P bond. While variable temperature NMR studies in solution have provided some insight,³² many conformations are not experimentally accessible.

For a representative phosphinophosphonium salt, $[\text{Ph}_3\text{P}-\text{PPh}_2][\text{GaCl}_4]$, compound **3** (figure 5.1(a)), the calculation of $^1J(^{31}\text{P}, ^{31}\text{P})$ has been used to obtain an estimate of R_{DD} , from the experimentally measured value of R_{eff} (see equation 2.29). From R_{DD} the P-P bond length may be estimated according to equation 2.20. $\text{H}_3\text{P}-\text{PH}_2^+$ is used as a model system for $\text{Ph}_3\text{P}-\text{PPh}_2^+$ since *ab initio* computational methods currently available are limited to small molecules for J -coupling calculations. To further examine the relationship between molecular structure and trends in J , calculations on $\text{H}_2\text{P}-\text{PH}_2$ have also been performed. In addition, the phosphorus chemical shift tensors have been characterized and these experimental results are complemented by *ab initio* calculation of phosphorus shielding tensors in a model compound, $(\text{CH}_3)_3\text{P}-\text{P}(\text{CH}_3)_2^+$.

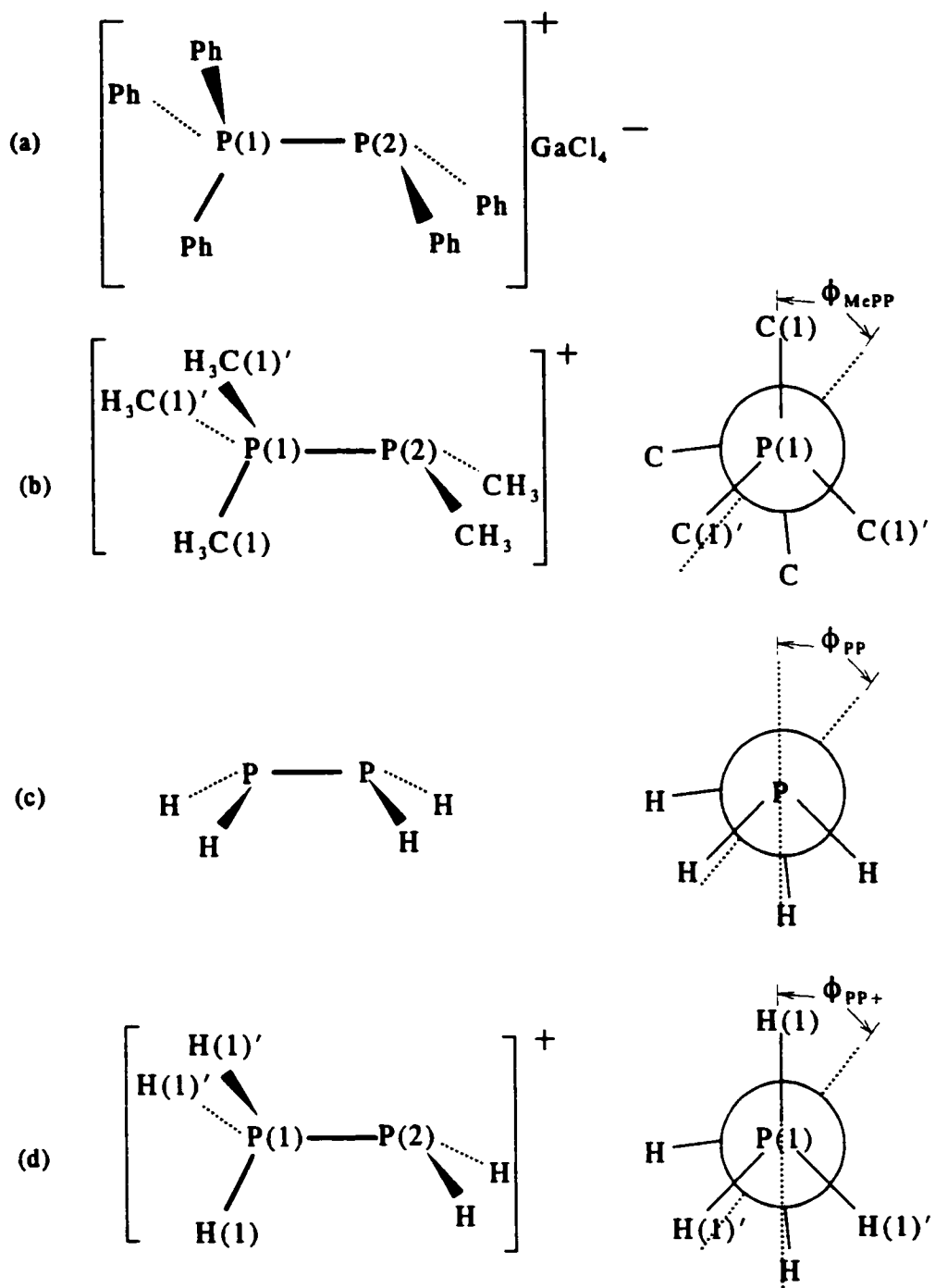


Figure 5.1 Structures of the molecules discussed in this chapter; (a) $[\text{Ph}_3\text{P}-\text{PPh}_2][\text{GaCl}_4]$, indicating the labelling convention for the two phosphorus nuclei; (b) $(\text{CH}_3)_3\text{P}-\text{P}(\text{CH}_3)_2^+$ and a Newman projection defining ϕ_{McPP} ; (c) $\text{H}_2\text{P}-\text{PH}_2$ and a Newman projection defining ϕ_{PP} ; (d) $\text{H}_3\text{P}-\text{PH}_2^+$ and a Newman projection defining, ϕ_{PP^+} .

5.2 Experimental and Computational Details

Sample Preparation: A sample of $[\text{Ph}_3\text{P-PPh}_2][\text{GaCl}_4]$ was provided by Dr. Edgar Ocando-Mavarez and Professor Neil Burford. All samples for NMR work were prepared in an inert atmosphere as this compound is air sensitive. Details and suggestions for handling air-sensitive NMR samples are presented in Appendix 2.

NMR Spectra: Phosphorus-31 NMR spectra were acquired for stationary or MAS samples of powdered crystalline $[\text{Ph}_3\text{P-PPh}_2][\text{GaCl}_4]$ at applied magnetic fields of 4.7 T (Chemagnetics CMX 200 spectrometer) and 9.4 T (Bruker AMX 400 spectrometer).

The standard CP experiment⁵⁴ with high-power proton decoupling was used in both cases. For experiments at 4.7 T, the sample was packed into a 4 mm (o.d.) zirconium oxide rotor and a proton 90° pulse of 3.0 μs , contact time of 5.0 ms, and recycle delay of between 5 and 8 s were used. Typical sweep widths were 50 kHz with acquisition times of 41 ms. Before Fourier transformation, 2048 points of zero filling was applied. Experiments at 9.4 T were performed on a sample packed into a 2.5 mm (o.d.) zirconium oxide rotor. Parameters similar to those for experiments at 4.7 T were used. All ^{31}P NMR spectra are referenced to the primary standard, 85% $\text{H}_3\text{PO}_4(\text{aq})$, by setting the isotropic peak in the ^{31}P NMR spectrum of solid $\text{NH}_4\text{H}_2\text{PO}_4$ to +0.8 ppm. Gaussian line broadening of between 20 and 40 Hz for the spectra of MAS samples and between 100 and 200 Hz for spectra of stationary samples was applied.

The 2D spin-echo experiment was performed at 4.7 T using parameters identical to the 1D experiments. For each t_1 increment, 224 transients were acquired, for a total of 64 increments. The sweep width in the F_2 dimension was 28.6 kHz and the

acquisition time was 12 ms. In the $F1$ dimension, the sweep width was 12.5 kHz. Gaussian line broadening of 200 Hz in $F1$ and 100 Hz in $F2$ was applied, followed by processing in magnitude mode. The experimental data were zero filled to 512 points \times 512 points.

The spectra of MAS samples were simulated using the program NMLAB,⁵⁰ while the spectra of stationary samples were simulated using WSOLIDS.⁴⁹ The $F1$ projection of the 2D spin-echo spectrum was calculated using SpinEcho.¹³⁹

Computational Details: Calculation of nuclear magnetic shielding tensors for $(\text{CH}_3)_3\text{P}-\text{P}(\text{CH}_3)_2^+$ was carried out at the HF level using the 6-311G** basis set on the phosphorus and carbon atoms and 3-21G on the hydrogen atoms. The structure was first optimized at the HF level using the 6-311G** basis set on all atoms, resulting in (see figure 5.1(b) for atom labelling) $\text{P}(1)-\text{P}(2) = 2.219 \text{ \AA}$, $\text{P}(2)-\text{C} = 1.848 \text{ \AA}$, $\text{P}(1)-\text{C}(1) = 1.816 \text{ \AA}$, $\text{P}(1)-\text{C}(1)' = 1.814 \text{ \AA}$, $\text{C}(1)-\text{P}(1)-\text{C}(1)' = 108.3^\circ$, $\text{C}(1)'\text{-P}(1)-\text{C}(1)' = 108.2^\circ$, $\text{C}-\text{P}(2)-\text{C} = 102.1^\circ$, $\text{C}(1)'\text{-P}(1)-\text{P}(2) = 108.0^\circ$ and $\phi_{\text{MePP}} = 180^\circ$. ϕ_{MePP} is the dihedral angle between the plane containing the $\text{P}(1)-\text{P}(2)$ bond and also bisecting the $\text{C}-\text{P}(2)-\text{C}$ bond angle and the plane containing the $\text{P}(1)-\text{P}(2)$ and $\text{P}(1)-\text{C}(1)$ bonds. All C-H distances were 1.08 \AA and H-C-H bond angles were 109.5° . All calculations were performed with Gaussian 98⁸⁴ using an IBM RS/6000 workstation.

Indirect ^{31}P , ^{31}P spin-spin coupling tensors for $\text{H}_2\text{P}-\text{PH}_2$ and $\text{H}_3\text{P}-\text{PH}_2^+$ were calculated using the MCSCF approach with complete active space self-consistent field (CASSCF) wavefunctions^{78,108} as implemented in DALTON, an *ab initio* electronic

structure program,¹⁷¹ installed on an IBM RS/6000 workstation. For CASSCF wavefunctions, it is necessary to choose active and inactive space combinations. The active space consists of the molecular orbitals into which electrons may be placed to produce configurations that are used to construct the electronic wavefunctions. It usually consists of a number of occupied and virtual molecular orbitals. The inactive space consists of the molecular orbitals which remain doubly occupied for all electron configurations. The selection of active and inactive spaces was made based on MP2 natural molecular orbital occupation numbers and energies.¹⁷² The inactive/active space used are given in the following format: for each molecular orbital symmetry, the number of inactive orbitals and active orbitals is given. For example, 1010/2131 indicates that there are four different molecular orbital symmetries. For the first symmetry type, 1 molecular orbital is inactive and 2 are active, 0 inactive and 1 active for the second symmetry, 1 inactive and 3 active for the third symmetry, and 0 inactive and 1 active for the fourth symmetry. Calculations of J for $\text{H}_2\text{P-PH}_2$ and $\text{H}_3\text{P-PH}_2^+$ were performed with cc-pVTZ (correlation-consistent polarization valence triple-zeta) basis sets¹⁷³ on all atoms.

An experimental geometry¹⁷⁴ was used for $\text{H}_2\text{P-PH}_2$ with the exception of ϕ_{PP} which was varied between 0° and 180° in 30° increments, keeping all other bond lengths and bond angles fixed. ϕ_{PP} is the dihedral angle between the planes which both contain the P-P bond but each one bisects one of the H-P-H bond angles (see figure 5.1(c)). The bond lengths and angles are as follows: P-P = 2.2191 Å, P-H = 1.4155 Å, H-P-H = 92.0° . The experimental value of ϕ_{PP} is 74.0° . For $\text{H}_2\text{P-PH}_2$, the

inactive/active space used to calculate ${}^1J(^{31}\text{P}, ^{31}\text{P})$ as a function of ϕ_{PP} (table 5.2) consisted of 55/54, which corresponds to a total of two unoccupied orbitals in the active space, one per molecular orbital symmetry. For studying the effect of other geometry factors (table 5.4), an inactive/active space consisting of 55/43, which does not include any unoccupied orbitals, was used.

For $\text{H}_3\text{P-PH}_2^+$, the geometry was optimized at the HF level with the 6-311++G(3df,3pd) basis set on all atoms. The optimized structure is as follows (see figure 5.1(d) for atom labelling): $\text{P}(1)\text{-P}(2) = 2.209 \text{ \AA}$, $\text{P}(1)\text{-H}(1) = 1.387 \text{ \AA}$, $\text{P}(1)\text{-H}(1)' = 1.386 \text{ \AA}$, $\text{P}(2)\text{-H} = 1.403 \text{ \AA}$, $\text{H}(1)\text{-P}(1)\text{-P}(2) = 116.6^\circ$, $\text{H}(1)'\text{-P}(1)\text{-P}(2) = 110.2^\circ$, $\text{H-P}(2)\text{-P}(1) = 92.4^\circ$, $\text{H}(1)'\text{-P}(1)\text{-H}(1)' = 106.3^\circ$, and $\text{H-P}(2)\text{-H} = 96.5^\circ$. Similar to the calculations for $\text{H}_2\text{P-PH}_2$, the angle ϕ_{PP^+} was varied between 0° and 180° . ϕ_{PP^+} is the dihedral angle between the plane containing the $\text{P}(1)\text{-P}(2)$ bond and also bisecting the $\text{H-P}(2)\text{-H}$ bond angle and the plane containing the $\text{P}(1)\text{-P}(2)$ and $\text{P}(1)\text{-H}(1)$ bonds. MCSCF calculations for the dependence of ${}^1J(^{31}\text{P}, ^{31}\text{P})$ on ϕ_{PP^+} for $\text{H}_3\text{P-PH}_2^+$ (table 5.3) were performed using an inactive/active space 10/8, i.e., one unoccupied orbital in the active space.

5.3 Results and Discussion

5.3.1 Phosphorus-31 NMR Spectra of $[\text{Ph}_3\text{P-PPh}_2][\text{GaCl}_4]$

The ${}^{31}\text{P}$ NMR spectra for a crystalline powder sample of $[\text{Ph}_3\text{P-PPh}_2][\text{GaCl}_4]$ are shown in figures 5.2 (obtained at 4.7 T) and 5.3 (obtained at 9.4 T) for various MAS rates. From the spectra acquired at the higher MAS rates, the isotropic chemical shifts

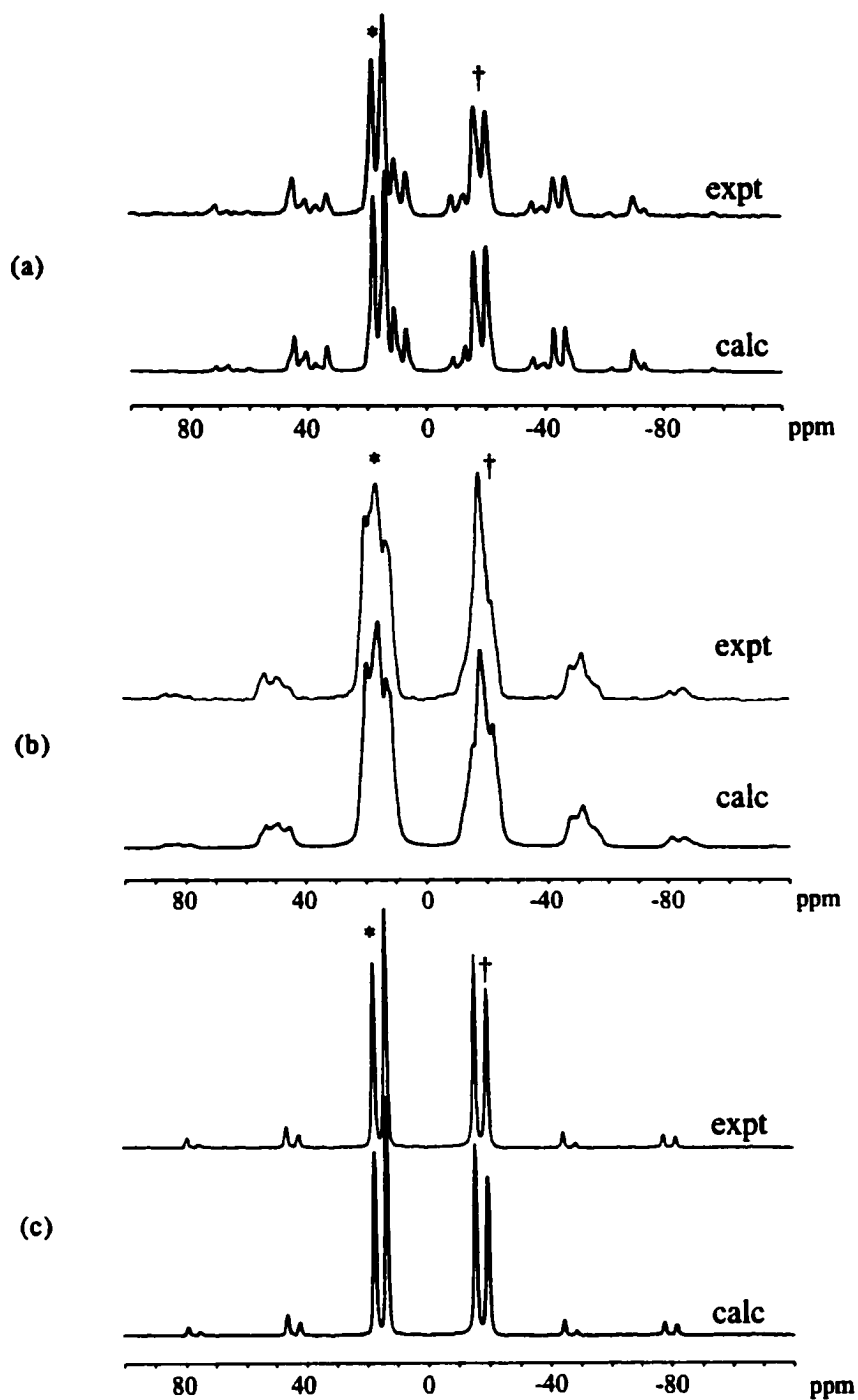


Figure 5.2 Experimental and calculated ^{31}P NMR spectra of MAS samples of $[\text{Ph}_3\text{P-PPh}_2][\text{GaCl}_4]$, acquired at 4.7 T. The spinning rates are (a) 2.17 kHz (128 transients), (b) 2.72 kHz (256 transients), and (c) 5.02 kHz (256 transients). In each case, 40 Hz of gaussian line broadening was applied. The asterisk and dagger mark the isotropic region for P(1) and P(2) respectively.

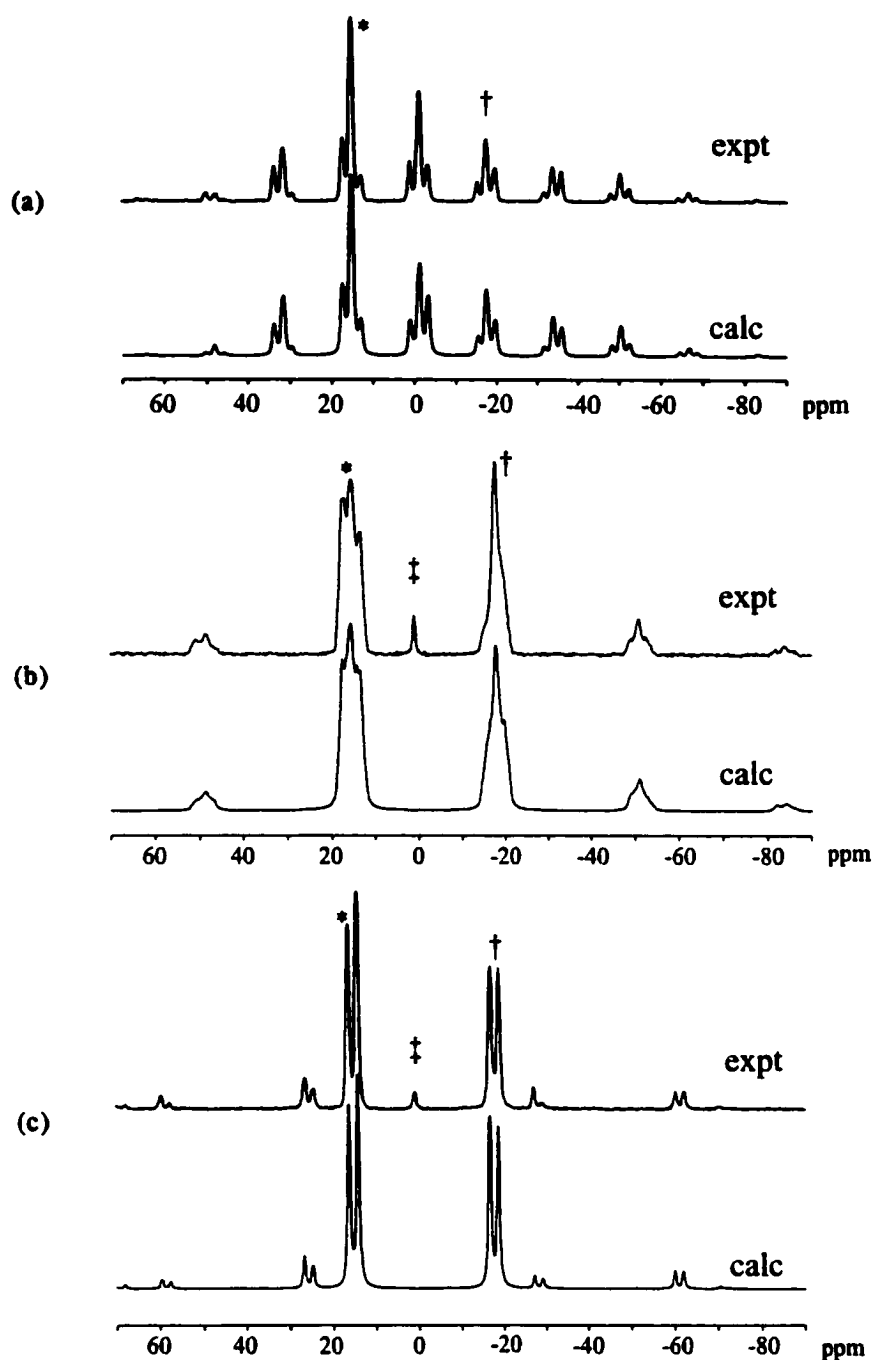


Figure 5.3 Experimental and calculated ^{31}P NMR spectra of MAS samples of $[\text{Ph}_3\text{P-PPh}_2][\text{GaCl}_4]$, acquired at 9.4 T. The spinning rates are (a) 2.65 kHz, (b) 5.38 kHz, and (c) 7.03 kHz. In each case, 512 transients were acquired and 20 Hz of gaussian line broadening was applied. The asterisk and dagger mark the isotropic region for P(1) and P(2) respectively. A signal possibly due to a decomposition product is indicated by ‡.

for each phosphorus nucleus and the magnitude of $^1J(^{31}\text{P}, ^{31}\text{P})_{\text{iso}}$ may be estimated and refined in subsequent simulations of all the NMR spectra. The data are summarized in table 5.1. The assignment of the phosphorus chemical shifts to sites in the molecule is made on the basis of known trends and on results of *ab initio* calculation of phosphorus nuclear magnetic shielding in a model system, $(\text{CH}_3)_3\text{P}-\text{P}(\text{CH}_3)_2^+$ (*vide infra*).

Calculations for nuclear magnetic shielding in $\text{Ph}_3\text{P}-\text{PPh}_2^+$ would entail a time-consuming geometry optimization since an experimental geometry is not available.

For this compound, $[\text{Ph}_3\text{P}-\text{PPh}_2][\text{GaCl}_4]$, the phosphorus chemical shifts obtained from a sample dissolved in CH_2Cl_2 compared to the solid state differ by less than 8 ppm. The impurity peak in figure 5.3 is attributed to a decomposition product. It is not observed in the spectra at 4.7 T (figure 5.2), probably due to differences in the effectiveness of the rotors at excluding air from the sample.

The difference between the isotropic chemical shifts of the two coupled phosphorus nuclei is 33.2 ppm, which is 2.61 kHz or 5.38 kHz at an applied magnetic field of 4.7 T or 9.4 T respectively. These conditions are ideal for the rotational resonance (RR) experiment,¹⁷⁵ whereby the dipolar coupling interaction is restored for a homonuclear spin pair when the difference between the isotropic chemical shifts is $n\nu_{\text{rot}}$ where n is typically 1 to 3. Indeed, the ^{31}P NMR spectra shown in figures 5.2(b) and 5.3(a),(b) were acquired under conditions of RR. While R_{eff} may have been measured from RR by generating Zeeman magnetization exchange curves, for this compound it was simpler to use the results of the 2D spin-echo experiment, presented below, to obtain R_{eff} .

Table 5.1: Phosphorus chemical shift tensor principal components and spin-spin coupling parameters for $[\text{Ph}_3\text{P-PPh}_2][\text{GaCl}_4]$.

parameter	P(1)		P(2)	
solution: ^a				
δ_{iso} / ppm	15.4		-10.6	
$^1J(^{31}\text{P}, ^{31}\text{P})$ / Hz	not observed			
solid state and <i>ab initio</i> data:				
	expt.	<i>ab initio</i> ^b	expt.	<i>ab initio</i> ^b
δ_{iso} / ppm ^c	15.4	-40	-17.8	-79
δ_{11} / ppm ^d	36	-22	23	3
δ_{22} / ppm	23	-43	-8	-73
δ_{33} / ppm	-14	-56	-68	-167
Ω / ppm	50	34	91	170
κ	0.48	0.28	0.32	0.10
$^1J_{\text{iso}}(^{31}\text{P}, ^{31}\text{P})$ / Hz	-323 ± 2			
R_{eff} / kHz	1.70 ± 0.05			

^a E. Ocando, N. Burford, unpublished results. The solvent is CH_2Cl_2 .

^b *Ab initio* data are for the optimized $(\text{CH}_3)_3\text{P-P}(\text{CH}_3)_2^+$ structure. Calculations are carried out at the HF level using 6-311G** basis set on phosphorus and carbon atoms while the 3-21G basis set was used on all the hydrogen atoms.

^c Experimental error on δ_{iso} is ± 0.1 ppm, obtained from spectra of MAS samples.

^d Experimental error on the principal components is ± 2 ppm, obtained from spectra of stationary samples.

The $F1$ projection from the 2D spin-echo ^{31}P NMR spectrum is shown in figure 5.4 along with simulations using opposite signs (figure 5.4(a)) and the same signs for $^1J(^{31}\text{P}, ^{31}\text{P})_{\text{iso}}$ and R_{eff} (figure 5.4(b)). From these simulations, $R_{\text{eff}} = 1.70 \pm 0.05$ kHz and $^1J(^{31}\text{P}, ^{31}\text{P})_{\text{iso}}$ is clearly negative relative to R_{eff} . Using the data from ^{31}P NMR spectra of MAS samples and the spin-spin coupling data from the 2D spin-echo spectrum, the ^{31}P NMR spectra obtained at two applied magnetic fields for a stationary sample may be analyzed. The best simulations are shown in figure 5.5 and the principal components of the two phosphorus chemical shift tensors as well as spin-spin coupling parameters which give the best overall fit to all the experimental spectra are given in table 5.1. The two features of note in the phosphorus nuclear magnetic shielding are that one of the phosphorus nuclei is more shielded than the other and its chemical shift tensor has a larger span. Based on known trends in phosphorus shielding, that phosphines are in general more shielded than phosphonium centres,^{4,176} the spectra may be assigned to the phosphorus nuclei as in table 5.1. In addition, calculated phosphorus chemical shift tensors in $(\text{CH}_3)_3\text{P}-\text{P}(\text{CH}_2)_2^+$ indicate that the phosphine centre, P(2), is more shielded and has a significantly larger span (table 5.1).

Regarding shielding tensor orientations in the molecular frame of reference, the position of the δ_{33} components relative to the P-P bond, given by β , and the orientations relative to each other, given by $\Delta\alpha$, have been determined experimentally. For P(1) and P(2), $\beta = 81 \pm 2^\circ$ and $78 \pm 2^\circ$ respectively and $\Delta\alpha = 25^\circ$. The third Euler angle, γ , is $2 \pm 5^\circ$ for P(1) and $78 \pm 2^\circ$ for P(2). Note that γ for P(1) has a larger error than γ for P(2). The angle γ determines whether δ_{11} or δ_{22} is closest to r_{pp} . The spectrum is

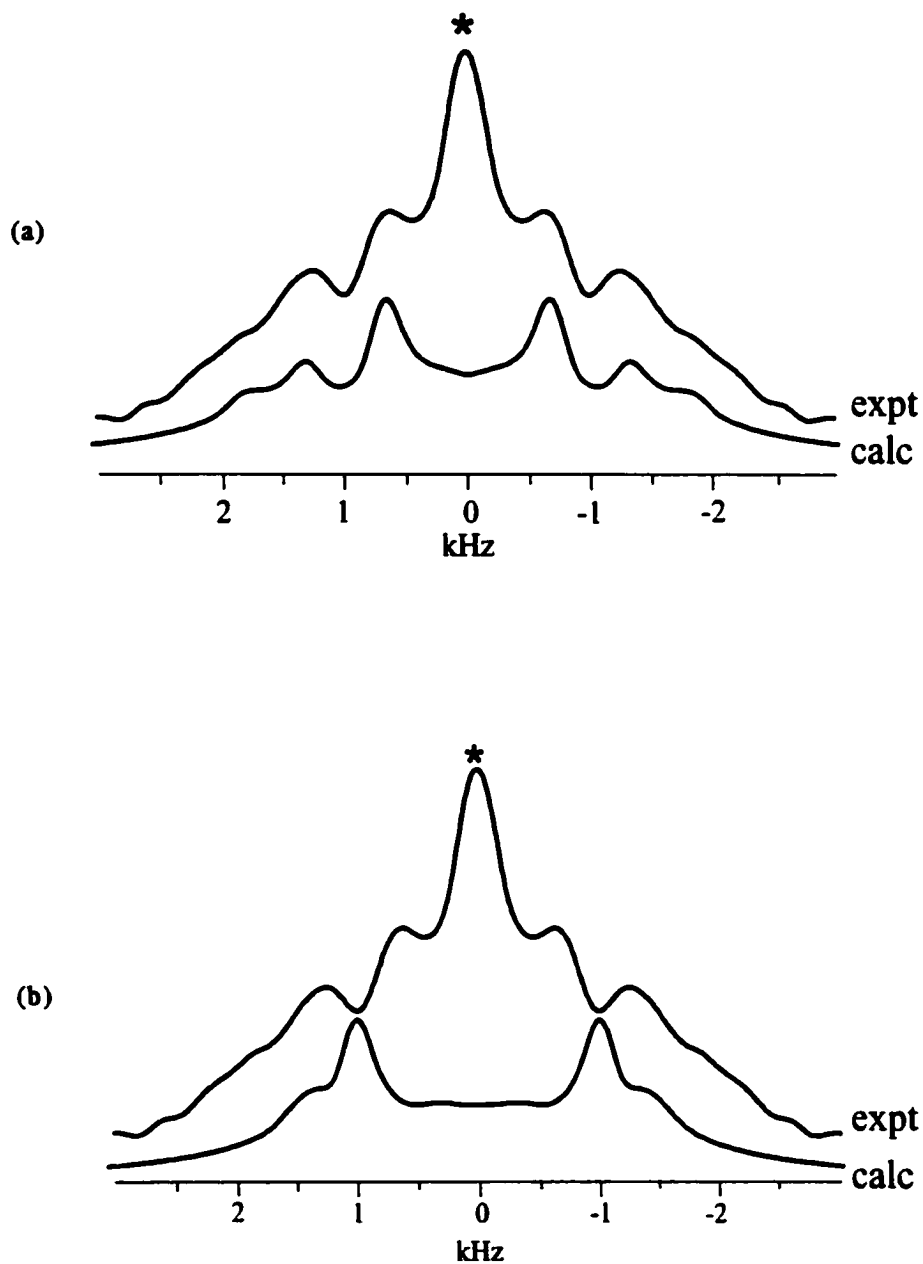


Figure 5.4 Experimental and calculated F_1 projections of the 2D spin-echo ^{31}P NMR spectrum of $[\text{Ph}_3\text{P-PPh}_2][\text{GaCl}_4]$ acquired at 4.7 T. The peak marked by an asterisk is an experimental artifact. Simulations are shown with $R_{\text{eff}} = 1.70$ kHz and (a) $^1J(^{31}\text{P}, ^{31}\text{P})_{\text{iso}} = -323$ Hz and (b) $^1J(^{31}\text{P}, ^{31}\text{P})_{\text{iso}} = +323$ Hz.

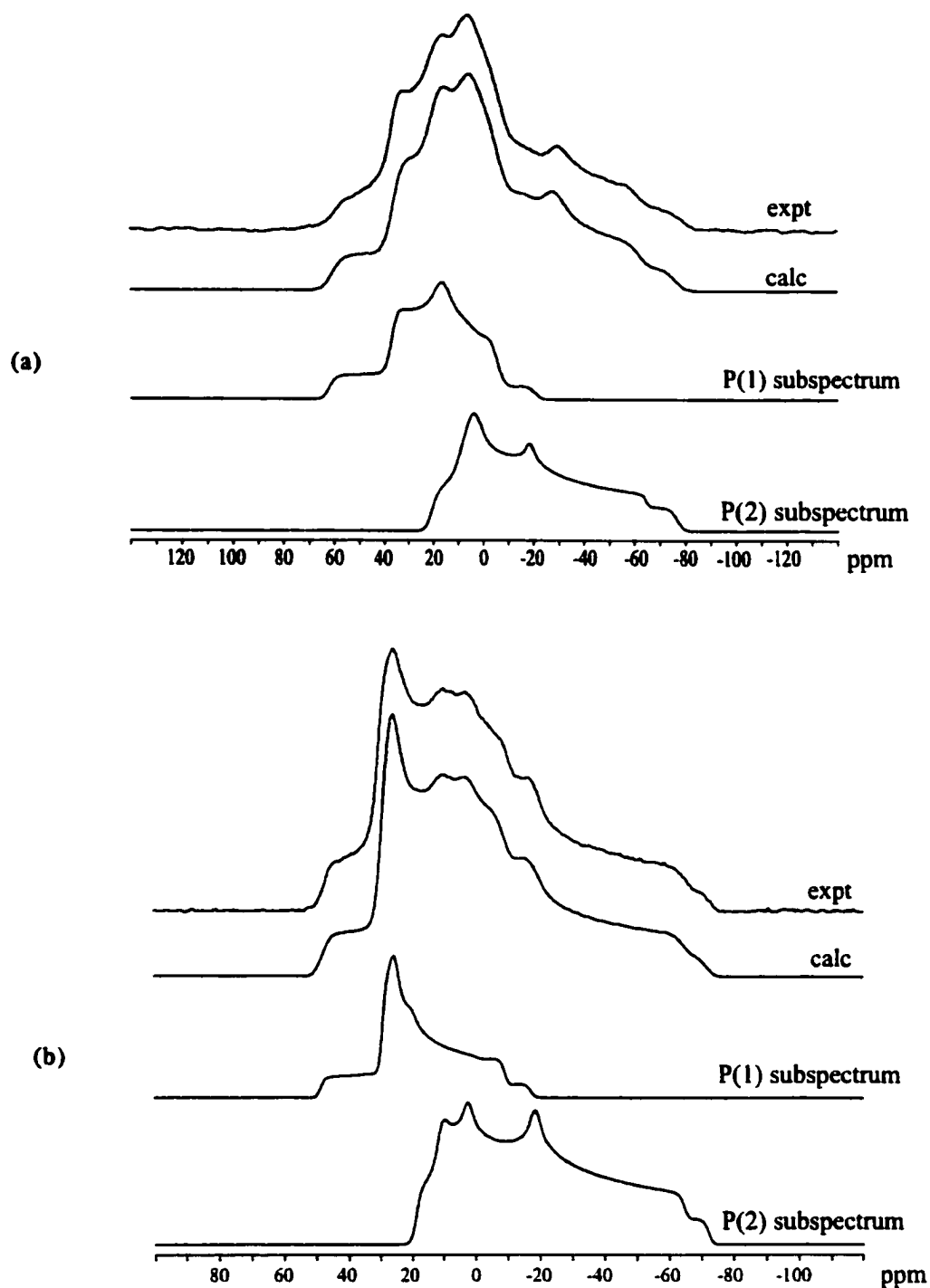


Figure 5.5 Experimental and calculated ^{31}P NMR spectra of stationary powder samples of $[\text{Ph}_3\text{P-PPh}_2][\text{GaCl}_4]$ acquired at (a) 4.7 T (5000 transients, 200 Hz gaussian line broadening) and (b) 9.4 T (3774 transients, 100 Hz gaussian line broadening). Also shown are the calculated subspectra for each phosphorus site.

relatively insensitive to γ for P(1) since the difference between δ_{11} and δ_{22} for P(1) is much smaller than for P(2); hence the position of δ_{11} and δ_{22} is not as easily defined in the case of P(1). The calculated orientation of the δ_{33} component for P(1) (figure 5.6(a)) is in agreement with experiment; however, this is not the case for P(2) where the δ_{33} component is calculated to be 34° away from the P-P bond (figure 5.6(b)). This is significantly different from the experimental result, $\beta = 78^\circ$. In addition, the calculations predict that the δ_{33} components for both tensors are aligned, i.e., $\Delta\alpha = 0^\circ$, whereas the experimental results predict an offset, $\Delta\alpha = 25 \pm 2^\circ$. While it may be tempting to further compare the experimental and calculated phosphorus shielding tensor orientations, it should be noted that calculations are performed on an optimized geometry of a model cation. In contrast to the situation for TMPS (chapter 3) and the phosphole tetramer (chapter 4), much less information is available about the experimental structure of $[\text{Ph}_3\text{P-PPh}_2][\text{GaCl}_4]$.

5.3.2 Dependence of $^1J(^{31}\text{P}, ^{31}\text{P})$ on conformation: $\text{H}_2\text{P-PH}_2$ vs. $\text{H}_3\text{P-PH}_2^+$

If one wishes to compare experimental and calculated results, as well as use the calculated J coupling to obtain structural information in these types of systems, knowledge of how J depends on the conformation is essential. $\text{H}_2\text{P-PH}_2$ and $\text{H}_3\text{P-PH}_2^+$ are prototypical molecules for such an investigation. Indirect experimental evidence that $^1J(^{31}\text{P}, ^{31}\text{P})_{\text{iso}}$ depends on conformation was first reported in 1970 in a variable temperature NMR study of P_2F_4 ¹⁷⁷ and in 1971 for 1,2-dimethyl-1,2-diphenyl biphosphine.¹⁷⁸ Since then, this phenomenon has been observed in a number of other

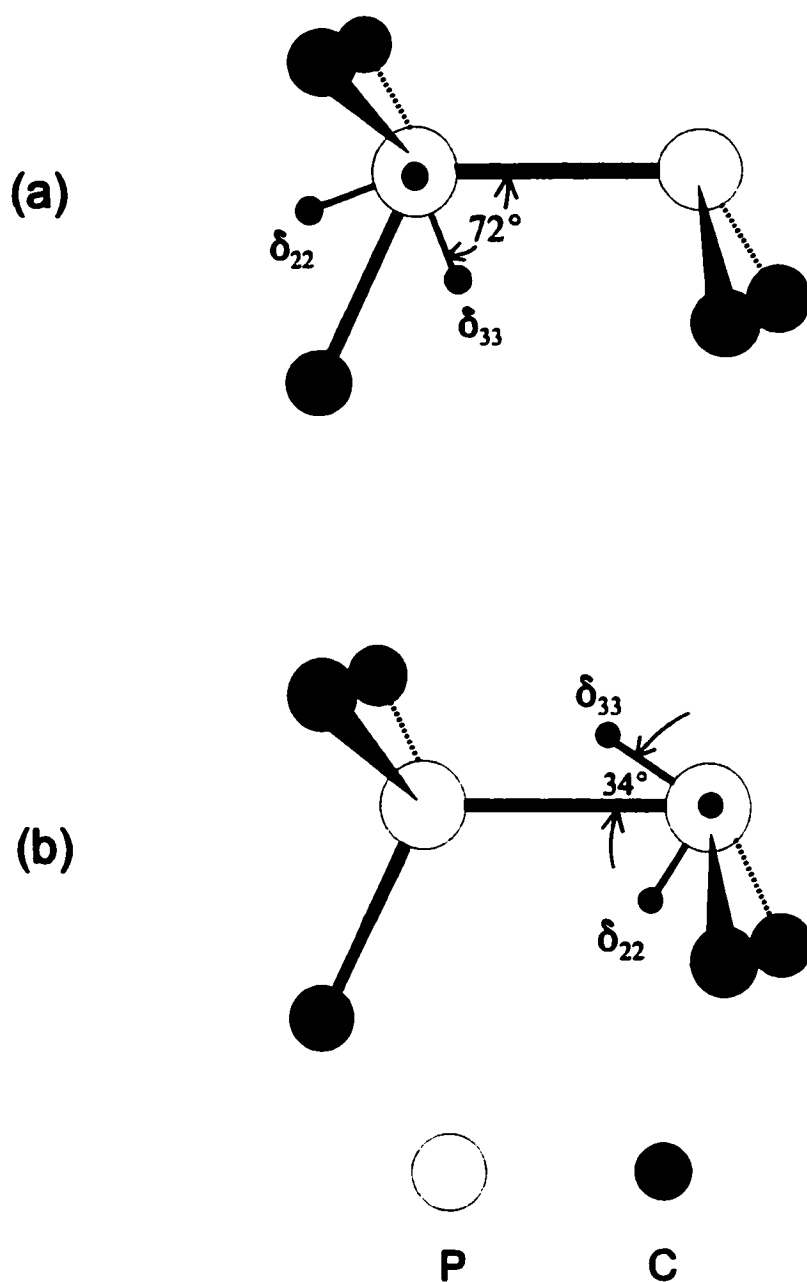


Figure 5.6 Calculated orientation of the phosphorus chemical shift tensors for (a) P(1) and (b) P(2) in $(\text{CH}_3)_3\text{P}-\text{P}(\text{CH}_3)_2^+$. In both cases, the δ_{11} component is perpendicular to the plane of the page. The hydrogen atoms have been omitted for clarity.

systems.^{32,179} The general trend for biphosphines appears to be as follows: a small positive $^1J(^{31}\text{P}, ^{31}\text{P})_{\text{iso}}$ is observed for the conformation where the formal lone pairs are *trans* with respect to each other ($\phi_{\text{PP}} = 180^\circ$) while $^1J(^{31}\text{P}, ^{31}\text{P})_{\text{iso}}$ is large and negative for the *cis* conformation ($\phi_{\text{PP}} = 0^\circ$).¹⁸⁰ In addition, biphosphines are not fixed in a particular conformation, hence the observed value of $^1J(^{31}\text{P}, ^{31}\text{P})_{\text{iso}}$ must be averaged over several conformations. The calculated potential energy curve for rotation of the PH_2 fragment about the P-P bond in $\text{H}_2\text{P-PH}_2$ indicates that the *cis* and *trans* arrangements of the formal electron lone pairs about the P-P bond have energies of 11.3 and 3.3 kJ mol^{-1} respectively relative to the energy minimum at $\phi_{\text{PP}} = 77^\circ$ (note that $RT = 2.45 \text{ kJ mol}^{-1}$ at $T = 295 \text{ K}$).¹⁸¹ Our calculations at the HF level of theory using the cc-pVTZ basis set on all atoms give results that are in qualitative agreement with reference 181 and indicate that the energy for rotation about the P-P bond is relatively flat for conformations between $\phi_{\text{PP}} = 60^\circ$ and $\phi_{\text{PP}} = 180^\circ$ (figure 5.7).

Shown in figure 5.8 is the dependence of $^1J(^{31}\text{P}, ^{31}\text{P})$ on ϕ_{PP} in $\text{H}_2\text{P-PH}_2$. The data are given in table 5.2. The experimental value for $^1J(^{31}\text{P}, ^{31}\text{P})_{\text{iso}}$ is $-108.2 \pm 0.2 \text{ Hz}$.¹⁸² While it is apparent that the quantitative agreement is not very good, it is evident that $^1J(^{31}\text{P}, ^{31}\text{P})$ is highly dependent on the dihedral angle. The FC mechanism is largely responsible for the dihedral angle dependence of $^1J(^{31}\text{P}, ^{31}\text{P})_{\text{iso}}$, although the SD mechanism makes a non-negligible contribution to the magnitude. An early molecular orbital SCF study also found a similar dependence of $^1J(^{31}\text{P}, ^{31}\text{P})_{\text{iso}}$ on ϕ_{PP} .¹⁸³ Our results are compared to results from other calculations^{184,185} in table 5.2. It is interesting to

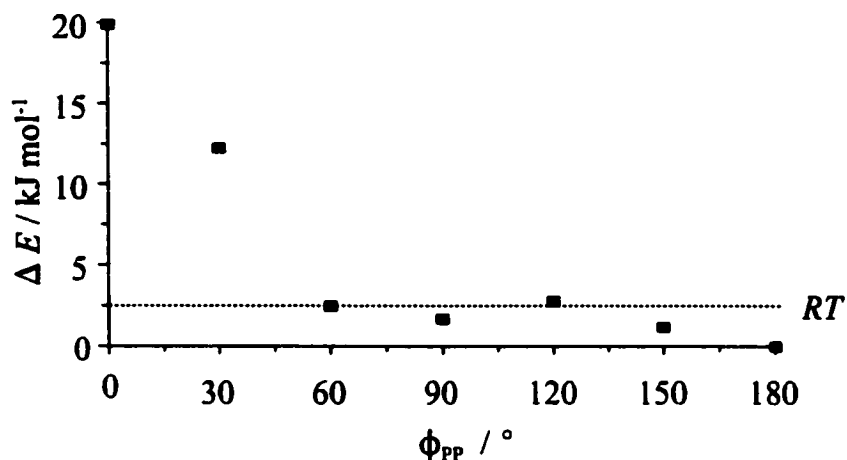


Figure 5.7 Plot of the total energy for $\text{H}_2\text{P-PH}_2$ as a function of ϕ_{PP} . All energies are relative to $\phi_{PP} = 180^\circ$.

note that the calculated ${}^1J(^{31}\text{P}, ^{31}\text{P})_{\text{iso}}$ results differ significantly with respect to the magnitude of the FC contribution; however, the trends are the same. The anisotropy in \mathbf{J} is calculated to be significantly larger than ${}^1J(^{31}\text{P}, ^{31}\text{P})_{\text{iso}}$ and it is also very dependent on ϕ_{PP} for $\text{H}_2\text{P-PH}_2$ as illustrated in figure 5.8(b).

In contrast to $\text{H}_2\text{P-PH}_2$, ${}^1J(^{31}\text{P}, ^{31}\text{P})$ for $\text{H}_3\text{P-PH}_2^+$ is relatively independent of ϕ_{PP^+} , defined in figure 5.1(d). Figure 5.9 illustrates the dependence of \mathbf{J} in $\text{H}_3\text{P-PH}_2^+$ on ϕ_{PP^+} with the data given in table 5.3. This result is reasonable, since rotation of the PH_3 group does not result in a significant change in the overall structure as is the case

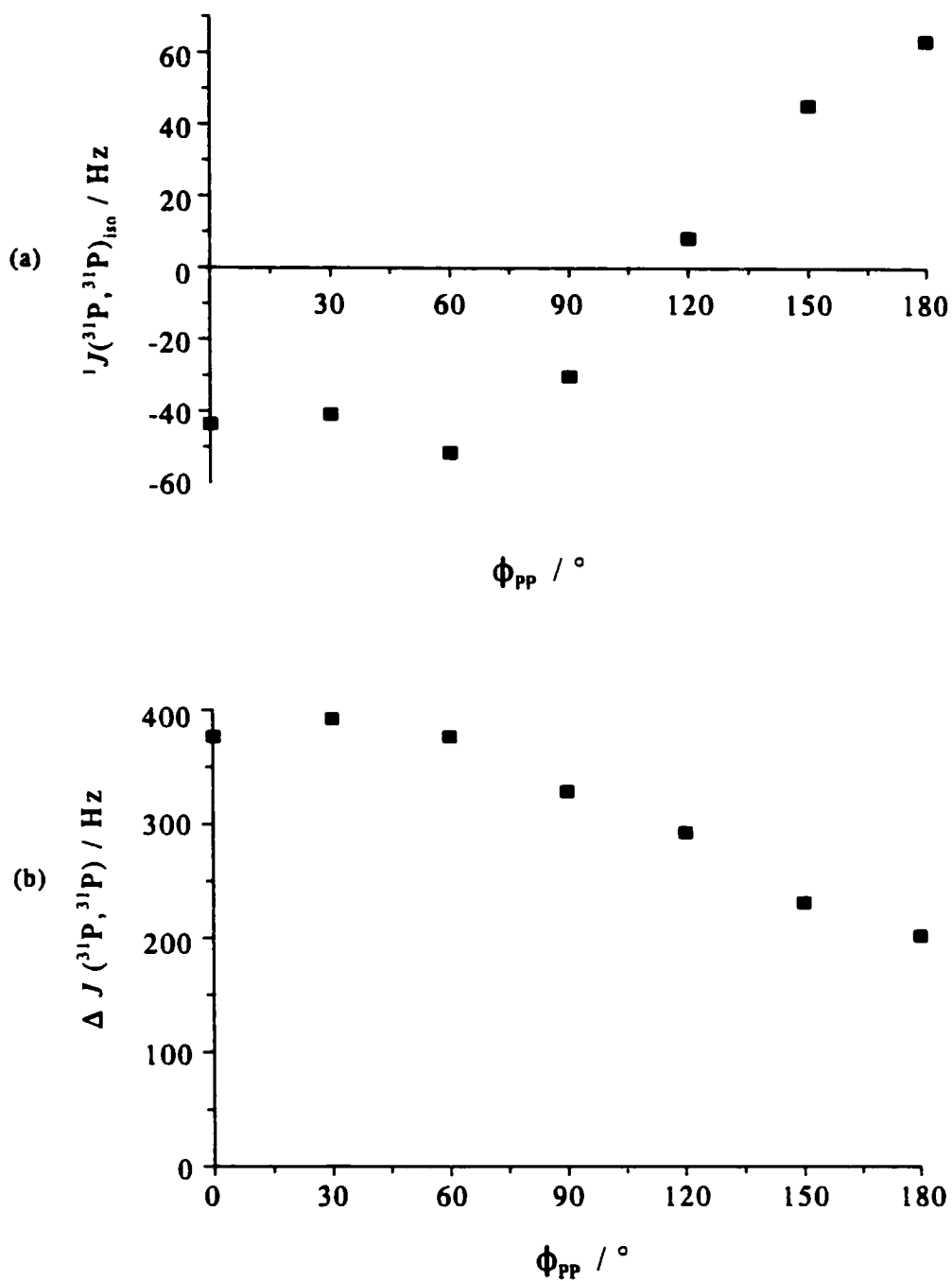


Figure 5.8 Calculated values of (a) ${}^1J({}^{31}\text{P}, {}^{31}\text{P})_{\text{iso}}$ and (b) ΔJ as a function of dihedral angle for $\text{H}_2\text{P-PH}_2$.

Table 5.2: Calculated values of ${}^1J({}^{31}\text{P}, {}^{31}\text{P})$ for $\text{H}_2\text{P-PH}_2$ as a function of ϕ_{PP} .

$\phi_{\text{PP}} / ^\circ$	${}^1J({}^{31}\text{P}, {}^{31}\text{P})_{\text{iso}}$ / Hz	$\Delta J({}^{31}\text{P}, {}^{31}\text{P})$ / Hz	Contributions to ${}^1J({}^{31}\text{P}, {}^{31}\text{P})_{\text{iso}}$ / Hz				
			DSO	PSO	SD	FC	
this work ^a							
0	-44	377	0.1	39	56	-139	
30	-41	393	0.1	24	50	-115	
60	-51	378	0.1	6	46	-103	
90	-30	330	0.1	4	47	-81	
120	8	294	0.1	10	66	-67	
150	45	232	0.1	8	50	-12	
180	64	203	0.1	6	52	6	
SCF MO / (12s9p) - [6s4p] ^b							
0	-238	-	-0.1 ^c		4	-242	
75	-165	-	-2		4	-166	
120	-70	-	-3		4	-71	
180	11	-	-2		4	9	
SOS-CI / STO-431G ^d							
0	-142	263	0.1	35	59	-236	
74	-125	221	0.1	6	54	-185	
180	35	57	0.1	12	63	-41	
SCF / (12s8p) - [6s4p] ^e							
81	-76	-	0	-0.2	118	-194	
expt ^f							
-	-108.2 ± 0.2	-	-	-	-	-	

^a Calculated using the MCSCF approach with cc-pVTZ basis set and an inactive/active space consisting of 55/54.

^b From reference 183.

^c The total orbital contribution is given. DSO + PSO.

^d SOS-CI (sum-over-states configuration interaction) data are from reference 184. STO stands for Slater-type orbital.

^e From reference 185. The basis set has added polarization functions.

^f From reference 182.

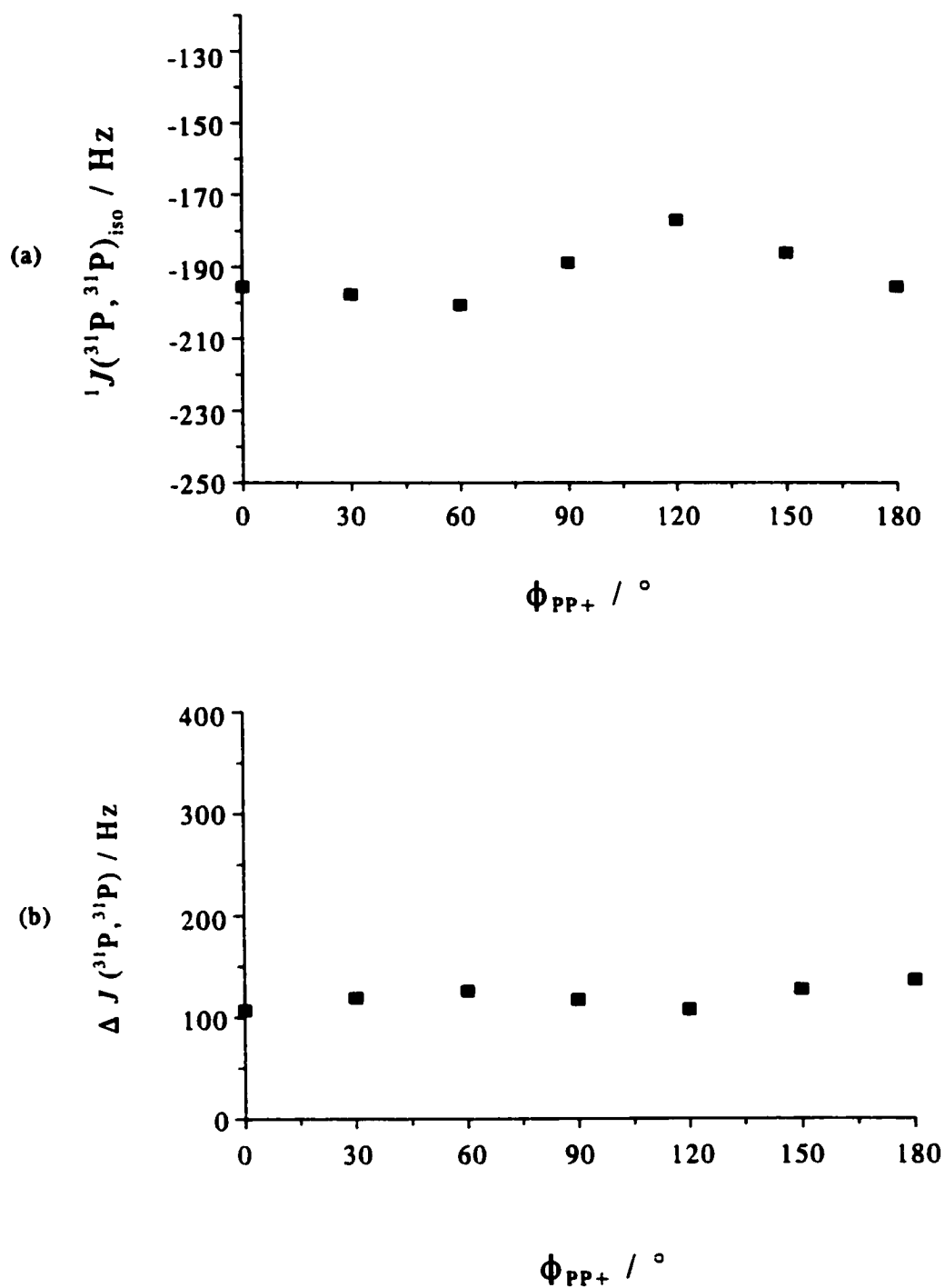


Figure 5.9 Calculated values of (a) ${}^1J({}^{31}\text{P}, {}^{31}\text{P})_{\text{iso}}$ and (b) ΔJ as a function of dihedral angle for $\text{H}_3\text{P-PH}_2^+$. The scale is the same as in figure 5.8 to emphasize the difference between the two molecules.

Table 5.3: Calculated values of ${}^1J({}^{31}\text{P}, {}^{31}\text{P})$ for $\text{H}_3\text{P-PH}_2^+$ as a function of ϕ_{PP^+} .^a

$\phi_{\text{PP}^+} / ^\circ$	${}^1J({}^{31}\text{P}, {}^{31}\text{P})_{\text{iso}} / \text{Hz}$	$\Delta J({}^{31}\text{P}, {}^{31}\text{P}) / \text{Hz}$	Contributions to ${}^1J({}^{31}\text{P}, {}^{31}\text{P})_{\text{iso}} / \text{Hz}$			
			DSO	PSO	SD	FC
0	-195	107	0.1	-7	4	-193
30	-198	120	0.1	-11	3	-189
60	-200	126	0.1	-15	2	-187
90	-189	118	0.1	-11	3	-181
120	-177	108	0.1	-7	3	-173
150	-188	128	0.1	-13	3	-176
180	-195	137	0.1	-18	2	-180

^a Calculations performed at the MCSCF level with the cc-pVTZ basis set using an inactive/active space of 10/8.

when one of the PH_2 groups in $\text{H}_2\text{P-PH}_2$ is rotated with respect to the P-P bond. For $\text{H}_3\text{P-PH}_2^+$, the magnitude of ${}^1J({}^{31}\text{P}, {}^{31}\text{P})_{\text{iso}}$ is much larger than in $\text{H}_2\text{P-PH}_2$, with the dominant contribution from the FC mechanism. For $\text{H}_3\text{P-PH}_2^+$, the anisotropy in \mathbf{J} is smaller relative to ${}^1J({}^{31}\text{P}, {}^{31}\text{P})_{\text{iso}}$ in contrast to the situation for $\text{H}_2\text{P-PH}_2$. The trend in ${}^1J({}^{31}\text{P}, {}^{31}\text{P})$ for $\text{H}_2\text{P-PH}_2$ vs. $\text{H}_3\text{P-PH}_2^+$ has also been reported in semi-empirical calculations of ${}^1J({}^{15}\text{N}, {}^{15}\text{N})_{\text{iso}}$ for the analogous nitrogen-containing compounds.¹⁸⁶ As well, it was noted that the calculated value of ${}^1J({}^{13}\text{C}, {}^{15}\text{N})_{\text{iso}}$ in methylamine is virtually independent of rotation of the NH_2 fragment about the C-N bond.¹⁸⁶

The replacement of one of the lone pairs in $\text{H}_2\text{P-PH}_2$ with a bonding pair (to a hydrogen atom) in $\text{H}_3\text{P-PH}_2^+$ results in a decrease in ${}^1J({}^{31}\text{P}, {}^{31}\text{P})_{\text{iso}}$ as well as a decrease in the anisotropy in \mathbf{J} . In terms of reduced coupling constants (see equation 2.24),

${}^1K(\text{P},\text{P})_{\text{iso}}$ for $\text{H}_2\text{P}-\text{PH}_2$ vs. $\text{H}_3\text{P}-\text{PH}_2^+$ with $\phi_{\text{PP}} = \phi_{\text{PP}^+} = 0^\circ$ are $-22 \times 10^{19} \text{ NA}^{-2}\text{m}^{-3}$ and $-99 \times 10^{19} \text{ NA}^{-2}\text{m}^{-3}$ respectively. This is contrary to the generally observed lone pair effect, where an *increase* in ${}^1K_{\text{iso}}$ is observed when a lone pair is replaced by a bond.^{32,187} For example, ${}^1K(\text{N},\text{C})_{\text{iso}}$ for $\text{CH}_3\text{CH}_2\text{CH}_2\text{NH}_2$ is $12.7 \times 10^{19} \text{ NA}^{-2}\text{m}^{-3}$ vs. $14.4 \times 10^{19} \text{ NA}^{-2}\text{m}^{-3}$ for $\text{CH}_3\text{CH}_2\text{CH}_2\text{NH}_3^+$,¹⁸⁸ and for $\text{P}(\text{CH}_3)_3$ vs. $\text{P}(\text{CH}_3)_4^+$, ${}^1K(\text{P},\text{C})_{\text{iso}} = -11.1 \times 10^{19} \text{ NA}^{-2}\text{m}^{-3}$ and $45.3 \times 10^{19} \text{ NA}^{-2}\text{m}^{-3}$ respectively.¹⁸⁹ Two exceptions are $(\text{CH}_3)_2\text{P}-\text{P}(\text{CH}_3)_2$ vs. $(\text{CH}_3)_2\text{P}-\text{P}(\text{S})(\text{CH}_3)_2$, with ${}^1K(\text{P},\text{P})_{\text{iso}} = 91 \times 10^{19} \text{ NA}^{-2}\text{m}^{-3}$ and ${}^1K(\text{P},\text{P})_{\text{iso}} = -114 \times 10^{19} \text{ NA}^{-2}\text{m}^{-3}$ respectively,¹⁸⁷ and $\text{Ph}_2\text{P}-\text{PPh}_2$ (${}^1K(\text{P},\text{P})_{\text{iso}} = -101 \times 10^{19} \text{ NA}^{-2}\text{m}^{-3}$)¹³ vs. $\text{Ph}_3\text{P}-\text{PPh}_2^+$ (${}^1K(\text{P},\text{P})_{\text{iso}} = -164 \times 10^{19} \text{ NA}^{-2}\text{m}^{-3}$, this work). It should be noted that ${}^1K(\text{P},\text{P})_{\text{iso}}$ for $\text{Ph}_2\text{P}-\text{PPh}_2$ is likely very dependent on the lone pair conformation and hence changes in the dihedral angle may change the trend with respect to $\text{Ph}_3\text{P}-\text{PPh}_2^+$.

Another factor that must be considered is a change in structure besides rotation about the P-P bond. It has been claimed that ${}^1J(^{31}\text{P}, ^{31}\text{P})_{\text{iso}}$ for $\text{RR}'\text{P}-\text{PRR}'$ is sensitive to the R-P-R' bond angle (where R, R' are any one of the following: H, an alkyl group, or phenyl).¹⁹⁰ To investigate the influence of geometry, ${}^1J(^{31}\text{P}, ^{31}\text{P})_{\text{iso}}$ was calculated for $\text{H}_2\text{P}-\text{PH}_2$ geometries where one bond length or angle was changed to match the corresponding parameter in the geometry used for $\text{H}_3\text{P}-\text{PH}_2^+$ (table 5.4). In this manner, the effect of changing each bond length or angle may be determined. The calculated ${}^1J(^{31}\text{P}, ^{31}\text{P})_{\text{iso}}$ values for $\text{H}_2\text{P}-\text{PH}_2$ using two different active spaces are given in the first two lines of table 5.4. This illustrates that using a larger active space (first line) does not significantly change the calculated coupling constant compared to the

results obtained using a smaller active space (second line). The next four lines present the calculated ${}^1J({}^{31}\text{P}, {}^{31}\text{P})_{\text{iso}}$ values obtained when a given bond length or angle in $\text{H}_2\text{P-PH}_2$ is changed to match the corresponding bond length or angle in $\text{H}_3\text{P-PH}_2^+$. As is evident from the data in table 5.4, none of the geometry differences between $\text{H}_2\text{P-PH}_2$ and $\text{H}_3\text{P-PH}_2^+$ can account for the difference in ${}^1J({}^{31}\text{P}, {}^{31}\text{P})_{\text{iso}}$ for these two molecules. Unfortunately, further MCSCF calculations on systems of this size are not possible with available computational resources.

Table 5.4: Geometry dependence of ${}^1J({}^{31}\text{P}, {}^{31}\text{P})_{\text{iso}}$ for $\text{H}_2\text{P-PH}_2$.^a

geometry alteration	${}^1J({}^{31}\text{P}, {}^{31}\text{P})_{\text{iso}} / \text{Hz}$
$\text{H}_2\text{P-PH}_2$ experimental geometry ($\phi_{\text{PP}} = 0^\circ$) ^a	-44
$\text{H}_2\text{P-PH}_2$ experimental geometry ($\phi_{\text{PP}} = 0^\circ$) ^b	-58
P-P in $\text{H}_2\text{P-PH}_2$ changed to 2.2192 Å ^b	-55
H-P-H in $\text{H}_2\text{P-PH}_2$ changed to 95° ^b	-52
H-P-H in $\text{H}_2\text{P-PH}_2$ changed to 106.37° ^b	-18
H-P in $\text{H}_2\text{P-PH}_2$ changed to 1.386 Å ^b	-67
$\text{H}_3\text{P-PH}_2^+$ ($\phi_{\text{PP}^+} = 0^\circ$) ^c	-195

^a From table 5.2.

^b MCSCF calculations using the cc-pVTZ basis set on all atoms and an inactive/active space of 55/43.

^c From table 5.3.

5.3.3 Estimate of r_{PP} in $[\text{Ph}_3\text{P-PPh}_2][\text{GaCl}_4]$

As was stated in the introduction (section 5.1), to obtain an estimate of the P-P bond length in $[\text{Ph}_3\text{P-PPh}_2][\text{GaCl}_4]$, it is necessary to have an estimate of the anisotropy in the J coupling, since it is experimentally inseparable from R_{DD} . With a value for ΔJ , one can obtain R_{DD} from R_{eff} according to equation 2.29. As mentioned in section 2.1.6, reliable measurements of ΔJ are scarce. An estimate of ΔJ may be obtained from *ab initio* calculations; however computer resources limit the size of the molecule one can use for J calculations. In this case, $\text{H}_3\text{P-PH}_2^+$ is the smallest possible model compound for $\text{Ph}_3\text{P-PPh}_2^+$. As the results for $\text{H}_3\text{P-PH}_2^+$ indicate that ΔJ is virtually independent of ϕ_{PP^+} (figure 5.9), one may use the average ΔJ over all conformers of $\text{H}_3\text{P-PH}_2^+$, 121 Hz. Using this value in equation 2.29, a value of 1.74 ± 0.05 kHz is obtained for R_{DD} , hence $r_{\text{PP}} = 2.25 \pm 0.03$ Å in $[\text{Ph}_3\text{P-PPh}_2][\text{GaCl}_4]$, according to equation 2.20. If one assumes that $R_{\text{eff}} = R_{DD}$, then $r_{\text{PP}} = 2.26 \pm 0.03$ Å which is within experimental error of the first estimate. In this case, ΔJ is relatively small, hence a reliable estimate of the vibrationally averaged P-P bond length may be obtained for R_{eff} . However, the *ab initio* calculations of J for $\text{H}_2\text{P-PH}_2$ indicate that one cannot necessarily assume that ΔJ for all one-bond P-P J -coupling tensors will be small.

5.4 Conclusions

The phosphorus chemical shift and ^{31}P - ^{31}P dipolar coupling tensors in $[\text{Ph}_3\text{P-PPh}_2][\text{GaCl}_4]$ have been characterized by solid-state NMR. By combining the experimental results with *ab initio* calculations of $^1J(^{31}\text{P}, ^{31}\text{P})$ for $\text{H}_3\text{P-PH}_2^+$, a reliable

estimate of the P-P bond length in $[\text{Ph}_3\text{P-PPh}_2][\text{GaCl}_4]$ has been obtained, $2.25 \pm 0.03 \text{ \AA}$. It should be noted that vibrational averaging and possible rocking motion of the P-P bond have been ignored. In addition, the dependence of indirect spin-spin coupling on lone pair conformation has been investigated for $\text{H}_2\text{P-PH}_2$ and $\text{H}_3\text{P-PH}_2^+$ using the MCSCF approach. It was found that $^1J(^{31}\text{P}, ^{31}\text{P})$ for $\text{H}_2\text{P-PH}_2$ is very dependent on conformation, in contrast to $\text{H}_3\text{P-PH}_2^+$.

Chapter 6: Conclusions

The phosphorus chemical shift and spin-spin coupling tensors for three different compounds containing P-P bonds have been characterized by solid-state ^{31}P NMR. The combination of experimental methods and *ab initio* calculations has proven to be very useful for exploring the tensor nature of each interaction.

For the first example, TMPS (chapter 3), the phosphorus NMR parameters were characterized by NMR studies on both a single crystal and a powder crystalline sample. There are two molecules in the asymmetric unit; however the difference between the two sites is very subtle, as evident in a redetermination of the X-ray crystal structure. This difference is also clearly evident in the ^{31}P NMR spectra, from which two unique phosphorus chemical shift tensors have been characterized. The tensor orientation is such that the direction of greatest shielding, δ_{33} , lies along the P=S bond. The experimental and calculated orientation of the phosphorus chemical shift tensors are in excellent agreement. It was also shown that the anisotropy in the ^{31}P , ^{31}P indirect spin-spin coupling for TMPS is less than 500 Hz, contrary to earlier reports for similar compounds.^{11,16} This compound serves as a benchmark for testing the reliability of *ab initio* calculations of nuclear magnetic shielding tensors.

The second system described in this thesis was the phosphole tetramer. Since a large single crystal was not available, the phosphorus NMR parameters for this compound were characterized by analysis of ^{31}P NMR spectra of powdered samples

(chapter 4). In this case, *ab initio* calculations of chemical shift tensor orientations proved to be invaluable. It was found that δ_{11} is closest to the P-P bond for both phosphorus chemical shift tensors. The δ_{33} component is situated in the same plane as the phosphole ring. The relative orientation of the δ_{33} components for the phosphorus nuclei reflects the local geometry of the phosphole rings.

The third compound described here, $[\text{Ph}_3\text{P-PPh}_2][\text{GaCl}_4]$, was prepared in the Burford lab. The solid-state ^{31}P NMR investigation of this compound provided the P,P bond length (chapter 5). *Ab initio* calculations of $^1\text{J}(^{31}\text{P}, ^{31}\text{P})$ on model systems provided insight into the dependence of J on molecular structure. For $\text{H}_2\text{P-PH}_2$, $^1\text{J}(^{31}\text{P}, ^{31}\text{P})$ is very dependent on the rotation of the PH_2 fragment about the P-P bond while it is nearly independent of rotation in $\text{H}_3\text{P-PH}_2^+$.

From the results of these three projects some general conclusions may be drawn. It is evident from the results for the phosphole tetramer and for $[\text{Ph}_3\text{P-PPh}_2][\text{GaCl}_4]$ that one cannot assume that the direction of greatest shielding corresponds to the generally perceived direction of greatest electron density, i.e., along the formal lone pairs. Furthermore, knowledge of the anisotropy in $^1\text{J}(^{31}\text{P}, ^{31}\text{P})$ is important for obtaining an estimate of the bond length from R_{eff} . The investigation of ΔJ in TMPS further establishes the observation that $\Delta J(^{31}\text{P}, ^{31}\text{P})$ is small in diphosphine disulfides, contrary to earlier reports.^{11,16} On the other hand, first-principle calculations indicate significant anisotropies for $^1\text{J}(^{31}\text{P}, ^{31}\text{P})$ in $\text{H}_2\text{P-PH}_2$ and $\text{H}_3\text{P-PH}_2^+$. In each of the projects discussed in this thesis, *ab initio* calculations of NMR parameters play a significant role. The reliability of *ab initio* calculations for characterizing phosphorus chemical shift tensor

orientations is established by comparison with results from a single-crystal ^{31}P NMR study of TMPS. For the phosphole tetramer, it is possible to fix the chemical shift tensor orientation in the molecular frame of reference by comparing calculated tensor orientations with the orientation information available from the analysis of spectra obtained from powder crystalline samples. First-principles calculations of $^1J(^{31}\text{P},^{31}\text{P})$ were necessary to establish that $\Delta J(^{31}\text{P},^{31}\text{P})$ makes a very small contribution to R_{eff} , hence a reliable estimate of r_{PP} could be obtained for $[\text{Ph}_3\text{P-PPh}_2][\text{GaCl}_4]$.

In the past few years, the value of *ab initio* calculations as a complement to experimental results in the field of NMR has been recognized. The continuous improvement and availability of computational methods and resources have undoubtedly contributed to extending the range of systems which may be studied. While *ab initio* calculations are yielding reliable qualitative results for nuclear magnetic shielding tensors, much more work needs to be done to reach the same level of confidence with J coupling. In this respect, it is essential that the results from first-principle calculations be compared with reliable experimental data. Some specific suggestions are given in the next chapter. At the same time, it is important for NMR spectroscopists to use more quantum chemistry methods and keep up to date with the latest developments in this field.

Chapter 7: Future Research Directions

7.1 Introduction

Several extensions of the research presented in this thesis are worthy of consideration. Suggestions include an investigation of phosphorus chemical shift tensors in other phosphinophosphonium cations (section 7.2) as well as further *ab initio* calculations (section 7.3). While the calculations of J appears to be promising, much more effort needs to be expended in this area. *Ab initio* calculations are presently limited to relatively small systems. The recent success of DFT approaches at calculating J for numerous spin pairs are most encouraging.^{121,122,123} Obviously, the potential of this approach for calculating $^1J(^{31}\text{P}, ^{31}\text{P})$ should be investigated. Section 7.4 presents some preliminary results and suggestions for further theoretical studies of indirect spin-spin coupling for systems containing phosphorus spin pairs. All the spin systems discussed in this thesis involve two coupled spin- $\frac{1}{2}$ nuclei. An example of a system consisting of three coupled spin- $\frac{1}{2}$ nuclei is outlined in section 7.5.

7.2 $[\text{Ph}_2(\text{Cl})\text{P}-\text{PPh}_2][\text{GaCl}_4]$

The precursor to $[\text{Ph}_3\text{P}-\text{PPh}_2][\text{GaCl}_4]$ (chapter 5), $[\text{Ph}_2(\text{Cl})\text{P}(1)-\text{P}(2)\text{Ph}_2][\text{GaCl}_4]$, has also been isolated.¹⁶⁹ In this case, the coupling of P(1) to a chlorine nucleus complicates the appearance of the spectra. Chlorine has two naturally occurring isotopes; ^{35}Cl : spin- $\frac{3}{2}$, N.A. = 75.53 % and ^{37}Cl : spin- $\frac{3}{2}$, N.A. = 24.47 %. Phosphorus-31 NMR spectra of MAS samples are shown in figure 7.1, obtained at

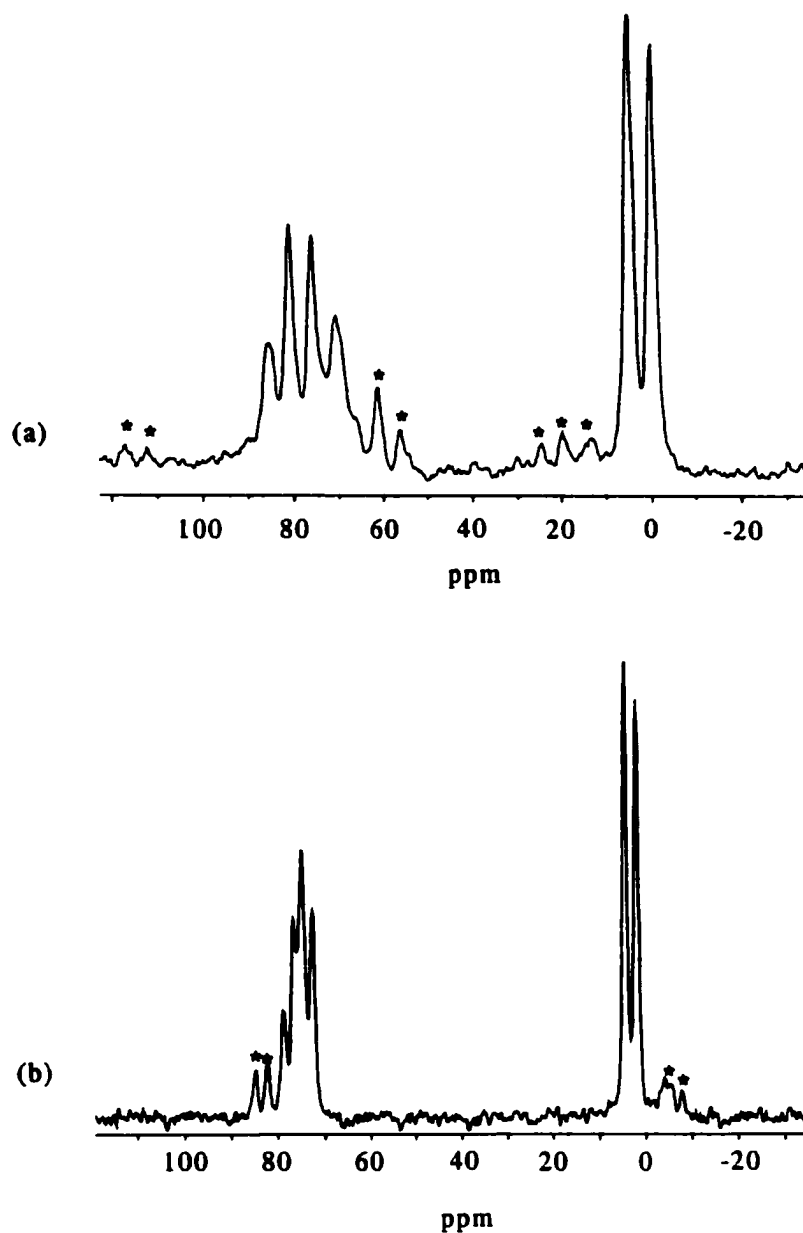


Figure 7.1 Phosphorus-31 NMR spectrum of solid $[\text{Ph}_2(\text{Cl})\text{P}-\text{PPh}_2][\text{GaCl}_4]$, acquired with MAS at (a) 4.53 kHz at an applied magnetic field of 4.7 T. Sixteen transients were acquired and 10 Hz of gaussian line broadening was applied. A spectrum acquired at an applied magnetic field of 9.4 T with MAS at 13 kHz is shown in (b). Sixteen transients were acquired and 50 Hz of gaussian line broadening was applied. The asterisks indicate spinning sidebands.

applied magnetic fields of 4.7 T and 9.4 T. The analysis of the spectra arising from a spin- $\frac{1}{2}$ nucleus coupled to a quadrupolar nucleus has been presented in the literature,^{191,192} however, many of the simulations are suspect, e.g., reference 192. Carbon-13 coupled to $^{35/37}\text{Cl}$ has been investigated in chloroketosulfones.¹⁹³ It is important that experiments be carried out at several applied magnetic fields, as is evident in reference 193. The line shape for $[\text{Ph}_2(\text{Cl})\text{P}-\text{PPh}_2][\text{GaCl}_4]$ is further complicated by the coupling of P(1) to the phosphine centre. Initial simulation of the MAS spectra proved to be unsuccessful. Preliminary ^{31}P NMR studies of $[\text{Ph}_2(\text{Cl})\text{P}-\text{PPh}_2][\text{GaCl}_4]$ by CP experiments indicate that the proton relaxation times are long; recycle delays in excess of 2 minutes were needed to avoid saturation. Further experiments on this compound are in progress.

7.3 *Ab Initio* Calculations of Phosphorus Chemical Shift Tensors

The results from *ab initio* calculations of phosphorus chemical shift tensors presented in this thesis indicate that qualitative agreement with experiment may be expected. However, there appears to be a systematic discrepancy between the experimental and calculated results. For all three compounds presented in this thesis, the values of δ_{iso} calculated at the HF level are more shielded by about 50 ppm. As mentioned in section 3.3.3, changes in the phosphorus chemical shift on the order of tens of ppm have been observed upon changing from the gas to liquid state. Clearly, the influence of intermolecular effects on the phosphorus chemical shift needs to be considered if one is to obtain quantitatively reliable results. Investigations along these

lines on model systems, such as PH_3 or P_4 for which the gas to liquid shifts are known (see section 3.3.3), are recommended.

7.4 Characterization of $^1J(^{31}\text{P}, ^{31}\text{P})$

While $^1J(^{31}\text{P}, ^{31}\text{P})_{\text{iso}}$ is large and negative in $\text{H}_2\text{P-PH}_2$,¹⁸² a large positive value, +720 Hz, is observed in molecules of the type $\text{H}_n(\text{CH}_3)_{3-n}\text{PPF}_5$,¹⁹⁴ and a value of +766 Hz was reported for the potassium salt of $\text{FO}_2\text{PPO}_2\text{F}^{2+}$.¹⁹⁵ Successful calculation of $^1J(^{31}\text{P}, ^{31}\text{P})_{\text{iso}}$ for these molecules which, together with $\text{H}_2\text{P-PH}_2$, span the range of observed $^1J(^{31}\text{P}, ^{31}\text{P})_{\text{iso}}$ values, would be of great value. A survey of INDO results (FC contribution only), which includes the above-mentioned molecules, has been reported.⁵⁷ In addition, a large negative values of $^1J(^{31}\text{P}, ^{31}\text{P})_{\text{iso}}$, approximately -480 Hz, have been observed for a series of diphospholes.¹⁹⁶ Given the success of MCSCF^{37,109,110} and DFT methods^{121,122,123} for calculating J coupling, application of these theoretical approaches to the above systems would be of interest. For the larger molecules, DFT may be the only possibility with currently available computer resources. Initial results are promising; however, systematic studies to reproduce experimental trends are warranted.

There are a number of other small phosphorus-containing molecules besides $\text{H}_2\text{P-PH}_2$ for which experimental data are available.⁵⁷ One system of fundamental importance is diphosphene, P_2H_2 , as well as the analogous nitrogen compound, diazene, N_2H_2 . Results for J from calculations using the MCSCF approach with the cc-pVTZ basis set for the *trans* isomers of these two compounds are given in table 7.1. For comparison, data from an early *ab initio* study¹⁹⁷ using smaller basis sets are also given.

Table 7.1: ${}^1J(X,X)$ and ${}^1K(X,X)$ for P_2H_2 and N_2H_2 .^a

	${}^1J(X,X)_{iso}/\text{Hz}$	$\Delta J(X,X)/\text{Hz}$	Contributions to ${}^1J_{iso}/\text{Hz}$			
			DSO	PSO	DS	FC
<i>trans</i> - N_2H_2 (X = ${}^{15}N$)						
CASI	-249	-220	0	-115	-16	-118
CASII	-25	74	0	10	1	-36
SOS CI ^b	-17	-	0	-15	0.2	-2
diazenes ^c	± 10 to 20					
<i>trans</i> - P_2H_2 (X = ${}^{31}P$)						
CASIII	-1985	1076	0.2	-531	-1069	-385
CASIV	-348	-1463	0	-386	49	-12
SOS CI ^d	-552	-	0	-498	9	-76
diphosphenes ^e	± 510 to 670					
			Contributions to ${}^1K_{iso} / 10^{19} \text{ NA}^{-2}\text{m}^{-3}$			
	${}^1K(X,X)_{iso} / 10^{19} \text{ NA}^{-2}\text{m}^{-3}$	$\Delta K(X,X) / 10^{19} \text{ NA}^{-2}\text{m}^{-3}$	DSO	PSO	DS	FC
<i>trans</i> - N_2H_2 (X = N)						
CASI	-2017	-1782	0	-932	-130	-956
CASII	-203	598	-0.3	79	12	-293
SOS CI ^b	-138	-	0.1	-122	2	-16
diazenes ^c	± 80 to 160					
<i>trans</i> - P_2H_2 (X = P)						
CASIII	-1006	174	0.1	-269	-542	-195
CASIV	-176	-742	0.1	-196	25	-6
SOS CI ^d	-280	-	0	-262	5	-39
diphosphenes ^e	± 260 to 340					

^a Calculations performed at the MCSCF level with cc-pVTZ basis set.

^b From reference 197. The geometry for *trans* N_2H_2 was not given.

^c From reference 201.

^d From reference 197, using the STO/6-31G** basis set. The geometry used for *trans* P_2H_2 is as follows: P-P = 2.034 Å, P-H = 1.44 Å, and P-P-H = 95.6°.

^e From reference 204.

The reduced coupling tensor, \mathbf{K} (equation 2.24), is also presented in table 7.1.

The molecular geometries used are as follows. For *trans*-P₂H₂, the P-P bond length = 2.00 Å, the P-H bond length = 1.40 Å and the P-P-H angle = 108°, based on typical values for diphosphenes.^{198,199} For *trans*-N₂H₂, the N-N bond length = 1.247 Å, the N-H bond length = 1.029 Å, and the N-N-H bond angle = 106.3°.²⁰⁰

The smallest active spaces used in both cases, 1010/1120 (denoted by CASI) for N₂H₂ and 4141/3120 (CASIII) for P₂H₂ do not include virtual molecular orbitals, and thus give the same results as an HF calculation.⁷⁸ The larger active spaces, 1010/2231 (CASII) for N₂H₂ and 4141/4231 (CASIV) for P₂H₂, include a virtual orbital for each molecular orbital symmetry. As is evident for N₂H₂, the magnitude of ${}^1J({}^{15}\text{N}, {}^{15}\text{N})_{\text{iso}}$ calculated with CASII is in reasonable agreement with experimental values that are typical of diazenes.²⁰¹ Unfortunately, the sign of this coupling is not known; however, early semi-empirical calculations predicted that ${}^1J({}^{15}\text{N}, {}^{15}\text{N})$ is negative except possibly in hydrazine type compounds.^{202,203} The MCSCF results discussed above and early *ab initio* results¹⁹⁷ for N₂H₂ in table 7.1 are in agreement with this prediction.

For P₂H₂, calculations using the larger active space, CASIV, predict a value of -348 Hz for ${}^1J({}^{31}\text{P}, {}^{31}\text{P})_{\text{iso}}$ and a large negative ΔJ of -1463 Hz. Unfortunately, no experimental data are available for P₂H₂; however typical values of ${}^1J({}^{31}\text{P}, {}^{31}\text{P})_{\text{iso}}$ for diphosphenes range between 510 and 670 Hz in magnitude, depending on the substituents.²⁰⁴ The sign of the coupling is not known, but it has been suggested^{180,204} that it is negative on the basis of early *ab initio* calculations which predicted a negative value, ${}^{197} {}^1J({}^{31}\text{P}, {}^{31}\text{P})_{\text{iso}} = -552$ Hz, due to the large negative contribution from the orbital

mechanism. The type of basis set used for the early *ab initio* calculations, STO/6-31G**, is known to be unreliable for indirect spin-spin coupling calculations.⁸ Semi-empirical approaches predict a large positive value, +830 Hz when only the FC mechanism is considered.⁵⁷

Also given in table 7.1 are the contributions of each mechanism to ${}^1J_{\text{iso}}$ and ${}^1K_{\text{iso}}$. For P_2H_2 , the magnitude of ${}^1J({}^{31}\text{P}, {}^{31}\text{P})_{\text{iso}}$ is dominated by the PSO contribution; however, it not definitive which mechanism dominates ${}^1J({}^{15}\text{N}, {}^{15}\text{N})_{\text{iso}}$ in N_2H_2 . Comparison of the contributions obtained using an active space with no virtual orbitals vs the results using one that does include virtual orbitals illustrates the triplet instability problem discussed in section 2.3.2 where the contributions that depend on the triplet states are known to be poorly calculated if virtual orbitals are not included in the MCSCF space. While calculations qualitatively predict the trend in ${}^1J_{\text{iso}}$ for P_2H_2 vs N_2H_2 , comparison of the values of ${}^1K_{\text{iso}}$ is more telling of problems with the *ab initio* results. In this case, the calculated results are clearly wrong compared to the experimental results, i.e., using the larger active space, the magnitude of ${}^1K_{\text{iso}}$ for N_2H_2 is larger than that for P_2H_2 , contrary to the experimental trend. For these systems, further work is necessary, possibly using restricted active spaces.^{97,110,205} Even for a molecule as small as P_2H_2 , extensive study of the dependence of the calculated \mathbf{J} on the active space is not possible with currently available computational resources. It should be noted that systems such as N_2H_2 and P_2H_2 , where there are multiple bonds and formal electron lone pairs, present a difficult computational challenge.⁸

7.5 NMR Spectra Arising from Three Coupled Homonuclear Spin- $\frac{1}{2}$ Nuclei in the Solid State

A logical extension to the investigations of spin pairs presented in this thesis is to systems of multiple coupled spins. Analysis of spectra arising from multiple spin systems are of interest in biomolecules where multiple labelling allows for more information to be extracted.²⁰⁶ The theory for the analysis of spectra arising from three coupled heteronuclear spin- $\frac{1}{2}$ nuclei has been presented in the literature, for the AA'X,²⁰⁷ ABX,²⁰⁸ and AX₂²⁰⁹ cases. The iterative fitting of MAS spectra arising from an ABX spin system to obtain chemical shift tensors has been reported.²¹⁰ In principle, the ambiguity regarding the orientation of the chemical shift tensor with respect to the molecular frame of reference, which is an inherent limitation of the dipolar-chemical shift method (section 2.2.2), is eliminated in the analysis of spectra for three coupled spins. For example, it was demonstrated for doubly ¹³C labelled L-alanine that the carbon chemical shift tensors obtained from an analysis of powder samples²¹¹ agreed well with results from a single-crystal NMR study.²¹² In this case, the presence of both the ¹³C-¹³C_α and ¹³C_α-¹⁴N spin pair was exploited to fix the carbon chemical shift tensors relative to the molecule.

The above discussion pertains to multiple heteronuclear spin systems. A homonuclear four spin system, the fully ¹³C labelled monoammonium salt of maleic acid, has been investigated by solid-state NMR.²¹³ An example of a homonuclear three spin system is illustrated in figure 7.2, where a linear arrangement of three phosphorus

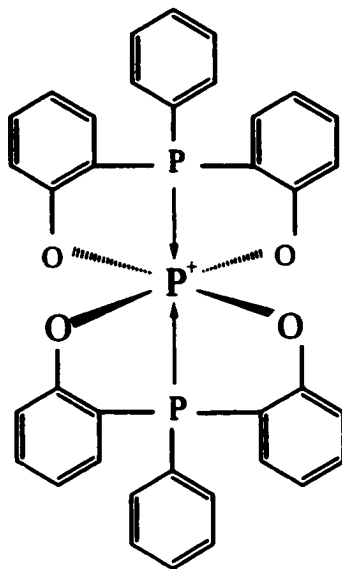


Figure 7.2 Structure of a phosphorus-containing homonuclear three-spin system.

nuclei is present.²¹⁴ A linear arrangement of phosphorus nuclei will simplify the analysis of the spectra. An investigation of the phosphorus chemical shift tensors and spin-spin coupling parameters in such a unique molecule would be a valuable contribution to an understanding of the relationship between structure and NMR parameters. A program available for simulating solid-state NMR spectra, SIMPSON,⁵¹ is capable of calculating spectra arising from multiple coupled spins with the inclusion of chemical shift, dipolar and spin-spin coupling interactions and may be useful for this project.

Appendix 1: Performing the 2D Spin-Echo NMR Experiment on the CMX Infinity 200 at the University of Alberta

The 2D spin-echo NMR spectra presented in this thesis were obtained using a Bruker MSL 200 spectrometer (figure 4.5) or a Varian Chemagnetics CMX Infinity 200 (figures 3.9 and 5.4). For the benefit of future users, the details of the procedure used to obtain 2D spin-echo NMR spectra using the CMX Infinity 200 and to process the data to a form that can be used for simulation with the program SpinEcho¹³⁹ are presented here. The following description pertains to the pulse program shown in figure 2.8. The phase cycling of Rance and Byrd was used.¹³⁸

After setting up the parameters for a standard 1D NMR experiment using CP, the π pulse on the X channel needs to be calibrated. This must be done using the same X power settings as used for CP. The important 2D parameters are *dw2*, *t1_evolve*, and *al2*. The dwell time for the second dimension, *dw2*, should be set so that the sweep width in the *F1* projection (sweep width = $1/dw2$) is larger than the largest splitting expected, i.e., larger than $2R_{\text{eff}}$ for a spin pair where the two nuclei are not magnetically equivalent and $3R_{\text{eff}}$ for the case of magnetic equivalence (see figure 2.4). The parameter *t1_evolve* corresponds to the time between the CP part of the pulse program and the π pulse as well as the time following the π pulse and before acquisition. In the version of the 2D spin-echo pulse sequence used on the CMX Infinity 200, the parameter is calculated based on the value of *al2*, which is the number of times

$t1_evolve$ is incremented, and $dw2$. The maximum value of $t1_evolve$ is $dw2*al2$.

Usually $al2 = 64$ experiments is acceptable.

Once the data are collected, they are processed using Spinsight software.²¹⁵ It is recommended that zero filling and gaussian line broadening be applied in both dimensions. To obtain a symmetric 2D NMR spectrum, it is necessary to process in magnitude mode for both dimensions. To ease simulation of the $F1$ projection with SpinEcho,¹³⁹ it is useful to have the file in a format that is usable with WSOLIDS⁴⁹ or other processing software available for PCs. At the time of preparation of this thesis, there is no direct method for doing this. Instead, a print out of the $F1$ projection is scanned and a program called SPECMAKE²¹⁶ which is part of the WSOLIDS⁴⁹ software package, is used to convert the scanned image to a data file. The print out of the $F1$ projection is obtained by executing a macro with Spinsight, called `1dshow_proj`. Note that in the display, Spinsight uses the wrong value of the dwell time to calculate the scale (dw instead of $dw2$). This is corrected by changing the value of dw to the value used for $dw2$ in the acquisition panel before the $F1$ projection is printed out. If the 2D spectrum is printed out, the scale for the $F1$ projection is correct. While it is not necessary to convert the spectrum data in this way, simulation of the spectra and preparation for publication is easier.

Appendix 2: Handling Air-Sensitive NMR Samples

This appendix is intended to provide some details with regards to handling air-sensitive samples for NMR studies. Some general strategies will first be presented, followed by some comments pertaining to specific rotor designs.

For samples that are extremely air-sensitive, sealed Pyrex MAS rotor inserts may be used.²¹⁷ The sample is heat sealed into the inserts or an epoxy sealant may be used. Heat sealing is generally more difficult given the small size of the inserts and the need to obtain as symmetric a seal as possible so as not to hamper MAS. If the sample is packed directly into the MAS rotors, an additional precautionary measure to avoid contact with air is to seal the rotor itself into a glass tube and break it open once the NMR experiment is set up.

The rotors used to obtain the NMR spectra presented in this thesis are manufactured by either Bruker or Varian-Chemagnetics. It has been the experience of the solid-state NMR group at Dalhousie University and University of Alberta that the Bruker rotors are generally sufficiently air-tight and no special precautions are needed beyond ensuring that the rotor caps are tight fitting. For the Varian-Chemagnetics rotors, there are a number of strategies for dealing with air-sensitive samples, for example the use of glass inserts as discussed above is a common solution. Inserts are commercially available for various Varian-Chemagnetics rotors. The rotor illustrated in figure A2.1 was used to obtain NMR spectra of air-sensitive samples on the Varian-Chemagnetics spectrometer. The only modification to the commercial design is an

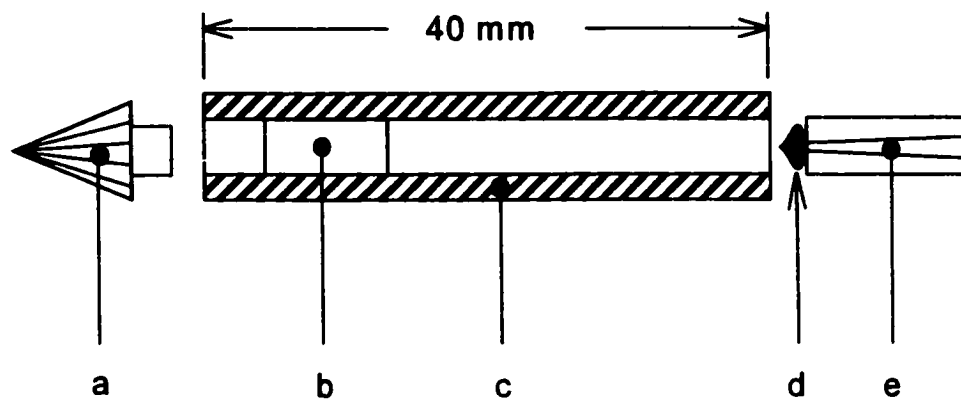


Figure A2.1 An illustration of a Varian-Chemagnetics rotor. (a) drive tip. (b) spacer. (c) zirconium oxide sleeve. (d) epoxy seal. (e) end cap, with a hole for variable temperature experiments.

epoxy seal applied to the inner surface of the end cap, which is manufactured with a vent hole for variable temperature experiments. The drive tips usually fit very tightly, hence there is no difficulty with excluding air at the other end of the rotor.

References

1. D. L. Pavia, G. M. Lampman, and G. S. Kriz. *Introduction to Spectroscopy*, 2nd Ed. Saunders College Publishing, Fort Worth, Texas. 1996.
2. U. Haerberlen. *In Advances in Magnetic Resonance*. Edited by J. S. Waugh. Academic Press, New York. 1976, Supplement 1, p. 1.
3. J. B. Robert and L. Wiesenfeld, *Physics Reports* **86**, 363 (1982).
4. K. R. Dixon. *In Multinuclear NMR*. Edited by J. Mason. Plenum Press, New York. 1987, p. 369.
5. C. J. Jameson, *Annu. Rev. Phys. Chem.* **47**, 135 (1996).
6. H. Fukui, *Prog. Nucl. Magn. Reson. Spectrosc.* **31**, 317 (1997).
7. A. C. de Dios, *Prog. Nucl. Magn. Reson. Spectrosc.* **29**, 229 (1996).
8. T. Helgaker, M. Jaszuński, and K. Ruud, *Chem. Rev.* **99**, 293 (1999).
9. C. J. Jameson. *In Modeling NMR Chemical Shifts: Gaining Insights into Structure and Environment*. Edited by J. C. Facelli and A. C. de Dios. American Chemical Society, Washington, DC. 1999, p. 1.
10. K. Eichele, G. Wu, R. E. Wasylshen, and J. F. Britten, *J. Phys. Chem.* **99**, 1030 (1995).
11. P. N. Tutunjian and J. S. Waugh, *J. Chem. Phys.* **76**, 1223 (1982).
12. J. B. Robert and L. Wiesenfeld, *Mol. Phys.* **44**, 319 (1981).
13. T. Nakai and C. A. McDowell, *J. Am. Chem. Soc.* **116**, 6373 (1994).
14. (a) S. Aime, R. K. Harris, E. M. McVicker, and M. Fild, *J. Chem. Soc., Dalton Trans.* 2144 (1976). (b) F. Sarikahya, Y. Sarikahya, I. Topaloğlu, and I. O. Şentürk, *Chimica Acta Turcica* **25**, 35 (1997).
15. R. K. Harris, L. H. Merwin, and G. Hägele, *J. Chem. Soc., Faraday Trans. 1.* **83**, 1055 (1987).
16. P. N. Tutunjian and J. S. Waugh, *J. Magn. Reson.* **49**, 155 (1982).

17. K. W. Zilm, G. G. Webb, A. H. Cowley, M. Pakulski, and A. Orendt, *J. Am. Chem. Soc.* **110**, 2032 (1988).
18. R. Challoner, C. A. McDowell, M. Yoshifuji, K. Toyota, and J. A. Tossell, *J. Magn. Reson. A* **104**, 258 (1993).
19. K. Eichele, G. C. Ossenkamp, R. E. Wasylishen, and T. S. Cameron, *Inorg. Chem.* **38**, 639 (1999).
20. G. M. Bernard, G. Wu, M. D. Lumsden, R. E. Wasylishen, N. Maigrot, C. Charrier, and F. Mathey, *J. Phys. Chem. A* **103**, 1029 (1999).
21. J. Fischer, A. Mitschler, F. Mathey, and F. Mercier, *J. Chem. Soc. Dalton Trans.* 841 (1983).
22. (a) F. S. Shagvaleev, T. V. Zykova, R. I. Tarasova, T. Sh. Sitdikova, and V. V. Moskva, *J. Gen. Chem. USSR* **60**, 1585 (1990). (b) N. Burford, T. S. Cameron, J. A. C. Clyburne, K. Eichele, K. N. Robertson, S. Sereda, R. E. Wasylishen, and W. A. Whitla, *Inorg. Chem.* **35**, 5460 (1996). (c) N. Burford, T. S. Cameron, D. J. LeBlanc, P. Losier, S. Sereda, and G. Wu, *Organometallics* **16**, 4712 (1997). (d) N. Burford and D. J. LeBlanc, *Inorg. Chem.* **38**, 2248 (1999).
23. R. K. Harris. *Nuclear Magnetic Resonance Spectroscopy*. John Wiley and Sons, Inc., New York. 1986, p. 10.
24. F. A. L. Anet and D. J. O'Leary, *Concepts in Magn. Reson.* **3**, 193 (1991).
25. F. A. L. Anet and D. J. O'Leary, *Concepts in Magn. Reson.* **4**, 35 (1992).
26. K. Schmidt-Rohr and H. W. Spiess. *Multidimensional Solid State NMR and Polymers*. Academic Press, London. 1994, p. 444.
27. J. Mason, *Solid State Nucl. Magn. Reson.* **2**, 285 (1993).
28. (a) C. J. Jameson, *Solid State Nucl. Magn. Reson.* **11**, 265 (1998). (b) R. K. Harris, *Solid State Nucl. Magn. Reson.* **10**, 177 (1998).
29. R. E. Wasylishen. *In Encyclopedia of Nuclear Magnetic Resonance*. Edited by D. M. Grant and R. K. Harris. Wiley Inc., Chichester, UK. 1996, p. 1685.
30. C. J. Jameson and J. Mason. *In Multinuclear NMR*. Edited by J. Mason. Plenum Press, New York. 1987, p. 3.

31. G. E. Pake, *J. Chem. Phys.* **16**, 327 (1948).
32. C. J. Jameson. *In Multinuclear NMR. Edited by J. Mason.* Plenum Press, New York, 1987, p. 89.
33. A. D. Buckingham, P. Pyykkö, J. B. Robert, and L. Wiesenfeld, *Mol. Phys.* **46**, 177 (1982).
34. W. T. Raynes, *Magn. Reson. Chem.* **30**, 686 (1992).
35. A. D. Buckingham and I. Love, *J. Magn. Reson.* **2**, 338 (1970).
36. H. W. Spiess, *NMR Basic Princ. Prog.* **15**, 55 (1978).
37. D. L. Bryce and R. E. Wasylishen, *J. Am. Chem. Soc.* **122**, 3197 (2000).
38. R. von Boeckh, G. Gräff, and R. Ley, *Z. Phys.* **179**, 285 (1964).
39. R. E. Wasylishen, K. C. Wright, K. Eichele, and T. S. Cameron, *Inorg. Chem.* **33**, 407 (1994).
40. M. D. Lumsden, R. E. Wasylishen, and J. F. Britten, *J. Phys. Chem.* **99**, 16602 (1995).
41. M. D. Lumsden, K. Eichele, R. E. Wasylishen, T. S. Cameron, and J. F. Britten, *J. Am. Chem. Soc.* **116**, 11129 (1994).
42. (a) W. P. Power, M. D. Lumsden, and R. E. Wasylishen, *J. Am. Chem. Soc.* **113**, 8257 (1991). (b) W. P. Power and R. E. Wasylishen, *Inorg. Chem.* **31**, 2176 (1992).
43. (a) D. L. VanderHart and H. S. Gutowsky, *J. Chem. Phys.* **49**, 261 (1968). (b) M. Linder, A. Höhener, and R. R. Ernst, *J. Chem. Phys.* **73**, 4959 (1980). (c) R. E. Wasylishen, R. D. Curtis, K. Eichele, M. D. Lumsden, G. H. Penner, W. P. Power, and G. Wu. *In Nuclear Magnetic Shieldings and Molecular Structure. Edited by J. A. Tossell.* Kluwer Academic Publishers, Dordrecht. 1993, p. 297.
44. W. P. Power and R. E. Wasylishen, *Ann. Rep. NMR Spectrosc.* **23**, 1 (1991).
45. (a) K. W. Zilm and D. M. Grant, *J. Am. Chem. Soc.* **103**, 2913 (1981). (b) G. Wu and R. E. Wasylishen, *Solid State Nucl. Magn. Reson.* **4**, 47 (1995).

46. H. van Willigen, R. G. Griffin, and R. A. Haberkorn, *J. Chem. Phys.* **67**, 5855 (1977).
47. (a) R. D. Curtis, J. W. Hilborn, G. Wu, M. D. Lumsden, R. E. Wasylishen, and J. A. Pincock, *J. Phys. Chem.* **97**, 1856 (1993). (b) M. D. Lumsden, G. Wu, R. E. Wasylishen, and R. D. Curtis, *J. Am. Chem. Soc.* **115**, 2825 (1993).
48. K. Eichele and R. E. Wasylishen, *J. Magn. Reson. A* **106**, 46 (1994).
49. K. Eichele and R. E. Wasylishen, WSOLIDS, 1994 and 2000.
50. B. Sun and R. G. Griffin, unpublished results.
51. M. Bak, J. T. Rasmussen, and N. C. Nielsen, *J. Magn. Reson.* **147**, 296 (2000).
52. (a) A. Kubo and C. A. McDowell, *J. Chem. Phys.* **92**, 7156 (1990). (b) E. Klaus and A. Sebald, *Angew. Chem. Int. Ed.* **34**, 667 (1995). (c) S. Dusold, E. Klaus, A. Sebald, M. Bak, and N. C. Nielsen, *J. Am. Chem. Soc.* **119**, 7121 (1997).
53. R. R. Ernst, G. Bodenhausen, and A. Wokaun. Principles of Nuclear Magnetic Resonance in One and Two Dimensions. Clarendon Press, Oxford. 1987.
54. A. Pines, M. G. Gibby, and J. S. Waugh, *J. Chem. Phys.* **59**, 569 (1973).
55. S. R. Hartmann and E. L. Hahn, *Phys. Rev.* **128**, 2042 (1962).
56. T. Nakai and C. A. McDowell, *Chem. Phys. Lett.* **217**, 234 (1994).
57. K. Eichele, R. E. Wasylishen, R. W. Schurko, N. Burford, and W. A. Whitla, *Can. J. Chem.* **74**, 2372 (1996).
58. S. Dusold, J. Kümmerlen, and A. Sebald, *J. Phys. Chem. A* **101**, 5895 (1997).
59. T. Nakai and C. A. McDowell, *Solid State Nucl. Magn. Reson.* **4**, 163 (1995).
60. (a) N. F. Ramsey, *Phys. Rev.* **77**, 567 (1950). (b) N. F. Ramsey, *Phys. Rev.* **78**, 699 (1950). (c) N. F. Ramsey, *Phys. Rev.* **83**, 540 (1951). (d) N. F. Ramsey, *Phys. Rev.* **86**, 243 (1952).
61. N. F. Ramsey, *Phys. Rev.* **91**, 303 (1953).
62. N. F. Ramsey. Molecular Beams. Oxford University Press, London. 1956.
63. P. Pyykkö, *Theor. Chem. Acc.* **103**, 214 (2000).

64. J. H. Van Vleck. *The Theory of Electric and Magnetic Susceptibilities*. Oxford University Press, London. 1932.
65. C. J. Jameson and J. Mason. *In Multinuclear NMR*. Edited by J. Mason. Plenum Press, New York. 1987, p. 51.
66. D. B. Chesnut, *Ann. Rep. NMR Spectrosc.* **29**, 71 (1994).
67. R. W. Schurko and R. E. Wasylshen, *J. Phys. Chem. A* **104**, 3410 (2000).
68. D. L. Bryce and R. E. Wasylshen, *J. Phys. Chem. A* **104**, 7700 (2000).
69. U. Fleischer, C. van Wüllen, and W. Kutzelnigg. *In Encyclopedia of Computational Chemistry*. Edited by P. von R. Schleyer. John Wiley and Sons, Chichester. 1998, p. 1927.
70. W. Kutzelnigg, U. Fleischer, and M. Schindler, *NMR Basic Princ. Prog.* **23**, 163 (1990).
71. S. I. Chan and T. P. Das, *J. Chem. Phys.* **37**, 1527 (1962).
72. C. W. Kern and W. N. Lipscomb, *J. Chem. Phys.* **37**, 260 (1962).
73. (a) R. Ditchfield, *Mol. Phys.* **27**, 789 (1974). (b) K. Wolinski, J. F. Hinton, and P. Pulay, *J. Am. Chem. Soc.* **112**, 8251 (1990). (c) G. Rauhut, S. Puyear, K. Wolinski, and P. Pulay, *J. Phys. Chem.* **100**, 6310 (1996).
74. M. Schindler and W. Kutzelnigg, *J. Chem. Phys.* **76**, 1919 (1982).
75. A. E. Hansen and T. D. Bouman, *J. Chem. Phys.* **82**, 5035 (1985).
76. T. A. Keith and R. F. W. Bader, *Chem. Phys. Lett.* **194**, 1 (1992).
77. (a) J. Gauss, *Chem. Phys. Lett.* **191**, 614 (1992). (b) J. Gauss, *Chem. Phys. Lett.* **229**, 198 (1994).
78. B. O. Roos, *Adv. Chem. Phys.* **69**, 399 (1987).
79. K. Ruud, T. Helgaker, R. Kobayashi, P. Jørgensen, K. L. Bak, and H. J. Aa. Jensen, *J. Chem. Phys.* **100**, 8178 (1994).
80. (a) M. Bühl, M. Kaupp, O. L. Malkina, and V. G. Malkin, *J. Comp. Chem.* **20**, 91 (1999). (b) V. G. Malkin, O. L. Malkina, M. E. Casida, and D. R. Salahub, *J. Am. Chem. Soc.* **116**, 5898 (1994). (c) V. G. Malkin, O. L. Malkina, and D. R. Salahub, *Chem. Phys. Lett.* **204**, 87 (1993). (d) V. G. Malkin, O. L.

- Malkina, and D. R. Salahub, *Chem. Phys. Lett.* **204**, 80 (1993).
81. G. Schreckenbach, R. M. Dickson, Y. Ruiz-Morales, and T. Ziegler. *In* **Chemical Applications of Density Functional Theory**. Edited by B. B. Laird, R. B. Ross, and T. Ziegler. American Chemical Society, Washington. 1996, p. 328.
82. (a) G. Schreckenbach, S. K. Wolff, and T. Ziegler, *J. Phys. Chem. A* **104**, 8244 (2000). (b) S. K. Wolff, T. Ziegler, E. van Lenthe, and E. J. Baerends, *J. Chem. Phys.* **110**, 7689 (1999).
83. Gaussian 94, Revision B.2, M. J. Frisch, G. W. Trucks, H. B. Schlegel, P. M. W. Gill, B. G. Johnson, M. A. Robb, J. R. Cheeseman, T. Keith, G. A. Petersson, J. A. Montgomery, K. Raghavachari, M. A. Al-Laham, V. G. Zakrzewski, J. V. Ortiz, J. B. Foresman, J. Cioslowski, B. B. Stefanov, A. Nanayakkara, M. Challacombe, C. Y. Peng, P. Y. Ayala, W. Chen, M. W. Wong, J. L. Andres, E. S. Replogle, R. Gomperts, R. L. Martin, D. J. Fox, J. S. Binkley, D. J. Defrees, J. Baker, J. P. Stewart, M. Head-Gordon, C. Gonzalez, and J. A. Pople, Gaussian, Inc., Pittsburgh, PA, 1995.
84. Gaussian 98, Revision A.4, M. J. Frisch, G. W. Trucks, H. B. Schlegel, G. E. Scuseria, M. A. Robb, J. R. Cheeseman, V. G. Zakrzewski, J. A. Montgomery, Jr., R. E. Stratmann, J. C. Burant, S. Dapprich, J. M. Millam, A. D. Daniels, K. N. Kudin, M. C. Strain, O. Farkas, J. Tomasi, V. Barone, M. Cossi, R. Cammi, B. Mennucci, C. Pomelli, C. Adamo, S. Clifford, J. Ochterski, G. A. Petersson, P. Y. Ayala, Q. Cui, K. Morokuma, D. K. Malick, A. D. Rabuck, K. Raghavachari, J. B. Foresman, J. Cioslowski, J. V. Ortiz, B. B. Stefanov, G. Liu, A. Liashenko, P. Piskorz, I. Komaromi, R. Gomperts, R. L. Martin, D. J. Fox, T. Keith, M. A. Al-Laham, C. Y. Peng, A. Nanayakkara, C. Gonzalez, M. Challacombe, P. Gill, B. Johnson, W. Chen, M. W. Wong, J. L. Andres, C. Gonzalez, M. Head-Gordon, E. S. Replogle, and J. A. Pople, Gaussian, Inc., Pittsburgh PA, 1998.
85. Æ. Frisch and M. J. Frisch. Gaussian 98 User's Reference, 2nd Ed. Gaussian Inc., Pittsburgh PA. 1999, p. 126.
86. C.J. Jameson. *In* Encyclopedia of Nuclear Magnetic Resonance. Edited by D. M. Grant and R. K. Harris. Wiley Inc. Chichester, UK. 1996, p. 1273.
87. A. K. Jameson and C. J. Jameson, *Chem. Phys. Lett.* **134**, 461 (1987).
88. R. E. Wasylishen, S. Mooibroek, and J. B. Macdonald, *J. Chem. Phys.* **81**, 1057 (1984).

89. C. J. Jameson, A. K. Jameson, and P. M. Burrell, *J. Chem. Phys.* **73**, 6013 (1980).
90. C. J. Jameson, A. C. de Dios, and A. K. Jameson, *Chem. Phys. Lett.* **167**, 575 (1990).
91. M. Gee, R. E. Wasylishen, and A. Laaksonen, *J. Phys. Chem. A* **103**, 10805 (1999).
92. J. E. Rich, M. N. Manalo, and A. C. de Dios, *J. Phys. Chem. A* **104**, 5837 (2000).
93. B. Celda, C. Biamonti, M. J. Arneau, R. Tejero, and G. T. Montelione, *J. Biomol. NMR* **5**, 161 (1995).
94. D. D. Laws, A. C. de Dios, and E. Oldfield, *J. Biomol. NMR* **3**, 607 (1993).
95. (a) A. J. Dingley and S. Grzesiek, *J. Am. Chem. Soc.* **120**, 8293 (1998). (b) A. J. Dingley, J. E. Masse, R. D. Peterson, M. Barfield, J. Feigon, and S. Grzesiek, *J. Am. Chem. Soc.* **121**, 6019 (1999). (c) F. Cordier and S. Grzesiek, *J. Am. Chem. Soc.* **121**, 1601 (1999). (d) G. Cornilescu, J.-S. Hu, and A. Bax, *J. Am. Chem. Soc.* **121**, 2949 (1999). (f) F. Cordier, M. Rogowski, S. Grzesiek, and A. Bax, *J. Magn. Reson.* **140**, 510 (1999).
96. C. Scheurer and R. Brüschweiler, *J. Am. Chem. Soc.* **121**, 8661 (1999).
97. D. L. Bryce and R. E. Wasylishen, *J. Biomol. NMR* **19**, 371 (2001).
98. H. Benedict, I. G. Shenderovich, O. L. Malkina, V. G. Malkin, G. S. Denisov, N. S. Golubev, and H.-H. Limbach, *J. Am. Chem. Soc.* **122**, 1979 (2000).
99. H. Fukui, *Prog. Nucl. Magn. Reson.* **35**, 267 (1999).
100. N. F. Ramsey. *In Experimental Nuclear Physics. Edited by E. Segrè.* John Wiley and Sons, New York. 1953, vol. 1, part III, p. 358.
101. J. Kowalewski and A. Laaksonen. *In Theoretical Models of Chemical Bonding. Edited by Z. B. Maksić.* Springer, Berlin. 1991, part 3, p. 387.
102. P. Pyykkö, *Chem. Phys.* **22**, 289 (1977).
103. V. Sychrovský, J. Gräfenstein, and D. Cremer, *J. Chem. Phys.* **113**, 3530 (2000).

104. I. Carmichael, *J. Phys. Chem.* **97**, 1789 (1993).
105. O. L. Malkina, D. R. Salahub, and V. G. Malkin, *J. Chem. Phys.* **105**, 8793 (1996).
106. V. G. Malkin, O. L. Malkina, and D. R. Salahub, *Chem. Phys. Lett.* **221**, 91 (1994).
107. M. F. Guest, V. R. Saunders, and R. E. Overill, *Mol. Phys.* **35**, 427 (1978).
108. O. Vahtras, H. Ågren, P. Jørgensen, J. J. Aa. Jensen, S. B. Padkjær, and T. Helgaker, *J. Chem. Phys.* **96**, 6120 (1992).
109. (a) A. Barszczewicz, T. Helgaker, M. Jaszuński, P. Jørgensen, and K. Ruud, *J. Magn. Reson. A* **114**, 212 (1995). (b) A. Barszczewicz, T. Helgaker, M. Jaszuński, P. Jørgensen, and K. Ruud, *J. Chem. Phys.* **101**, 6822 (1994). (c) J. Kaski, P. Lantto, J. Vaara, and J. Jokisaari, *J. Am. Chem. Soc.* **120**, 3993 (1998). (d) J. Kaski, P. Lantto, T. T. Rantala, J. Schroderus, J. Vaara, and J. Jokisaari, *J. Phys. Chem. A* **103**, 9669 (1999).
110. D. L. Bryce and R. E. Wasylishen, *J. Am. Chem. Soc.* **122**, 11236 (2000).
111. J. F. Stanton and R. J. Bartlett, *J. Chem. Phys.* **98**, 7029 (1993).
112. S. A. Perera, H. Sekino, and R. J. Bartlett, *J. Chem. Phys.* **101**, 2186 (1994).
113. S. A. Perera, R. J. Bartlett, and P. von R. Schleyer, *J. Am. Chem. Soc.* **117**, 8476 (1995).
114. J. Oddershede, P. Jørgensen, and D. L. Yeager, *Comput. Phys. Rep.* **33**, 2 (1984).
115. J. Oddershede. *In Methods in Computational Molecular Physics. Edited by S. Wilson and G. H. F. Dierksen. Plenum Press, New York, 1992, p. 303.*
116. T. Enevoldsen, J. Oddershede, and S. P. A. Sauer, *Theor. Chem. Acc.* **100**, 275 (1998).
117. S. A. Perera and R. J. Bartlett, *J. Am. Chem. Soc.* **122**, 1231 (2000).
118. H. Fukui, *J. Chem. Phys.* **65**, 844 (1976).
119. T. Enevoldsen, L. Visscher, T. Saue, H. J. Aa. Jensen, and J. Oddershede. *J. Chem. Phys.* **112**, 3493 (2000).

120. J. Khandogin and T. Ziegler, *J. Phys. Chem. A* **104**, 113 (2000).
121. J. Autschbach and T. Ziegler, *J. Am. Chem. Soc.*, **123**, 3341 (2001).
122. J. Autschbach and T. Ziegler, *J. Chem. Phys.* **113**, 936 (2000).
123. J. Autschbach and T. Ziegler, *J. Chem. Phys.* **113**, 9410 (2000).
124. T. Helgaker, M. Jaszuński, K. Ruud, and A. Górska, *Theor. Chem. Acc.* **99**, 175 (1998).
125. J. Vaara, J. Kaski, and J. Jokisaari, *J. Phys. Chem. A* **103**, 5675 (1999).
126. A. Viste, M. Hotokka, L. Laaksonen, and P. Pyykkö, *Chem. Phys.* **72**, 225 (1982).
127. (a) K. Krüger, G. Grossmann, U. Fleischer, R. Franke, and W. Kutzelnigg, *Magn. Reson. Chem.* **32**, 596 (1994). (b) G. Ohms, U. Fleischer, and V. Kaiser, *J. Chem. Soc., Dalton Trans.* 1297 (1995).
128. A.-R. Grimmer, R. Peter, and E. Fechner, *Z. Chem.* **18**, 109 (1978).
129. (a) R. J. Iuliucci, C. G. Phung, J. C. Facelli, and D. M. Grant, *J. Am. Chem. Soc.* **118**, 4880 (1996). (b) R. J. Iuliucci, C. G. Phung, J. C. Facelli, and D. M. Grant, *J. Am. Chem. Soc.* **120**, 9305 (1998). (c) R. W. Schurko, R. E. Wasylshen, and H. Foerster, *J. Phys. Chem. A* **102**, 9750 (1998). (d) D. L. Bryce and R. E. Wasylshen, *J. Phys. Chem. A* **103**, 7364 (1999).
130. (a) T. Vosegaard, P. Daugaard, E. Hald, and H. J. Jakobsen, *J. Magn. Reson.* **142**, 379 (2000). (b) T. Vosegaard, J. Skibsted, and H. J. Jakobsen, *J. Phys. Chem. A* **103**, 9144 (1999). (c) T. Vosegaard, E. Hald, V. Langer, H. J. Skov, P. Daugaard, H. Bildsøe, and H. J. Jakobsen, *J. Magn. Reson.* **135**, 126 (1998).
131. (a) SADABS, G. M. Sheldrick, and Bruker AXS, Inc., Madison, Wisconsin, 53719 USA. (b) R. H. Blessing, *Acta Crystallogr.* **A51**, 33 (1995).
132. S. N. Dutta, and M. M. Woolfson, *Acta. Crystallogr.* **14**, 178 (1961).
133. SHELXTL (5.10) program library (G. Sheldrick, Siemens XRD, Madison Wisconsin).
134. J. S. Rollett, *Computing Methods in Crystallography*. Pergamon Press, New York. 1965.

135. E. Prince. *Mathematical Techniques in Crystallography and Material Science*. Springer-Verlag, Berlin. 1994.
136. (a) M. A. Kennedy and P. D. Ellis, *Concepts in Magn. Reson.* **1**, 35 (1989). (b) M. A. Kennedy and P. D. Ellis, *Concepts in Magn. Reson.* **1**, 109 (1989). (c) K. Eichele, J. C. C. Chan, R. E. Wasylshen, and J. F. Britten, *J. Phys. Chem. A* **101**, 5423 (1997).
137. D. W. Alderman, M. S. Solum, and D. M. Grant, *J. Chem. Phys.* **84**, 3717 (1986).
138. M. Rance and R. A. Byrd, *J. Magn. Reson.* **52**, 221 (1983).
139. SpinEcho, K. Eichele and R. E. Wasylshen, unpublished.
140. A. D. Becke, *J. Chem. Phys.* **98**, 5648 (1993).
141. C. Lee, W. Yang, and R. G. Parr, *Phys. Rev. B*, **37**, 785 (1988).
142. R. K. Harris and R. G. Hayter, *Can. J. Chem.* **42**, 2282 (1964).
143. (a) J. M. Millar, A. M. Thayer, D. B. Zax, and A. Pines, *J. Am. Chem. Soc.* **108**, 5113 (1986). (b) T. Nakai, J. Ashida, and T. Terao, *Mol. Phys.* **67**, 839 (1989).
144. J. D. Lee and G. W. Goodacre, *Acta Crystallogr.* **B27**, 302 (1971).
145. M. G. Munowitz and R. G. Griffin, *J. Chem. Phys.* **76**, 2848 (1982).
146. Y. Ishii, T. Terao, and S. Hayashi, *J. Chem. Phys.* **107**, 2760 (1997).
147. J. Herzfeld and A. E. Berger, *J. Chem. Phys.* **73**, 6021 (1980).
148. R. E. Wasylshen, W. P. Power, G. H. Penner, and R. D. Curtis, *Can. J. Chem.* **67**, 1219 (1989).
149. G. Heckmann and E. Fluck, *Mol. Phys.* **23**, 175 (1972).
150. C. J. Jameson, *Bull. Magn. Reson.* **3**, 3 (1980).
151. R. Sillanpää, Ö. Ergin, and S. Çelebi, *Acta Crystallogr.* **C49**, 767 (1993).
152. F. Mathey, F. Mercier, F. Nief, J. Fischer, and A. Mitschler, *J. Am. Chem. Soc.* **104**, 2077 (1982).

153. G. Wu and R. E. Wasylishen, *J. Chem. Phys.* **99**, 6321 (1993).
154. G. Wu, B. Sun, R. E. Wasylishen, and R. G. Griffin, *J. Magn. Reson.* **124**, 366 (1997).
155. teXsan for Windows version 1.05: Crystal Structure Analysis Package, Molecular Structure Corporation (1997-8).
156. (a) D. B. Chesnut and K. D. Moore, *J. Comp. Chem.* **10**, 648 (1989). (b) D. B. Chesnut, B. E. Rusiloski, K. D. Moore, and D. A. Egolf, *J. Comp. Chem.* **14**, 1364 (1993).
157. S. Duangthai and G. A. Webb, *Organic Magn. Reson.* **21**, 199 (1983).
158. D. B. Chesnut and L. D. Quin, *J. Am. Chem. Soc.* **116**, 9638 (1994).
159. D. B. Chesnut and E. F. C. Byrd, *Heteroatom Chem.* **7**, 307 (1996).
160. G. M. Bernard, G. Wu, and R. E. Wasylishen, *J. Phys. Chem. A* **102**, 3184 (1998).
161. (a) F. Mathey, *Chem. Rev.* **88**, 429 (1988). (b) F. Mathey, *Coordination Chem. Rev.* **137**, 1 (1994).
162. (a) L. Nyulászi, *J. Phys. Chem.* **100**, 6194 (1996). (b) A. Dransfeld, L. Nyulászi, and P. v. R. Schleyer, *Inorg. Chem.* **37**, 4413 (1998). (c) F. G. N. Cloke, P. B. Hitchcock, P. Hunnabell, J. F. Nixon, L. Nyulászi, E. Niecke, and V. Thelen, *Angew. Chem. Int. Ed.* **37**, 1083 (1998).
163. L. Nyulászi, *Chem. Rev.*, in press, 2001.
164. K. Eichele, R. E. Wasylishen, J. M. Kessler, L. Solujić, and J. H. Nelson, *Inorg. Chem.* **35**, 3904 (1996).
165. R. D. Curtis, B. W. Royan, R. E. Wasylishen, M. D. Lumsden, and N. Burford, *Inorg. Chem.* **31**, 3386 (1992).
166. J. B. Grutzner. *In Recent Advances in Organic NMR Spectroscopy. Edited by J. B. Lambert and R. Rittner.* Norell Press, Landisville, NJ. 1987, chapter 2, p. 17.
167. G. H. Penner and R. E. Wasylishen, *Can. J. Chem.* **67**, 1909 (1989).
168. G. Wu, R. E. Wasylishen, W. P. Power, and G. Baccolini, *Can. J. Chem.* **70**, 1229 (1992).

169. N. Burford, E. Ocando-Mavarez, unpublished.
170. U. Haubenreisser, U. Sternberg, and A.-R. Grimmer, *Mol. Phys.* **60**, 151 (1987).
171. "DALTON, an *ab initio* electronic structure program", written by T. Helgaker, H.J. Å. Jensen, P. Jørgensen, J. Olsen, K. Ruud, H. Ågren, T. Andersen, K.L. Bak, V. Bakken, O. Christiansen, P. Dahle, E.K. Dalskov, T. Enevoldsen, B. Fernandez, H. Heiberg, H. Hettema, D. Jonsson, S. Kirpekar, R. Kobayashi, H. Koch, K.V. Mikkelsen, P. Norman, M.J. Packer, T. Saue, P.R. Taylor, and O. Vahtras; Release 1.0 (1997).
172. (a) H. J. Aa. Jensen, P. Jørgensen, H. Ågren, and J. Olsen, *J. Chem. Phys.* **88**, 3834 (1988). (b) J. Guilleme and J. S. Fabián, *J. Chem. Phys.* **109**, 8168 (1998).
173. T. H. Dunning, Jr., *J. Chem. Phys.* **90**, 1007 (1989).
174. J. R. Durig, L. A. Carreira, and J. D. Odom, *J. Am. Chem. Soc.* **96**, 2688 (1974).
175. (a) E. R. Andrew, A. Bradbury, R. G. Eades, and V. T. Wynn, *Phys. Lett.* **4**, 99 (1963). (b) D. P. Raleigh, M. H. Levitt, and R. G. Griffin, *Chem. Phys. Lett.* **146**, 71 (1988). (c) D. L. Bryce and R. E. Wasylshen. *In Encyclopedia of Spectroscopy and Spectrometry. Edited by J. C. Lindon, G. E. Tranter, and J. L. Holmes. Academic Press, San Diego. 2000, p. 2136.*
176. (a) G. A. Olah and C. W. McFarland, *J. Org. Chem.* **34**, 1832 (1969). (b) B. E. Mann, *J. Chem. Soc., Perkin Trans. 2*, 30 (1972). (c) S. O. Grim, E. F. Davidoff, and T. J. Marks, *Z. Naturforsch.* **26b**, 184 (1971). (d) G. P. Schiemenz, *Phosphorus 3*, 125 (1973).
177. R. W. Rudolph and R. A. Newmark, *J. Am. Chem. Soc.* **92**, 1195 (1970).
178. H. C. E. McFarlane and W. McFarlane, *J. Chem. Soc., Chem. Commun.* 1589 (1971).
179. W. McFarlane, N. H. Rees, L. Constanza, M. Patel, and I. J. Colquhoun, *J. Chem. Soc., Dalton Trans.* 4453 (2000).
180. C. J. Jameson. *In Phosphorus-31 NMR Spectroscopy in Stereochemical Analysis. Edited by J. G. Verkade and L. D. Quin. VCH Publishers, Inc., Deerfield Beach, Fla. 1987, p. 205.*

181. U. C. Singh, P. K. Basu, and C. N. R. Rao, *J. Mol. Struct.* **87**, 125 (1982).
182. R. M. Lynden-Bell, *J. Chem. Soc., Faraday Trans.* **57**, 888 (1961).
183. J. P. Albrand, H. Faucher, D. Gagnaire, and J. B. Robert, *Chem. Phys. Lett.* **38**, 521 (1976).
184. V. Galasso, *J. Chem. Phys.* **80**, 365 (1984).
185. D. Chakraborty and P. Chandra, *J. Mol. Struct.* **434**, 75 (1998).
186. J. M. Schulman, J. Ruggio, and T. J. Venanzi, *J. Am. Chem. Soc.* **99**, 2045 (1977).
187. V. M. S. Gil and W. von Philipsborn, *Magn. Reson. Chem.* **27**, 409 (1989).
188. S. Berger and J. D. Roberts, *J. Am. Chem. Soc.* **96**, 6757 (1974).
189. W. McFarlane, *Proc. R. Soc. London, Ser. A.* **306**, 185 (1968).
190. H. C. E. McFarlane and W. McFarlane, *J. Chem. Soc., Chem. Commun.* 582 (1975).
191. (a) D. L. VanderHart, H. S. Gutowsky, and T. C. Farrar, *J. Am. Chem. Soc.* **89**, 5056 (1967). (b) H. W. Spiess, U. Haeberlen, and H. Zimmermann, *J. Magn. Reson.* **25**, 55 (1967). (c) M. M. Maricq and J. S. Waugh, *J. Chem. Phys.* **70**, 3300 (1979). (d) E. Menger and W. S. Veeman, *J. Magn. Reson.* **46**, 257 (1982). (e) J. G. Hexem, M. H. Frey, and S. J. Opella, *J. Chem. Phys.* **77**, 3847 (1982). (f) J. Böhm, D. Fenzke, and H. Pfeifer, *J. Magn. Reson.* **55**, 197 (1983). (g) D. L. Sastry, A. Naito, and C. A. McDowell, *Chem. Phys. Lett.* **146**, 422 (1988). (h) A. C. Olivieri and R. K. Harris, *Prog. Nucl. Magn. Reson. Spectrosc.* **24**, 435 (1992).
192. N. Zumbulyadis, P. M. Henrichs, and R. H. Young, *J. Chem. Phys.* **75**, 1603 (1981).
193. K. Eichele, R. E. Wasylshen, J. S. Grossert, and A. C. Olivieri, *J. Phys. Chem.* **99**, 10110 (1995).
194. C. W. Schultz and R. W. Rudolph, *J. Am. Chem. Soc.* **93**, 1898 (1971).
195. H. Falius and M. Murray, *J. Magn. Reson.* **10**, 127 (1973).

196. F. Breitsameter, K. Polborn, and A. Schmidpeter, *Eur. J. Inorg. Chem.* **1907** (1998).
197. V. Galasso, *Chem. Phys.* **83**, 407 (1984).
198. A. H. Cowley and N. C. Norman, *Prog. Inorg. Chem.* **34**, 1 (1986).
199. D. G. Gilheany. *In The Chemistry of Organophosphorus Compounds. Edited by F. R. Hartley.* John Wiley and Sons, Chichester. 1990, p. 43.
200. J. Demaison, F. Hegelund, and H. Bürger, *J. Mol. Struct.* **413**, 447 (1997).
201. M. Witanowski, L. Stefaniak, and G. A. Webb, *Ann. Rep. NMR Spectrosc.* **11b**, 1 (1981).
202. T. Khin and G. A. Webb, *J. Magn. Reson.* **33**, 159 (1979).
203. M. Witanowski, L. Stefaniak, and G. A. Webb, *Ann. Rep. NMR Spectrosc.* **11b**, 140 (1981).
204. H.-P. Schrödel and A. Schmidpeter, *Phosphorus, Sulphur, and Silicon* **129**, 69 (1997).
205. P.-Å. Malmqvist, A. Rendell, and B. O. Roos, *J. Phys. Chem.* **94**, 5477 (1990).
206. (a) Y. Ishii and R. Tycko, *J. Am. Chem. Soc.* **122**, 1443 (2000). (b) F. M. Marassi, A. Ramamoorthy, and S. J. Opella, *Natl. Aca. Sci. U.S.A.* **94**, 8551 (1997). (c) C. H. Wu, A. Ramamoorthy, and S. J. Opella, *J. Magn. Reson. A*, **109**, 270 (1994). (d) A. Ramamoorthy, C. H. Wu, and S. J. Opella, *J. Magn. Reson. B*, **107**, 88 (1995).
207. G. Wu and R. E. Wasylshen, *Mol. Phys.* **83**, 539 (1994).
208. R. Challoner and C. A. McDowell, *J. Magn. Reson.* **98**, 123 (1992).
209. H. Bai and R. K. Harris, *J. Magn. Reson.* **96**, 24 (1992).
210. S. Dusold and A. Sebald, *Mol. Phys.* **95**, 1237 (1998).
211. M. Bak and N. C. Nielsen, *J. Chem. Phys.* **106**, 7587 (1997).
212. A. Naito, S. Ganapathy, K. Akasaka, and C. A. McDowell, *J. Chem. Phys.* **74**, 3190 (1981).
213. S. Dusold, H. Maisel, and A. Sebald, *J. Magn. Reson.* **141**, 78 (1999).

214. H. Luo, R. McDonald, and R. G. Cavell, *Angew. Chem. Int. Ed.* **37**, 1098 (1998).
215. Spinsight 4.1, Varian Associates, Inc., 1998.
216. SPECMAKE, a program by K. Eichele, 1998.
217. P. J. Giammatteo, W. W. Hellmuth, F. G. Ticehurst, and P. W. Cope, *J. Magn. Reson.* **71**, 147 (1987).